Unconditionally convergent time domain adaptive and time-frequency techniques for epicyclic gearbox vibration

by

Peter Paul Schön

Dissertation submitted in partial fulfilment of the requirements for the degree Master of Engineering in the Faculty of Engineering, Built Environment and Information Technology, the University of Pretoria

June 2005

Abstract

Condition monitoring of epicyclic gearboxes through vibration signature analysis, with particular focus on time domain methods and the use of adaptive filtering techniques for the purpose of signal enhancement, is the central theme of this work. Time domain filtering methods for the purpose of removal of random noise components from periodic, but not necessarily stationary or cyclostationary, signals are developed. Damage identification is accomplished through vibration signature analysis by nonstationary time-frequency methods, belonging to Cohen's general class of time-frequency distributions, strictly based in the time domain.

Although a powerful and commonly used noise reduction technique, synchronous averaging requires alternate sensors in addition to the vibration pickup. For this reason the use of time domain techniques that employ only the vibration data is investigated. Adaptive filters may be used to remove random noise from the nonstationary signals considered. The well-known Least Mean Squares algorithm is employed in an adaptive line enhancer configuration. To counter the much discussed convergence difficulties that are often experienced when the least mean squares algorithm is applied, a new unconditionally convergent algorithm based on the spherical quadratic steepest descent method is presented. The spherical quadratic steepest descent method has been shown to be unconditionally convergent when applied to a quadratic objective function.

Time-frequency methods are succinctly employed to analyse the vibration signals simultaneously in the time and frequency domains. Transients covering a wide frequency range are a clear and definite indication of impacting events as gear teeth mate, and observation of such events on a time-frequency distribution are used to indicate damage to the transmission. The pseudo Wigner-Ville distribution and the Spectrogram, both belonging to Cohen's general class of time-frequency distributions are comparatively used to the end of damage identification.

It is shown that an unconditionally convergent adaptive filtering technique used in conjunction with time-frequency methods can indicate a damaged condition in an epicyclic gearbox, where the non-adaptively filtered data did not present clear indications of damage.

Acknowledgements

My thanks goes to prof. P.S. Heyns and Mr. C.J. Stander for their guidance during the course of this work. I am especially grateful for being allowed the freedom to chart my own course through the research, while knowing that assistance would be rendered whenever required.

Prof. J.A. Snyman provided me with all assistance needed to implement the SQSD algorithm. For his assistance and insight into optimization methods I am grateful.

For many insightful discussions on digital signal processing techniques and implementations, whenever the need arose, I am grateful to Mr. L. Staphorst, and Mr. P. de Villiers.

Table of Contents

Nomenclature

A	:	maximum step size for adaptive algorithm
Γ	:	adaptive demodulation convergence parameter matrix
Δ	:	delay
α	:	exponential decay constant
$\alpha_{m,l}$	:	initial phase angle of amplitude modulation function
$\beta_{m,l}$	:	initial phase angle of phase modulation function
γ	:	adaptive demodulation convergence parameter
ε_g	:	gradient tolerance
ε_n	:	error signal at time n
ε_w	:	LMS step size convergence tolerance
ε_x	:	SQSD step size convergence tolerance
θ	:	frequency shift variable
λ	:	convergence or iterative step size parameter
σ	:	exponential decay constant for Gaussian window function
τ	:	time shift variable
$\varphi(\theta,\tau)$	:	time-frequency distribution kernel
$\varphi_{k,m}(t)$	:	phase modulation law at iteration k
φ_m	:	original or initial phase angle of m-th harmonic
$A(\theta,\tau)$	:	symmetrical ambiguity function
ΔB	:	separation between discrete frequency components
$C(f)$	:	Fourier transform of c(t)
E	:	total energy of a signal
$E(t)$	:	instantaneous energy density of signal
$E\{\cdot\}$	:	expected value
$G(q)$	:	digital filter
$H(\omega)$	:	Fourier transform of window function h(t)
$H\{\cdot\}$	:	Hilbert transform
L	:	number of significant harmonics in amplitude or phase modulation functions / adaptive filter length
M	:	number of significant harmonics in x(t)
$P(t,\omega)$	:	time-frequency distribution
P_i	:	phase angle of planet gear i
$P_S(t,\omega)$	:	Spectrogram time-frequency distribution
Q_{mr}	:	phasor sum of different planet gear phase spectra
$\mathbf{R}$	:	input autocorrelation matrix
$S(\omega)$	:	Fourier transform of time signal s(t)
$\lvert S(\omega)\rvert^2$	:	energy density spectrum
T_g	:	number of gear teeth
T_s	:	sampling period
W	:	filter bandwidth
$W(t,\omega)$	:	Wigner-Ville time-frequency distribution
$X_A(t)$	:	Fourier series representation of $x_A(t)$
$X_k(t)$	:	time domain amplitude and phase modulated gear meshing vibration at iteration k

X_m : amplitude of m-th harmonic
$Y(f)$: Fourier transform of y(t)
Z_a : number of teeth on annular gear
Z_p : number of teeth on the planetary gear
Z_s : number of teeth on sun gear
$a_{k,m}(t)$: amplitude modulation law at iteration k
a_m : amplitude modulation function of m-th harmonic
b_m : phase modulation function of m-th harmonic
$c(t)$: train of ideal impulses
c_k : SQSD curvature at iteration k
d : SQSD step size parameter
e_k : exact error signal at instant k
$e_{k,m}(t)$: additive noise at iteration k
f_a : planet to annulus gear corresponding tooth mesh frequency
f_c : carrier rotation frequency
f_m : gear mesh frequency
f_p : planet gear rotation frequency
f_r : shaft rotation frequency
$f_r(n)$: shaft rotation frequency as function of discrete time variable
f_s : sampling frequency
f_{sg} : sun gear rotation frequency
$h(k)$: transfer function
$h(t)$: window function (spectra and time-frequency distributions)
k : iteration number; summation index
l : index of harmonic number in amplitude or phase modulation functions
m : index of harmonic number
n : discrete time variable
p : summation limit – number of elements in weight vector
$\mathbf{p}$: cross correlation vector between desired response and input components
q : shift operator - $qu(t)=u(t+1)$
r : sideband number
$s(t)$: time signal
$|s(t)|^2$: instantaneous energy
t : continuous time variable
$u(t)$: input sequence
$\mathbf{w}_0$: starting filter weight vector
$\mathbf{w}_k$: filter weight vector at instant k
$x(n)$: discrete time domain amplitude and phase modulated gear meshing vibration
$x(t)$: continuous time domain amplitude and phase modulated gear meshing vibration
$x_A(t)$: complex analytical signal associated with x(t)
$x_i(t)$: imaginary part of complex analytical signal $x_A(t)$
$x_k(t)$: time domain amplitude and phase modulated gear meshing

vibration at iteration k

$x_r(t)$: real part of complex analytical signal $x_A(t)$

$y_a(n)$: averaged signal, computed from x(n)

$y_F(n)$: discrete time filtered signal

y_k : measured data point at sampling instant k

y_n : measured signal sample at time n

$z^{-\Delta}$: delay of Δ samples

1 Introduction

Condition monitoring of an epicyclic gearbox through vibration signature analysis is the central theme of this work. A particular focus will be maintained on strictly time domain methods: time-frequency methods for signature interpretation and the use of adaptive filtering techniques for the purpose of signal enhancement.

This work arises from a need experienced by the South African Air Force maintenance function: Effective condition based maintenance techniques are required for the ageing fleet of C-130 Hercules aircraft operated by the air force. Of particular interest for the purpose of this work is the monitoring of the main engine gearbox driving the airscrew, and driven by a gas-turbine engine.

Systems used in the production of goods and delivery of services constitute the vast majority of most industry's capital (Wang, 2002). Physical equipment is susceptible to failure through breakdown, deterioration in performance through age and use and to obsolescence due to improvements in technology (Jonsson, 2000). Jonsson further states that the rising importance of streamlining processes and achieving process control and flexibility raises the cost of disturbances. Wang (2002) points out that for certain systems, including military and transportation systems, it is extremely important to avoid failure during actual operation because such failure can be dangerous or disastrous.

Condition-based maintenance techniques provide assessments of a system's condition, based on data collected on the system through continuous monitoring or inspection, with the aim of determining maintenance requirements prior to the occurrence of failure. Grall, Bérenguer and Dieulle (2002) point out that many structures and mechanical systems suffer increasing wear with age and usage, and are subject to random failures resulting from this deterioration. Deterioration and failures of such systems might incur high costs due to losses resulting from delays, unplanned interventions on the systems and safety hazards.

In-service costs for aircraft are mainly those for (i) the fuel consumed and (ii) the replacement of the system's components (Naeem, Singh & Probert, 2001). Any rise in life expectancy of an aircraft's gas-turbine engines directly lowers the life-cycle cost. Life-cycle cost depends upon the class of mission undertaken, operating conditions therein experienced and the rate of in-service engine deterioration. Naeem, Singh and Probert (2001) observed that the extent to which the in-service deterioration of an aircraft's engines adversely affects: (i) the rate of fuel usage (ii) the aircraft's effectiveness and (iii) its operational life is not clearly established and is subjective to the observer.

High-performance military aero engines are complex in design and have to operate under severe mechanical stresses and at high temperatures. Designers and users of aircraft incorporating these engines continually seek greater reliability, increased availability, enhanced performance and improved safety as well as low life-cycle costs.

Effective condition based maintenance therefore has an important role to play in the effective management of production or service delivery systems. The aircraft under consideration fit into the class of service delivery systems, providing a transportation service. Current reliability safeguards such as damage tolerant or fail-safe designs, redundancy and safe-life determination techniques (Samuel & Pines, Article in Press) do not provide for optimized maintenance expenditure.

There are currently three approaches to the detection of faults in geared systems: acoustic signal analysis, debris monitoring and vibration analysis (Wang, Ismail & Golnaraghi, 2001). Vibration-based diagnostic monitoring techniques have been the most popular due to the relative ease of instrumentation and measurement. When vibration features of a component are obtained, its health condition can be determined by comparing these patterns with those corresponding to its normal and failure conditions, either by visual inspection or by inference approaches.

1.1 Problem Discussion

The gearbox under consideration is a dual-stage epicyclic gearbox that drives the airscrew, as well as several auxiliary devices. The gearbox is a complex machine with a large reduction ratio of 13.54:1. The gearboxes thus play a critical role in the propulsion system of the aircraft. A generally applicable methodology of dealing with the vibration signatures of these gearboxes is sought, rather than a specific application of a particular method to a specific gearbox.

Vibration limits as specified by the engine manufacturer have become inapplicable and insufficient for the purpose of condition monitoring on the engines employed on South African Air Force aircraft. This is due to extensive modification programs conducted during the years of socio-political isolation of South Africa. A specific concern of the air force is the problem of distinguishing between vibration signatures of engines being run simultaneously.

Engines are preferably not to be run unsymmetrical, as the airframe may incur damage in this way. It is further preferred to run all four engines simultaneously, rather than just running two engines at a time. The complexity of the structure of the airframe causes complex attenuation of the respective vibration signatures, complicating identification of the exact

source of a particular signature. A degree of uncertainty is thus present when examining data recorded at a specific engine as to the origin of all contributions to the measurement; a problem experienced by the South African Air Force's maintenance function on the C-130 aircraft.

Transmission path effects on the vibration signals are unknown: the effects of the aircraft structure on the signals are highly dependant on the measurement point. Furthermore, knowledge of the exact nature of the signals is absent as the exact defect being experienced by the system may be unknown. Also, different defects may be simultaneously present.

The working conditions of the aero-engine gearbox under consideration introduce additional complications into the analysis. The gearbox functions under fluctuating load conditions, due to the variable pitch airscrew and flow-induced effects. The fact that the gearbox is driven by a gas turbine engine further complicates the situation by the introduction of stochastic and deterministic vibrations to the system.

Accurate analysis of vibration spectra and wave forms can provide useful information pertinent to the source of the vibration. When the vibrations being studied result from physical interactions in a mechanical system, the vibration wave carries in it useful information regarding the system condition and operation. The condition of the system may therefore be inferred from deciphering of the useful information encoded in the vibration signal.

Various attempts have been made at developing methods to accommodate complex epicyclic gearboxes for the purpose of condition monitoring. Many of the works in this field have helicopter main drive gearboxes as subject (Randall, 2001; Antoni & Randall, 2004; McFadden 1988). Numerous attempts at condition monitoring of planetary gearboxes have also been made elsewhere, the articles of Meltzer and Ivanov (2001, parts I and II) addressing in particular the scenario of operation under varying speed conditions using time-frequency methods.

A review of vibration-based techniques for helicopter transmission diagnostics is provided by Samuel and Pines (Article in Press). Helicopter main rotor drive gearboxes are more often than not of the epicyclic kind. It is stated by the authors that condition based maintenance has yet to be completely realized. They observe that rotorcraft safety and reliability is presently sought by manufacturers through conservative safety factors on design and component safe-life estimates, and recommended frequent scheduled maintenance. Three techniques are specified by Samuel and Pines as currently in use: damage tolerant or fail-safe designs, redundancy and safe-life determination techniques. Statistical techniques, spectral analysis, time-frequency methods, mathematical modelling and adaptive signal

processing techniques are among the vibration analysis techniques discussed by Samuel and Pines (Article in Press).

Dalpiaz, Rivola and Rubini (2000) provide a survey and assessment of the sensitivity of several gearbox diagnostic techniques. Their review in particular compares time-frequency and cyclostationary analysis based techniques to more established cepstrum analysis and time-synchronous averaging techniques. Among the time-synchronous averaging techniques considered are included amplitude and phase demodulation techniques.

Wang, Ismail and Golnaraghi (2001) focus on time-frequency techniques, specifically the wavelet transform, statistical measures and amplitude and phase demodulation. Time-synchronous averaging and the residual signal analysis technique are grouped under filtering conditions by these authors.

From the reviews provided by Samuel and Pines (Article in Press), Dalpiaz et al. (2000) and Wang et al. (2001) it is clear that no technique can be singled out as the mantra of gearbox vibration signature analysis. The performance of a specific analysis technique in a specific situation depends on the conditions of the analysis, and on the vibration data itself. A multi-pronged approach should thus be considered prudent if accurate and reliable diagnoses are to be made. Choice of the most appropriate techniques will certainly be guided by prior knowledge of the data to be analyzed.

Considering the selection of a set of most appropriate techniques, the analyst should draw on his or her knowledge of the particular scenario under consideration. Data characteristics such as spectral content and stationarity, or cyclostationarity, should be considered in the selection process. Machine characteristics are therefore equally important, as these influences in their turn the nature of the vibration signature recorded. Additionally the characteristics of the analysis techniques govern their effectiveness and applicability to certain scenarios.

To this end a literature review is presented as the remainder of this chapter. Prominent vibration analysis techniques will be briefly discussed, and their applicability to the present application considered.

1.2 Characterising Gearbox Vibrations

Fundamental to, and characteristic of, gear vibration is a periodic amplitude and phase modulated signal at the tooth-meshing frequency, and harmonics of the tooth-meshing frequency (Randall, 1982). Periodic signals at the tooth mesh frequency are due to deviations from the perfect involute gear tooth profile, and may be observed from seemingly perfect newly manufactured gearboxes. Sources of such deviations from the tooth profile are tooth deflection under load and geometrical errors from the manufacturing process. These deviations from the perfect involute profile cause amplitude

and frequency modulations of the carrier frequency, i.e. gear mesh frequency. Harmonics of the base tooth-meshing frequency are generated due to periodically varying compliance as the load is shared between different numbers of teeth.

Any deviation from the ideal tooth profile will result in precession of the contact point around the ideal pitch circle. This in turn implies that contact between points on the circumference of the teeth will not occur at the expected times, thus influencing the time domain vibration signature. Deviations from the ideal tooth profile may result from manufacturing errors, load effects, damage to gear teeth or assembly errors such as eccentricity. Amplitude and phase modulation of the carrier gear mesh signal will result from deviations from the ideal tooth profile (Randall, 1982).

Amplitude modulation effects result from sensitivity of the vibration amplitude to tooth loading. Fluctuation of the load will cause a corresponding variation in the amplitude of the vibration signal. The modulating frequency for gear vibrations will generally be related to the shaft frequency of the gear, for effects related to gear rotation. Randall (1982) reports that a highly localized fault, e.g. on one tooth, will tend to give a modulation by a short pulse of the order of the tooth-mesh period, and repeated every revolution. Notably it is explained by Randall that a more distributed fault that is wider in the time domain will make the corresponding envelope in the frequency domain narrower and higher.

Frequency modulations may result from non-constant rotational speed or non-uniform tooth spacing. Randall (1982) argues that the same fluctuations in tooth contact pressure which give rise to amplitude modulation must simultaneously apply a fluctuating torque to the gears, and result in angular velocity fluctuations at the same frequency. These fluctuations may be modelled in mathematical gear models as phase modulations, as in McFadden (1986), or as frequency modulations, as in Bonnardot, El Badaoui, Randall, Daniere and Guillet (Article in Press).

Apart from the causes of modulation discussed previously, fluctuation of the external load will also cause amplitude and frequency, or phase, modulation, without having anything to do with the gearbox's condition. The frequency of the modulation may however be used in some cases to distinguish external load related modulations from modulations caused by internal defects.

Planet gears in epicyclic gearboxes are not stationary: they rotate about the sun gear, between the sun gear and the ring or annular gear. This implies that there is relative motion between some of the gear components and a stationary measurement location on the gear case. This relative motion causes an apparent amplitude modulation of the meshing signals originating

from the planet gears: a phenomenon termed planet pass modulation by Forrester and Blunt (2003). McFadden and Smith (1985) noted that epicyclic gearbox vibration may be modulated by the motion of the planet gears with the rotation of the gear cage.

McFadden and Smith (1985) explained the asymmetry often observed in the spectra of epicyclic gear system's vibration at the hand of an argument involving the planetary gear layout geometry and the resulting phase of the vibration of the different planetary gears relative to each other. McFadden and Smith show that the phase angle of any component in the vibration spectrum of an epicyclic gear is determined solely by the initial position of the planet gear relative to the transducer, by the number of teeth on the annulus and by the meshing harmonic and sideband order, assuming that the time delay caused by the propagation of the vibration around the annulus is small.

Dowling (1993) highlights several characteristics regarding the nature of machine signals. He points out that a fault signal often originates in a moving component and is transmitted to stationary components through a complicated path, as is the case with gears. This transmission path may result in a complicated transfer function, or even a time varying transfer function. Dowling also points to the impulsive nature of vibration phenomena that generate wide-band spectral content signals which in turn interact with the system natural frequencies and mode shapes. Vibration signals associated with transient events may further not be repetitive in the earliest stages of development.

Stationarity of vibration signals may be employed in a constructive manner in the analysis of vibration signatures. Capdessus, Sidahmed and Lacoume (2000) defines a random signal x(t) as n-th order stationary if its time-domain n-th order moment does not depend on time t. A random signal x(t) is considered by these authors to show cyclostationarity at the n-th order if its time domain n-th order moment is a periodical function of time t. Elsewhere, Antoni, Bonnardot, Raad and El Badaoui (2004) define a cyclostationary process as a stochastic process that exhibits some hidden periodicities in its structure.

Kinematical variables in rotating machinery are periodic with respect to some of the rotation angles. This implies that the signals emanating from such machinery are intrinsically angle-cyclostationary rather than time-cyclostationary, as reported by Antoni, Bonnardot, Raad and El Badaoui (2004). Proposition 2 presented by Antoni et al. (2004) states that a wide-sense angle-cyclostationary process sampled by a bijective mapping will be wide-sense time-cyclostationary if, and only if, the speed fluctuation of the system is itself a wide-sense cyclostationary process. For randomly

fluctuating angular speed, this implies that the time sampled signal will not be cyclostationary.

For the purpose of machinery diagnostic monitoring, stationary analysis is most frequently employed. This may be due to the fact that before catastrophic failure occurs, the fault signal appears in a repetitive manner. Dowling (1993) argues that non-stationary analysis is required for optimum incipient failure detection because failure signals: a) are non-stationary; b) are not repetitive in the earliest stages; c) consist of several active frequency components; and d) often occur over several time scales.

1.3 Filtering of Vibration Signals

As a preparatory step before vibration signal analysis, various filtering operations can be performed on the measured signal with the purpose of signal enhancement, for instance noise reduction or narrow-band filtering as required by certain narrow-band techniques. Separation of periodic signal components from random components may be used to distinguish between different vibration signatures: separating gear and bearing signals as in Antoni and Randall (2001).

Conventional digital filtering techniques may be applied to remove energy from frequency bands that contain no useful or unwanted information. For the preservation of signal phase, the technique of forward-backward filtering may be employed (Gustafsson, 1996). This technique can be used with finite impulse response as well as infinite impulse response digital filters to great effect.

Adaptive signal processing encompasses signal processing algorithms which are adjustable in such a way that their performance, according to some criterion, improves through contact with their operating environment. Adaptive systems are therefore time varying and nonlinear, and the principle of superposition does not hold for these systems. Adaptive systems' adjustments usually depend on finite-time average signal characteristics, rather than on instantaneous values of signals (Widrow & Stearns, 1985).

A common element in many of the applications of adaptive signal processing is that some element of a problem is unknown and must be learned, or some system component is changing in an unknown manner and therefore must be tracked (Alexander, 1986). Adaptive filters are commonly used in the following circumstances: when filter characteristics are required to be variable; when there is spectral overlap between signal and noise; or if the band occupied by noise is unknown or time varying. Conventional filters applied to the above cases would lead to unacceptable distortion of the desired signal (Ifeachor & Jervis, 2002).

Filtering nonstationary signals is a major area of application for adaptive filters (Widrow & Kamenetsky, 2003). Widrow and Kamenetsky further state that when the statistical character of an input signal changes gradually, randomly and unpredictably, a filtering system that can automatically optimize its input-output response in accord with the requirements of the input signal could yield superior performance relative to that of a non-adaptive system.

An adaptive filter has the property that its frequency response function is adjustable to improve its performance in accordance with some performance function, allowing the filter to adapt to changes in the input signal. Adaptive filters are capable of tracking the statistics of nonstationary signals, provided that the changes in signal statistics occur slowly relative to the convergence time of the adaptive filter (Elliott, 2001).

Adaptive systems under consideration here all make use of performance functions that determine the system output. This performance function has to be chosen such that it will lead to a measurable improvement in the system output characteristics. Closed loop adaptive systems will be considered. The closed loop adaptive system involves automated experimentation with adjustments of the system characteristics, in an ordered manner. Knowledge of the resulting outcomes of the adjustments is then used to make further adjustments to the adaptive system, in order to improve its performance relative to the performance function.

Synchronous averaging is an ensemble averaging technique where knowledge of the repetition frequency of a desired signal, or a second synchronous noise free signal is used to compute a synchronised ensemble average of the desired signal. McFadden (1987) proposes a revised model for the time domain averaging process that is more complicated than the previously used comb filter model, proposed by Braun (1975). The model proposed applies a rectangular window to the signal in the time domain, and samples the Fourier transform of the signal in the frequency domain.

Generally a key phasor reference signal is required when performing synchronous averaging (Fyfe & Munck, 1997). Although it is possible to use knowledge of the frequency of the signal, this approach requires little or no variation in the rotational velocity of the component and is therefore limited in its application.

This work will focus on signal processing techniques that do not require additional information, other than that contained in the vibration signal. Due to requirements surrounding the certification of sensors for operation in an aerospace environment, the use of additional sensors is highly unattractive. Diagnostic techniques capable of reliable diagnosis with minimal hardware requirements are preferred. Conventional order tracking techniques use an

additional sensor to provide the key phasor reference. Conventional order tracking techniques are therefore unattractive from the perspective adopted in this work.

1.4 Time-Frequency Methods

Many of the conventional signal analysis techniques employed require periodicity of the fault signal. Dowling (1993) points out that in contrast, most if not all faults are non-periodic in the earliest stages of development. For some cases, by the time the fault exhibits an identifiable periodic structure, it is already well developed. Conventional techniques do not adequately track non-stationary signals, and don't adequately describe the internal fine structure of transients.

Time frequency analysis aims to describe the evolution of the frequency or spectral content of a signal over time. What makes a particular representation of a signal significant is that the characteristics of the signal are understood better in that representation because the representation is characterised by a physical quantity that is important in nature or for the situation at hand.

Considering a simple time varying signal, incorporating amplitude and phase modulation, it should be noted that there exists an infinite number of ways of choosing different pairs of amplitudes and phases that generate the same signal (Cohen, 1995). By utilising a complex mathematical description of the signal, and fixing the imaginary part, the amplitude and phase of a signal can however be specified in an unambiguous manner.

Time energy density and the frequency energy density are insufficient to describe the physical signal because they do not fully describe what is occurring. From the frequency energy density, or spectrum, it is clear which frequencies were present, but it is not clear when those frequencies existed. Hence the need to describe the temporal variation of the energy spectral content.

As gear faults develop, the frequency spectrum will develop with the fault. Time-frequency analyses can then be used to monitor the progression of the fault, as it develops. Localised faults may also be obscured by averaging techniques, which makes time-frequency analysis more attractive from a diagnostic point of view.

Vibration data from gearboxes can exhibit various non-linear and transient events, and analysing such events require techniques that go beyond the classical Fourier spectral analysis approach as noted by Staszewski, Worden and Tomlinson (1997). Oehlmann, Brie, Tomczak and Richard (1997) argue that vibration signals, representative of physical processes in a gearbox, are nonstationary multi-component signals that include tooth meshing, fault

transients, gearbox resonance vibrations and system and sensor transmission characteristics.

1.5 Gear Condition Monitoring

Modern techniques for gear diagnostics are based on the analysis of vibration signals measured on a gearbox's casing. The aim is to detect the presence and the type of a fault at an early stage of development. The evolution of a fault condition is monitored in order to estimate the machine's residual life and choose an adequate maintenance strategy. Vibration-based monitoring techniques currently available for the detection of gear faults can be classified according to the analysis domain as follows: frequency/cepstrum analysis, time/statistical analysis and time - frequency analysis (Wang, Ismail & Golnaraghi, 2001).

Spectral analysis may be unsuitable to detection of gear failures at an early stage, especially in the case of local faults, which primarily affect sidebands in the spectrum. Several gear pairs and other mechanical components usually contribute to the overall vibration. Hence it may be very difficult to evaluate the spacing and evolution of sideband families in a spectrum. For this reason, many researchers have proposed the application of other vibration analysis techniques, such as cepstrum, time-synchronous average and related techniques, time-frequency distribution techniques, cyclostationary analysis, signal modelling techniques, high-resolution spectral analysis techniques and advanced statistical methods (Dalpiaz, Rivola & Rubini, 2000).

Techniques currently used for gear condition monitoring, as well as techniques for noise reduction will be discussed in the form of a brief literature review. Filtering techniques will cover the topics of synchronous averaging and adaptive filtering. Damage identification techniques will be divided under subsections of spectral or cepstral analysis, amplitude and phase demodulation techniques, time-frequency techniques and an energy technique used in conjunction with time-frequency distributions.

1.5.1 Adaptive Signal Processing Applications

Impulsive signals originating from machinery were studied by Lee & White (1998). The presence of a fault in machinery may be indicated by the presence of, or increase in, impulsive signal elements. Impulsive signal elements result from a change of stiffness or a change in mass of the system. The emphasis of Lee and White's effort was on the pre-processing of measured signals to permit more accurate characterization of fault related impulsive components.

Lee and White employed an enhancement scheme based on a two-stage Adaptive Line Enhancer, as opposed to for instance a synchronous averaging scheme. The filtered signals were represented in the time-frequency domain to obtain simultaneous spectral and temporal information.

Accelerometer signals were augmented by Hernandez (2001) using a Recursive Least Squares algorithm. A single accelerometer was mounted in a bus for the purpose of taking acceleration measurements during a performance test. Noise present in the signals studied by Hernandez occupied a frequency band very close to the band of the acceleration signal.

Hernandez (2001) addressed the optimization of various filter parameters, including the number of taps and the so called forgetting factor of the Recursive Least Squares algorithm. Application of Hernandez's methodology delivered an increase in signal to noise ratio of 20dB, from 13.23dB before the filter to 33.64dB after the filter.

Guidelines for the choice of parameters of the least mean squares algorithm were proposed by Antoni and Randall (2001). Their application of choice is vibration data obtained from helicopter gearboxes, which are in general epicyclic gearboxes. The guidelines proposed by the authors stem from thorough examination of the properties of the signal to be filtered, and the desired result of the filtering process.

Specific guidelines are offered by Antoni and Randall (2001) for setting of the filter length, or number of coefficients employed, the forgetting factor and the choice of initial weight vector. Introduction of an exponentially decreasing forgetting factor is further proposed in order to enhance the accuracy of the filtered signal, while maintaining an acceptable convergence rate. It is additionally shown that reliable estimates of the forgetting factor may be made from an autocorrelation matrix of the input signal, having moderate size, much smaller than the length of the filter.

Improvements in the signal-to-noise ratio of a signal obtained from a variable reluctance type wheel speed sensor are presented by Hernandez (2003). The wheel speed sensor is a common component of many of the modern Automatic Braking Systems (ABS) installed in modern motorcars. The author desired to improve the low speed response obtained from the sensor, for improved performance at slow vehicle speeds.

Considerations of speed of convergence led Hernandez (2003) to using a Frequency Domain Least Mean Squares (FDLMS) adaptive filtering algorithm. The author concluded that satisfactory gains in signal-to-noise ratio were obtained by comparing the power spectral densities of filtered and unfiltered signals. The adaptive algorithm was employed in the adaptive line enhancer configuration.

1.5.2 *Synchronous Averaging*

By synchronizing the sampling of the vibration data with the rotation of a particular gear of interest and calculating the ensemble average of the vibration over numerous revolutions, a signal is obtained which is

determined solely by the vibration produced by the gears on the particular shaft, or identically in phase with that shaft. In the time domain, the signal average will show the pattern of the tooth meshing vibration including amplitude and phase modulations, over one revolution, while the frequency domain gives the tooth meshing components and all the modulation sidebands at the shaft rotation frequency (McFadden, 1986). This technique, discussed by McFadden and Smith (1985) is known as time-synchronous averaging, and has been used extensively in condition monitoring of gearboxes.

For the purpose of condition monitoring on rotating machines, the cyclic nature of the vibration signals can be employed. Methods have been developed that utilise the cyclostationarity of rotating machine vibration phenomena. Order tracking is such a method, and uses multiples of the running speed as frequency base, in stead of absolute frequencies. Computed order tracking makes use of constant sampling per time basis, and then uses software algorithms to resample the data at constant angular increments. Fyfe and Munck (1997) reported that computed order tracking is however extremely sensitive to the timing accuracy of the key phasor pulses. Accordingly, it is desirable to employ a shaft encoder with high resolution for this purpose. Order tracking is nothing more than angular domain resampling of the time domain vibration signal, and is used as precursory step, before performing synchronous averaging.

Synchronous averaging, though prevalent in conventional gearbox condition monitoring, produces considerable difficulties when applied to epicyclic gearboxes. Multiplicity of contact regions between gears combined with the motion of the planet gears are significant contributors to these difficulties. McFadden (1991) proposed a technique, based on the proximity of a specific planet gear to the transducer, to calculate the time domain average of individual planetary gears as well as that of the sun gear.

Proximity of a specific planetary gear to the measurement location on the annulus, in tandem with the variations in the amplitude of the transfer function between planet gear and transducer implies that the contribution made by that gear to the total vibration signal will be most significant. Transmission of the vibration signal through the structural transfer function, sampling, and appropriate selection of a windowing function produces a signal dominated by vibration from a specific planetary gear. Subsequent mapping of the windows, with respect to angular position on the gear, into their correct positions in the time domain average produces a signal from which the time domain average may be computed. A detailed analysis is presented in order to clearly establish the conditions under which the technique developed by McFadden (1991) is applicable.

Patents have arisen from development of techniques to deal with the planet pass modulation – the observation that the gear vibration signal of a planetary gear is modulated by a periodic function with period synchronised to the planet carrier rotation (Forrester & Blunt, 2003). A technique is presented by Forrester and Blunt (2003) that alleviates the discontinuities present in techniques that employ a principle similar to that of McFadden (1991), and performs averaging over shorter total time. The technique performs separation of the total measured signal into contributions from each planet gear, using all of the available vibration data.

Representative signal averages are produced for each planet gear by employing a selective continuous time filter into the averaging process. The time filter proportionally divides the total vibration signal into contributions from each planet, using a window function. With careful selection of the window function's characteristics and the signal averaging parameters, separation is performed with minimum leakage of vibration from other planetary gears.

Forrester and Blunt (2003) present an application of their technique to a small planetary gearbox with 3 planet gears. They successfully indicate a small fault condition on one of the teeth of a planetary gear, using the kurtosis value of the averaged signal. Flank wear was simulated by removal of a small amount of material from one of the planetary gear teeth.

1.5.3 *Spectral and Cepstral Analysis*

The most significant components in gear vibration spectra are the tooth-meshing frequencies and their harmonics, together with sidebands, which are due to modulation phenomena. Sidebands of the mesh frequency occur as a result of a modulating rotational motion, caused by a failure of mating teeth to impact one another at the proper time, as discussed by Goldman (1999). Incrementation in the number and amplitude of the sidebands may indicate a fault condition. Randall (1982) reports that the spacing of the sidebands is related to the particular source. Faults localised on one tooth, or over a few teeth, such as cracks and spalls, produce modulation effects during the engagement of the faulted teeth, and are repeated once each revolution of the gear. The spectrum presents a large number of sidebands of the tooth-meshing frequency and its harmonics, spread over a wide frequency range, spaced by the rotation frequency of the faulted gear and characterised by low amplitude. Transient additive impulses may be produced, giving rise to low-frequency components.

In most gear systems the tooth meshing frequency and its harmonics dominate the spectrum. For epicyclic gearboxes, McFadden and Smith (1985) proposed a simple model to explain why the principal component of the spectrum is slightly removed from the gear meshing frequency. A theoretical development is presented that clearly shows that while the motion of a single

planet gear past an observer location on the annular gear produces symmetrical sidebands about the tooth meshing frequency, the phase angle of planet gears relative to one another may cause destructive interference, obscuring certain components of the spectrum.

Three test cases are used by McFadden and Smith (1985) to illuminate the validity of their technique: a compressor drive gearbox, a Sea King helicopter gearbox and a turbine engine reduction gearbox. The suppression, or lack thereof, of gear mesh harmonics, or sidebands of the harmonics, is indicated to be a function of the geometric layout of the planetary gears. It is importantly noted by the authors that the asymmetry is strictly an artefact of the measurement of the vibration at a fixed location, and not a feature of epicyclic gear vibration itself.

A particular difficulty when monitoring epicyclic gearboxes is the constantly varying transmission path for at least the planet gears. A further practical issue is the infeasibility of mounting a shaft encoder in order to successfully perform rotation sampling in the angular domain, or synchronous averaging. This problem may not exist for industrial applications, but becomes an issue when gearboxes on aero engines are considered. Multiple gears running at the same meshing frequency are also present – i.e. planetary gears.

Oppenheim and Shafer (1989) define the real cepstrum as the inverse Fourier transform of the logarithm of the magnitude of a signal's Fourier transform. Randall (1982) points out that the cepstrum is thus useful for detecting any periodic structure in the spectrum, in the case of gear vibration signals the families of sidebands resulting from amplitude and frequency modulation of the gear mesh carrier signal.

Articles by Dalpiaz, Rivola and Rubini (2000) as well as El Badaoui, Guillet and Daniere (2004) report that the cepstrum is less sensitive to transducer location when synchronous averaging is employed. Both sets of authors however also indicate that synchronous averaging, although advantageous, is not essential in all cases. Results presented by Dalpiaz et al. reinforce this statement.

Modulation phenomena, of which several may simultaneously be present in the vibration signal, each produce a different family of sidebands characterised by the spacing of the sidebands in the spectrum. The spacing between sidebands is determined by the modulation frequency. Changes in the number and amplitude of the sidebands may indicate deterioration in condition. Each family of sidebands produces a peak in the cepstrum at a quefrency corresponding to the reciprocal of the spacing of the spectrum components, as well as rahmonics at multiples of the base quefrencies. As noted by Dalpiaz et al. (2000), the fundamental cepstrum component represents the average sideband level over the whole spectrum.

1.5.4 *Demodulation Techniques*

Spectral analysis, though a sufficient technique for simpler gearboxes, is inadequate for analysis of more complex epicyclic gearboxes. For simple gearboxes, modulation sidebands (Randall, 1982) are identifiable in the spectrum. When a more complex epicyclic gearbox is considered, identification of modulation sidebands becomes difficult due to the increased complexity of the spectrum: more frequency components are present (McFadden, 1986). Further complexity is introduced for epicyclic gearboxes by obscuring of possibly the gear mesh frequency itself, and some of the sidebands, due to interference between signal components as proposed by McFadden and Smith (1985).

Phase modulation's importance in gear vibration analysis was first noted by McFadden and Smith (1985). In the year following, McFadden (1986) presented a signal model by means of which the amplitude and phase modulation could be extracted from the time domain average of a gear vibration signal as the instantaneous phase and amplitude of the analytical signal, computed by means of the Hilbert transform. The author applied the demodulation technique to a data set obtained from helicopter main rotor gearboxes, successfully indicating the presence and growth of a fatigue crack in the spiral bevel pinion.

Hilbert transform based demodulation was further extended by McFadden (1988) to the detection of the location of a fatigue crack in a gear, by analysing the phase of the change in the meshing vibration. An identical model to McFadden's earlier publication in 1986 was used unmodified to calculate an analytical signal. Rotation of the analytical signal vector was removed, initial phase cancelled and the difference between modulated and un-modulated vectors was calculated.

Frequency domain techniques were used for band pass filtering, obtaining the analytical function, removing the uniform rotation of the analytical function vector, removal of the initial phase and computing the difference between modulated and un-modulated signals. Conversion by the inverse complex Fourier transform produces the complex difference signal. Examination of the locus of the difference signal in the complex plane indicated damage to the gear under consideration. An irregularity in this locus at a certain angle was then used to predict the position of the fatigue crack present in the gear. McFadden (1986) points out that the technique is applicable only to gears with spiral or helical tooth forms.

Adaptive demodulation applied to gear vibration signals was presented by (Brie, Tomczak, Oehlmann and Richard (1996). An abrupt change detection algorithm was coupled to the adaptive demodulation algorithms. Normal amplitude and phase modulations present in healthy gear vibration signals

are slowly time variant, while defects introduce abrupt variations in the vibration signal.

Superiority of the adaptive demodulation approaches over the conventional Hilbert transform approach is shown from considerations of signal bandwidth. Mathematical proof is presented of the spectral bandwidth of random amplitude and phase modulations, and it is pointed out that the Hilbert transform approach makes use of only a single filter, while the adaptive approaches use multiple filters.

Algorithms based on the recursive least squares, as well as least mean squares architectures are presented by Brie, Tomczak, Oehlmann and Richard (1996). An important advantage of the LMS algorithm presented is found therein that access is provided to individual amplitude and phase parameters of the various harmonics.

Application of the techniques presented by Brie, Tomczak, Oehlmann and Richard (1996) to an automotive gearbox demonstrated the success of the RLS adaptive demodulation scheme, as well as that of the change detection algorithm. Synchronous averaging was performed on the data measured from the test rig, followed by adaptive demodulation.

1.5.5 *Time-Frequency Methods*

The Wigner-Ville distribution is a well known time-frequency distribution, and has been applied to widely divergent fields and problems. It fits into Cohen's general class of time-frequency distributions (Cohen, 1989). Staszewski, Worden and Tomlinson (1997) applied the Wigner-Ville distribution to the gearbox diagnostics problem, in conjunction with pattern recognition techniques. Importantly the authors note that the Wigner-Ville distribution results in two-dimensional patterns exhibiting fault features that are difficult to interpret. Statistical and neural network based pattern recognition techniques are used by the authors to detect spur gear fault conditions.

Staszewski et al.(1997) show that gearbox fault detection using the Wigner-Ville distribution is achievable and feasible. Moreover, it is explicitly stated that local fault detection on spur gears is possible. It is remarked that the removal of background meshing vibration from the signal improves the visibility of impulsive features caused by certain types of faults. The weighted form of the Wigner-Ville distribution attenuates interference terms in the time-frequency domain, but also results in a reduction in the frequency resolution and a loss of sensitivity regarding fault detection.

Acoustic and vibration signal analysis by means of the Wigner-Ville distribution was compared by Baydar and Ball (2001). Three local fault conditions – broken tooth, cracked tooth and localised wear – on helical gears

were considered. Synchronously averaged data was analysed using the smoothed pseudo-Wigner-Ville distribution. Detection of faults rested on the observation of patterns indicative of impulsive transients in the time-frequency distribution, resulting from impacts due to the fault local conditions.

Faults were monitored in a progressive manner by Baydar and Ball (2001). Several progressive stages of each fault were considered. The time-frequency distributions of both the vibration and acoustic signals permit the successful identification of the various types of gear failures considered by the authors. The choice of the Wigner-Ville distribution is motivated by considering that the properties and theoretical background, as well as computational aspects of the numerical evaluation of the distribution are well established in literature.

Gearbox vibrations, including gear and bearing signals, were analyzed by Oehlmann, Brie, Tomczak and Richard (1997). The authors point out that shocks induced by faults in gears and bearings cause an increase of mechanical system energy, which in turn leads to rising frequency and amplitude of the vibration signal. They choose the optimal kernel method, belonging to Cohen's general class of time-frequency distributions, to generate time-frequency distributions of the measured vibration signals. Brie et al. sought a low-pass kernel function which covers maximum energy in the ambiguity plane. To this end the kernel volume was kept smaller than some lower bound, determined experimentally.

Two structures in the time frequency distributions were identified by Brie et al: firstly amplitude modulations of the gear mesh carrier signal and secondly time-frequency components with approximately linear frequency variations, i.e. chirp signals. It is noted by the authors that the sensor location influences the time-frequency representation. The structures identified remain observable, but the amplitude is modified.

Unsteady speed in a planetary gear system was considered by Meltzer and Ivanov (2003). The Choi-Williams distribution was preferred by these authors as a result of examining the kernels of the Wigner-Ville, spectrogram and Choi-Williams distributions in the ambiguity plane. The basis of their choice is formed by arguments relating to the resolution of the transforms in time and frequency, as well as the suppression of terms in certain regions of the ambiguity plane.

Experimental verification was carried out by Meltzer and Ivanov (2003) on a three stage epicyclic gearbox intended for use in a passenger vehicle. Angle-equidistant and time-equidistant sampling scenarios were investigated. For the time-equidistant sampling scenario, the kernel of the Choi-Williams distribution was modified to account for the variation in speed that occurred

during the tests. This modification to the kernel was successfully applied to the diagnosis of fault conditions in the gear drive by the authors.

Application of another energy distribution belonging to Cohen's (1989) general class, the spectrogram, was published by Wang and McFadden (1993) in a 2-article series. While the first article deals with the time-frequency method, the second one concerns mainly image identification techniques applied to the damage detection problem. McFadden and Wang used synchronously averaged data, with components at the meshing frequency removed to enhance the synchronously averaged signal. The authors successfully indicate a fault condition in the gearbox under consideration by indicating a spreading out of energy on the frequency axis at the order of a spall damaged tooth.

Wang and McFadden (1993) describe the Wigner-Ville distribution as inappropriate for the analysis of gear vibration signals. The spectrogram is preferred by these authors as a result of the inherent non-linearity of the Wigner-Ville distribution, taking into account the subtlety of gear fault signatures. Recommendations are further made by the authors regarding the choice of a suitable window function, and setting the parameters governing such a function.

1.5.6 *Instantaneous Energy Density*

The marginal conditions of time-frequency distributions state that ideally summing up the energy distribution for all frequencies at a particular time should give the instantaneous energy, and summing up over all times at a particular frequency should give the energy density spectrum (Cohen, 1989). Loutridis (Article in press) argues that faults are by their nature transient events, and cause a parcelling of the energy of the vibration signal. Significant change is hence to be expected in the energy density the moment damaged teeth are engaged.

Loutridis calculates the instantaneous energy density as the integral of the absolute value of the Wigner-Ville distribution in the frequency domain, at a particular time instant. This is equivalent to satisfying the time marginal for strictly positive distributions, where the absolute value has no effect. The Wigner-Ville distribution is not strictly positive, but a good approximation is still obtained according to Loutridis (Article in Press). Continuous wavelet transforms and the empirical mode decomposition technique are also considered by Loutridis, and similar energy densities are derived.

For the Wigner-Ville distribution, the wavelet transform based scalogram and the empirical mode decomposition technique, Loutridis demonstrates effectiveness of the instantaneous energy density technique. The author does however point out that the sensitivity of the energy feature based on the Wigner-Ville distribution is slightly better than for the continuous wavelet

transform and empirical mode decomposition technique. Further advantages of the Wigner-Ville distribution mentioned by Loutridis is its relative simplicity and fast computation time. Reliable predictions were obtained by the author for all three methods, for gear tooth cracks ranging from 15% up to 75% of the gear tooth root.

1.6 Scope of Work

Condition monitoring of epicyclic gearboxes through analysis of vibration data based in the time domain will form the centrepiece of this work. Time domain filtering techniques will be developed for the purpose of removing random noise from the periodic, or possibly pseudo periodic, vibration signal. In this sense, pseudo periodic is meant to imply a periodic signal of which the period is subject to seemingly random perturbations in the time domain, on a scale smaller than the total periodic signal length. The signals studied will not be identically stationary, nor cyclostationary.

It has been shown by Antoni, Bonnardot, Raad and El Badaoui (2004) that sampling of these same signals in the angular, or order domain does produce cyclostationary signals. Order tracking requires the use of a reference signal, and will be excluded from this work due to this fact.

Bonnardot, El Badaoui, Randall, Daniere and Guillet (Article in Press) presents a technique where only the vibration signature is used to perform order tracking. Their technique is limited by the speed fluctuation that can successfully be accommodated. The effect of the structural transfer function on the vibration signal is further implicitly assumed to be negligible, and indeed appears to be for the data considered by the authors. Further research and development work is required on the technique of Bonnardot et al. (Article in Press).

Adaptive signal processing techniques will be employed for the purpose of noise reduction in this work. The vibration signatures from the epicyclic gearbox considered are expected to be nonstationary in the time domain. Nonstationarity of the signals being processed makes the use of adaptive filtering techniques attractive, as noted by Widrow and Kamenetsky (2003).

Time domain based damage identification techniques that do not require stationarity of the signal, will be considered. The time domain has an important advantage in that rotational speed variations are preserved in time domain data. Synchronous averaging removes the effect of shaft speed variations from rotating machine vibration data.

Nonstationarity of the expected vibration data once more will influence the choice of damage identification techniques, as for the filtering techniques before. Dowling (1993) provides several arguments that may be used to

strengthen the choice of nonstationary analysis techniques for data based in the time domain, as discussed under section 1.2.

Time-frequency methods are an obvious choice for the purpose of signal analysis and defect identification or diagnosis. Periodicity of the signals processed by time-frequency methods is not required. Time frequency methods have been applied to vibration analysis by several authors, as discussed under sections 1.4 and 1.5.5. Time-frequency distributions for which the properties are well known and documented will be considered in this work. The instantaneous energy density criterion, proposed by Loutridis (Article in Press) will be considered in conjunction with the selected time-frequency distributions.

From considering the effects that gear defects may have on the phase or instantaneous frequency, and amplitude of the vibration signal generated, the use of amplitude and phase demodulation makes intuitive sense. McFadden presented two cases where damage to a gear tooth could successfully be indicated by demodulated data from the synchronous average of vibration data (Mcfadden, 1986 and McFadden, 1988). It is expected that the synchronous averaging process will enhance the diagnostic ability of demodulation techniques. Amplitude and phase demodulation will not be applied to the time domain data considered in this work.

Implications of using exclusively time domain techniques to perform gear damage identification have not been commented on to date. Synchronous averaging, which is widely used to reduce the noise in vibration signals, is in this case not applicable due to the lack of a rotational reference. The time domain filtering and signal analysis techniques discussed will be assessed in terms of their usefulness for the purpose of damage diagnosis. The effect of the adaptive filtering methods on the noise represented in especially the Wigner-Ville distribution will be considered.

2 Filtering of Gear Vibration Signals

Filters are defined, in the signal processing context, by Ifeachor and Jervis (2002) as systems that selectively change the wave shape, amplitude-frequency and/or phase-frequency characteristics of a signal in a desired manner. For the purpose of signature based diagnostics, waveform features are used to relate to some state of the system emitting the wave. Filters may be usefully employed to enhance or suppress certain waveform characteristics, as an aid to diagnostic techniques.

Reduction of noise in a measured signal is an eminent application area of filters. Specific applications in signal processing for mechanical diagnosis include enhancement of periodic or deterministic signal components (Braun, 1975), separation of periodic and random components (Randall, 2001), and selection of frequency bands of interest (Braun & Seth, 1979).

Discussions in this work will restrict themselves to digital filtering, or discrete time filtering techniques. Ordinary digital filtering, primarily by finite impulse response implementations, was employed for the purpose of frequency band selection in some cases. Adaptive filtering techniques were further employed for the purpose of random noise reduction.

Adaptive filtering of machine vibration signals was a primary consideration at the initiation of this work. Much of this current chapter is therefore devoted to adaptive filtering techniques. For the sake of completeness, certain pertinent digital filtering topics will be briefly discussed, as well as the synchronous averaging technique.

2.1 Digital Filtering Techniques

Finite Impulse Response (FIR) filters, as opposed to infinite impulse response (IIR) implementations, have an impulse response of finite duration. The finite impulse response filter's input and output signals are related by the convolution sum of equation 2.1:

$$y_F(n) = \sum_{k=0}^{N-1} h(k)x(n-k) \tag{2.1}$$

where: $y_F(n)$: discrete time filtered signal
$h(k)$: transfer function
$x(n)$: discrete time signal

Although FIR filters have no physical equivalent, they do posses a number of attractive properties. In this work the FIR structure was exclusively utilised. Ifeachor and Jervis (2002:321) present a list of attractive properties of FIR filters that will be briefly discussed in the following paragraphs.

Linear phase response is realizable with a suitable FIR structure. Four types of linear phase response FIR filters are classifiable, depending on whether the filter length N is even or odd, and whether the impulse response exhibits positive or negative symmetry.

Type 1 linear phase FIR filters have positive symmetry of the impulse response, and an odd number of coefficients. Type 2 linear phase FIR filters have positive symmetry and even number of coefficients, but its frequency response is zero at half the sampling frequency's value. Type 2 is thus not suited for high pass filtering applications.

Types 3 and 4 linear phase response FIR filters both exhibit negative impulse response symmetry, with odd and even numbers of coefficients, respectively. The frequency response of both types is zero at the frequency of zero, making them unsuitable as low pass filters. Additionally type 3 filters have zero frequency response at half the sampling frequency, making it also unsuitable as a high pass filter. Both types 3 and 4 introduce 90° phase shift, making them useful in the design of differentiators and Hilbert transformers.

Finite impulse response filters are realized non-recursively, by direct evaluation of equation 2.1. Stability of IIR filters can not always be guaranteed. FIR filters suffer less from the effects of using a limited number of bits used in the implementation, such as roundoff noise and coefficient quantization errors, than IIR filters. FIR filters do however require a larger number of coefficients for sharp cut-off characteristics than IIR filters.

McFadden's (1986 & 1988) technique for damage identification by phase demodulation uses the vibrations signal's phase to identify damaged gear teeth. Ordinary digital filtering by FIR implementation may cause an unacceptable distortion of the phase characteristics at the frequency of interest. Zero phase distortion filtering for FIR as well as IIR digital filters is achievable using the forward-backward filtering technique, discussed by Gustafsson (1996).

Gustafsson (1996) describes the procedure as applying a filter G(q) forward (obtaining $y_{Ff}(t)$ in equation 2.2) and then backward on the reversed filtered signal, and then reversing the output again:

$$y_{Ff}(t) = G(q)u(t)$$
$$y^{R}_{Ffb}(t) = G(q)y^{R}_{Ff}(t) \qquad (2.2)$$

where: G(q) : digital filter
u(t) : input sequence
q : shift operator - qu(t)=u(t+1)

The superscript R denotes reversed sequences while subscripts f for forward and b for backward are used. The total effect is a zero phase filter with transfer function $|G(e^{i\omega})|^2$; in effect the order of the filter is thus doubled.

Without employing the initial conditions as per Gustafsson's method, transients are expected at the start and end of the forward-backward filtered sequence. These portions of the waveform may however be discarded if ample data is available for analysis.

2.2 Synchronous Averaging

Distinction is made between time domain averaging and synchronous averaging in this work. Although related, time domain averaging is in the strict sense an ensemble averaging process that takes place in the time domain. Synchronous averaging on the other hand, in as far as its application to rotating machine signals go, is an ensemble average computed in the angular or rotation domain.

2.2.1 Time Domain Averaging

Time domain averaging of a function x(t), digitized at a sampling interval nT, is described by (Braun, 1975):

$$y_a(nT) = \frac{1}{N}\sum_{r=0}^{N-1} x(nT - rmT) \qquad (2.3)$$

where: x(nT) : digitized function x(t)
y_a(nT) : averaged x(nT)
N : number of averages computed
mT : averaged period

Time domain averaging is a method well suited to the extraction of periodic waveforms from a noisy signal. Noise components tend to cancel in the ensemble average computed, leaving an improved estimate of the periodic signal (McFadden, 1986). It is further remarked in both McFadden (1986) and Braun (1975) that increasing the number of averages N, narrows the teeth of the comb filter and reduces the amplitude of the side lobes between the teeth.

Braun (1975) discusses a comb filter model for the time domain averaging process. McFadden (1986) points out two problems with the comb filter model: a) the model assumes knowledge of the noisy signal over an infinite

time interval; b) though the time domain average approximates a desired periodic signal, it is not exactly periodic and can thus only be represented by a signal which is defined over an infinite time.

Assuming that the signal is known for all time t implies that the time domain average is defined for all time. Examining the signal over a finite time in effect applies a window to the signal, which has to be taken into consideration when examining the properties of the time domain average.

To explain the non-exact periodicity of the comb filter model, consider a train of N ideal impulses c(t), of amplitude 1/N and spaced at mT. The time domain average can now be computed as the convolution of the train of ideal impulses c(t) and the signal x(t). The convolution theorem is further handy to compute the Fourier transform Y(f) of the time domain average as a product (McFadden, 1986):

$$\begin{aligned} y(t) &= c(t) * x(t) \\ Y(f) &= C(f) \cdot X(f) \end{aligned} \tag{2.4}$$

C(f) is however continuous in f, and hence for general X(f) the Fourier transform of the time domain average Y(f) will be continuous in f. This implies that the time domain average can not be periodic in mT. Noise components which are not harmonically related to the repetition frequency 1/mT may thus be passed by the comb filter, albeit at reduced amplitude. The estimate of the time domain average will therefore not be exactly periodic, and can only be represented completely by a signal which extends over infinite time.

Applying a rectangular window to the time domain signal removes the need for knowledge of the signal for infinite time. The resulting windowed signal's time domain average is however still not exactly periodic. McFadden (1986) describes further a procedure for sampling the Fourier transform of the signal in the frequency domain. This sampling procedure may be conveniently realized by computation of the Fourier transform of the windowed time domain average. This Fourier transform is then multiplied by the Fourier transform of the sampling function, and the inverse Fourier transform is computed to obtain the time domain average back in the time domain.

2.2.2 *Synchronous Averaging*

Order domain analysis relates a rotating machine vibration signal to the rotational speed of a shaft. The sampling base is hence in the angular domain, as opposed to conventional time domain sampling. Order tracking requires sampling of the signal at constant angular increments, as opposed to the conventional time domain sampling method that employs constant time increments. Sampling, when performing order tracking, takes place at a rate

proportional to the shaft's angular velocity, and is hence ideally invariant to shaft speed fluctuations.

Digital resampling of a time domain signal into the angular domain by numerical techniques is known as computed order tracking. Fyfe and Munck (1997) discus several important factors surrounding the implementation of computed order tracking. Sketch outlines of the hardware and algorithms required for such implementations are also provided.

In addition to the hardware required for conventional temporal sampling, order tracking requires a phase reference signal connected to a rotational reference on the rotating machine. A key-phasor signal from some form of shaft encoder is generally used. This signal is used to extract signal amplitudes at constant angular increments, providing a signal sampled in the angular or order domain.

Fyfe and Munck (1997) point out two distinct estimation processes that occur during order tracking: the correct placement of angular sample points on the independent time axis, and the estimation of the resampled points on the dependant amplitude axis. Estimation of the correct placement of angular sample points on the time axis is highly dependant on the accuracy of the synchronous reference signal. Once the appropriate positions of the angular sampling points on the independent time axis have been computed, the appropriate amplitude of the resampled signal can be computed, generally using an interpolation method. The order of the interpolation employed also plays an important role with regard to the accuracy of the final resampled signal.

Fyfe and Munck (1997) conclude from their study that the single most important factor influencing the spectral accuracy is the precision with which the key-phasor arrival times can be determined. Use of higher order interpolation schemes is also noted to improve accuracy. It is noted by the authors that due to delays inherent in the electronic circuitry surrounding the key-phasor, the accuracy of the method decreases as the shaft speed increases. Bossley, McKendrick, Harris and Mercer (1999) note that for periods of fast acceleration and deceleration, the accuracy of order tracking is similarly reduced.

Synchronous averaging of epicyclic gearbox vibration data was addressed by McFadden (1991). Based on the distinction made in this work between time domain averaging and synchronous averaging, what McFadden refers to as time domain averaging is here referred to as synchronous averaging. Computing a synchronous average from an epicyclic gearbox's vibration signal is complicated by the motion of the planet gears, and the multiplicity of contact regions between the planet gears and the sun and annular gears. The motion of the planetary gears relative to the stationary measurement

point further implies that the signals generated by the planetary gears are modulated at the carrier rotation frequency; a phenomenon termed planet pass modulation by Forrester and Blunt (2003).

McFadden's technique for calculating the synchronous averages of the vibration signals of the different gears rest thereon that the planet gear closest to the transducer will make the most significant contribution to the signal measured by the transducer. McFadden considers a total vibration signal sensed by the transducer, but windowed by application of a rectangular window when the gear moves past the transducer. The signal recorded in such a manner is then considered to be representative mainly of the particular gear, and the specific teeth that were engaged at this particular time.

By taking into consideration the relative angular velocities of the gears, it is possible to determine which teeth were in mesh at specific times. If adequate measurements are made, a synchronous average may now be computed by suitably arranging the small windowed portions of the total signal recorded, and computing an ensemble average. This average will be considered a synchronous average, assuming that the signal is recorded using constant angular sampling.

2.3 Adaptive Filtering

An adaptive filter is essentially a digital filter with self adjusting characteristics. The Least Mean Squares (LMS) and Recursive Least Squares (RLS) algorithms are two of the most widely used algorithms in adaptive signal processing, according to Ifeachor and Jervis (2002:645). An adaptive filter has the property that its frequency response is automatically adjusted to improve its performance in accordance with some criterion, allowing the filter to adapt to changes in the input signal characteristics. The adaptive filter is thus capable of tracking the statistics of nonstationary signals, provided the changes in signal statistics occur slowly compared with the convergence time of the adaptive filter (Elliott, 2001). The convergence time of the adaptive filter thus has bearing on the characteristics of the signal being filtered. An algorithm that converges too fast may be as undesirable as an algorithm with excessively slow convergence properties.

With statistically stationary inputs, the quadratic performance surface of an adaptive filter algorithm is fixed, and the optimal Wiener solution is fixed (Widrow & Kamenetsky, 2003). With non-stationary inputs, this performance surface changes randomly, and the optimal Wiener solution is not fixed but is a randomly moving target.

A common property of the applications of adaptive signal processing is that some element of the problem is unknown and must be learned, or some component of a possibly unknown system is changing in an unknown manner and must be tracked. Hence the physical processes encountered may

be either time varying or unknown, or both. Stochastic methods, based upon derivations using the statistical properties of the data signals are commonly employed in adaptive algorithms. The primary statistical measure used is the ensemble average, or mean, of a squared prediction error function (Alexander, 1986).

An adaptive process may be regarded as a method for moving generally "downhill" on a performance surface, defined by an appropriate criterion. Widrow and Stearns (1985) describe an adaptive filter as a filter of which the structure is adjustable in such a way that its behaviour improves through contact with its signal environment.

2.3.1 *Adaptive Algorithms for Filter Applications*

Adaptive algorithms are applied to a very broad range of applications. Among this plethora is counted search algorithms, control algorithms, signal processing applications and neural networks. Numerous algorithms, and variants of these algorithms, have been developed by different researchers. Some algorithms are tailored to specific applications, while others have retained a more general scope of applicability.

The Least Mean Squares algorithm is widely employed for adaptive filtering, and is the basis of most adaptive filters used in practice (Lee & White, 1998; Ifeachor & Jervis, 2002; Elliott, 2001; Widrow & Kamenetsky, 2003).

2.3.2 *Adaptive Noise Cancellation*

From a digital signal processing perspective, Ifeachor and Jervis (2002) considers an adaptive filter to consist of two distinct parts: a digital filter with adjustable coefficients; and an adaptive algorithm which is used to adjust the coefficients of the filter. The basic component of most adaptive filtering systems is the adaptive linear combiner (Widrow & Walach, 1984; Widrow & Stearns, 1985), which forms an output signal from the weighted sum of a set of input signals:

$$\begin{aligned} y_k &= \mathbf{w}_k^T \mathbf{x}_k \\ &= \sum_{i=1}^{p} w_i x_{k-i+1} \end{aligned} \qquad (2.5)$$

where: y_k : filter output at sampling instant k
$\mathbf{w}_k$: filter weight vector at sampling instant k
$\mathbf{x}_k$: filter input vector at sampling instant k

Superscript T indicates the vector transpose, while subscript k indicates the sampling instant and p is the number of elements in vectors x or w. The first and second lines of equation 2.5 are equivalent: the first line makes use of the vector notation form, while the second uses the summation notation form. A

schematic representation of the adaptive linear combiner is shown below, in figure 2.1.

In the case of the adaptive filter, it is common that the input vector x is formed from the last p data samples at the k'th sampling instant, as opposed to p distinct data points occurring simultaneously.

The mathematical realisation as in equation 2.5 uses a transversal or finite impulse response structure. Although other forms are available, notably the infinite impulse response or lattice structures, the finite impulse response structure is most widely used for reasons of simplicity and numerical stability (Ifeachor & Jervis, 2002).

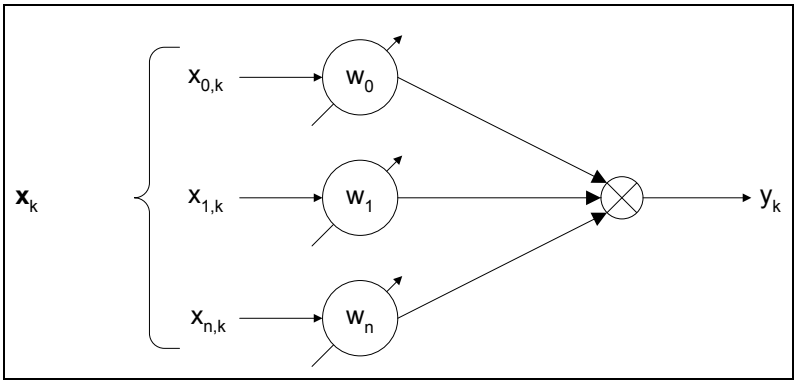

Figure 2.1: Adaptive Linear Combiner

Most noteworthy among the noise cancelling applications of adaptive filters are the adaptive noise canceller and the adaptive line enhancer. While the adaptive noise canceller uses a contaminated input, as well as a reference input correlated with the buried signal, the adaptive line enhancer uses a single input signal. A delayed version of the single input signal is used to decorrelate the noise component and remove it from the device's output. The adaptive line enhancer is the primary configuration used in this work. A schematic diagram is shown in figure 2.2.

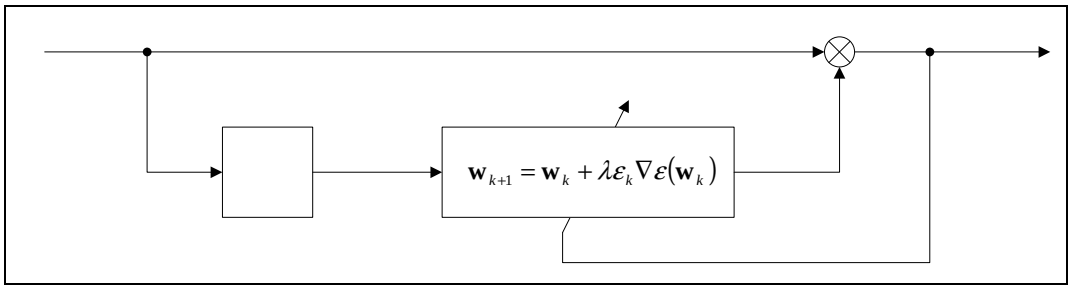

Figure 2.2: LMS Adaptive Line Enhancer

The filter uses a single input, denoted in figure 2.2 as y_k. This input simultaneously takes two paths: it goes directly to a summing node, and it branches of into a delay, denoted $z^{-\Delta}$. After having passed through the delay

it enters the digital filter operation; in this case an FIR configuration. The filter output is then passed to the summing node, where it is subtracted from the sample y_k to form the error term. The error term is fed back to the adaptive algorithm, which in turn adjusts the coefficients of the digital filter.

2.3.3 Adaptive Filters as an Optimization Problem

An adaptive filter may be viewed as an in-line optimization problem. The filter weights become the design variables, and the filter error becomes the objective function that is to be minimized. From this perspective, the general adaptive filtering problem may be formally stated as an optimization problem:

$$\begin{aligned} f(\mathbf{w}) &= y_k - \mathbf{w}_k^T \mathbf{x}_k \\ &= y_k - \sum_{i=1}^{n} w_i x_{k-i+1} \\ \min_{\mathbf{w}} & \; f(\mathbf{w}), \;\; \mathbf{w} = [w_1, w_2, \ldots, w_n]^T \in R^n \end{aligned} \tag{2.6}$$

During the execution of the adaptive filter algorithm, a key step is the updating of coefficients from one iteration to the next. Gradient based algorithms require the calculation or estimation of the performance surface gradient for this step. From the definition of the LMS criterion:

$$\begin{aligned} f(\mathbf{w}_k) &= E\{\varepsilon_k^2\} \\ \frac{\partial}{\partial \mathbf{w}_k} f(\mathbf{w}_k) &= \frac{\partial}{\partial \mathbf{w}_k}\left(E\{\varepsilon_k^2\}\right) \\ &= -2E\{\varepsilon_k \nabla \varepsilon(\mathbf{w}_k)\} \end{aligned} \tag{2.7}$$

The gradient expression $E\{\varepsilon_k \nabla \varepsilon(\mathbf{w}_k)\}$ is commonly estimated by an instantaneous value. Statistical expected value is denoted as $E\{\cdot\}$. Updating of coefficients for steepest descent based adaptive schemes then takes the following general form:

$$\mathbf{w}_k = \mathbf{w}_{k-1} + \lambda \varepsilon_{k-1} \nabla \varepsilon(\mathbf{w}_{k-1}) \tag{2.8}$$

where λ in this case represents a generalized convergence, or iterative step size, parameter. Equation 2.8 expresses the updating of the current weight vector, $\mathbf{w}_k$, in terms of the previous weight vector $\mathbf{w}_{k-1}$. In figure 2.2, the next weight vector, $\mathbf{w}_{k+1}$, is updated in terms of the present weight vector $\mathbf{w}_k$ – a form found to be more convenient for computational implementation. The two forms are considered equivalent, in spite of the difference in notation.

2.3.4 Formulating Adaptive Algorithms

Stochastic and deterministic methods have been used to formulate adaptive algorithms (Alexander, 1986). Statistical concepts such as Wiener (Ifeachor &

Jervis, 2002) and Kalman filter theory, as well as deterministic approaches such as the method of least squares have been used (Haykin, 1986). Different formulations hold advantages of particular insights that may be gained into the operation of the algorithm as a result of choosing that specific formulation.

Wiener formulations use a transversal finite impulse response filter, defined by a set of tap weights, as the structural basis for an adaptive filter implementation. For stationary inputs the mean-squared error is shown by Widrow and Stearns (1985) to be precisely a second order function of the tap weights in the transversal filter. The error surface is thus a multidimensional hyper-paraboloid. The optimum Wiener solution is defined by the tap weights corresponding to the minimum point on the error surface.

A matrix equation, known as the normal equation, defining the optimum Wiener solution is modified, classically by use of the method of steepest descent. This modification employs a gradient vector whose value depends on the correlation matrix of the tap inputs in the transversal filter and on the cross-correlation vector between the desired response and the tap inputs. Instantaneous values are used for the correlations so as to estimate the gradient vector.

Kalman filtering problems are stated in terms of a plant equation that describes the system dynamics in terms of a state vector, and a measurement equation that describes the measurement errors incurred. The Kalman approach in adaptive filtering as applied to vibration data has been investigated by among others Vold, Mains and Blough (1997) and Herlufsen, Gade, Konstantin-Hansen and Vold (1999) in a range of publications on the Vold-Kalman order tracking filter. Kalman formulations will not be employed in this work.

Formulations based on the classical method of least squares differs from the Wiener and Kalman approaches in that it uses deterministic measures from the start. A performance index consisting of a sum of weighted error squares is minimized. The error or residual is defined as the difference between some desired response and the output of the filter. A prominent algorithm that makes use of this formulation is the recursive least-squares algorithm.

2.3.5 *Adaptive Algorithms as Predictors*

There lies a philosophical advantage in considering an adaptive algorithm from the viewpoint of a linear predictor. Consider again equation 2.8 for updating of coefficients:

$$\mathbf{w}_k = \mathbf{w}_{k-1} + \lambda \varepsilon_{k-1} \nabla \varepsilon(\mathbf{w}_{k-1}) \tag{2.9}$$

It is clear from equation 2.9 that parameters from the previous step, k-1, are used to estimate, or predict, the values of the current step, k. The "past" is therefore used in predicting the "present", using a performance function to adjust the coefficients.

In the linear form, adaptive prediction may be formulated as follows:

$$y(t) = \sum_{i=0}^{L} w_i x(t - \Delta - i) \tag{2.10}$$

where Δ denotes a delay in number of sample points.

2.3.6 *Least Mean Squares Adaptive Filter*

Classically, the least mean squares adaptive algorithm has been developed from the basis of the steepest descent general optimization algorithm. The basic steepest descent method is however modified to use a fixed step size, as opposed to performing a line search at each iteration to find a local minimum along the search direction. The progression from the classical method of steepest descent to the LMS algorithm is shown here as a basis for the derivation of an adaptive algorithm that utilises the Spherical Quadratic Steepest Descent (SQSD) method of Snyman and Hay (2001).

2.3.6.1 Method of Steepest Descent

When using a conventional steepest descent implementation, a gradient tolerance ε_g - a small number close to zero – is defined and used to stop the algorithm when the gradient is sufficiently close to zero, and hence near enough to the optimum value sought. For this constant step size formulation, the gradient tolerance becomes redundant as it is desired that the algorithm should maintain a tracking capability.

Normally a "step size" limit ε_w would be defined to stop the algorithm once the steps between iterations becomes so small that adequate proximity to the sought optimum has been obtained. For the constant step size algorithm, using a step size denoted as λ, this limit becomes inappropriate. A starting point $\mathbf{w}_0$ for the parameter variable, denoted $\mathbf{w}$ is required, and let the iteration number be denoted as k.

Test for proximity to the sought optimum by comparing the computed gradient to the gradient tolerance ε_g:

$$\|\nabla f(\mathbf{w}_{k-1})\| < \varepsilon_g, \quad \mathbf{w}^* = \mathbf{w}_{k-1} \tag{2.11}$$

For an algorithm employing explicit line searches, a line search would be performed at this point to determine the optimal step size λ. This line search in the direction defined by the gradient expression of equation 2.11 may

involve function evaluations. For this formulation, using a constant step size, this step becomes redundant.

Parameter vector **w** is updated according to the steepest descent equation:

$$\mathbf{w}_k = \mathbf{w}_{k-1} - \lambda \nabla f(\mathbf{w}_{k-1}) \tag{2.12}$$

Although the last step in the conventional algorithm becomes redundant in the constant step size formulation, it is stated for the sake of completeness. Test for proximity to the sought optimum by comparing the new point on the performance surface, $\mathbf{x}_m$, to the previous point $\mathbf{x}_{m-1}$:

$$\left\|\mathbf{w}_k - \mathbf{w}_{k-1}\right\| < \varepsilon_w, \quad \mathbf{w}^* = \mathbf{w}_k \tag{2.13}$$

The exclusion of the step that terminates the optimization process by limiting the minimum step size results therein that the algorithm will continue to "oscillate" about the sought minimum. It is necessary to exclude this step if the algorithm is to maintain a tracking capability.

2.3.6.2 Steepest Descent to LMS

The least mean squares algorithm is based on the steepest descent algorithm. The most prominent difference between the two algorithms is the way in which the gradient of the performance surface is obtained. From Alexander (1986):

$$\begin{aligned} f(\mathbf{w}_k) &= E\{\varepsilon_k^2\} \\ \frac{\partial}{\partial \mathbf{w}_k} f(\mathbf{w}_k) &= \frac{\partial}{\partial \mathbf{w}_k}\left(E\{\varepsilon_k^2\}\right) \\ &= E\left\{\frac{\partial}{\partial \mathbf{w}_k}\varepsilon_k^2\right\} \\ &= 2E\left\{\varepsilon_k \frac{\partial}{\partial \mathbf{w}_k}\varepsilon_k\right\} \end{aligned} \tag{2.14}$$

From the formula for the prediction error ε_k, equation 2.6, it follows:

$$\frac{\partial}{\partial \mathbf{w}_k}\varepsilon_k = \frac{\partial}{\partial \mathbf{w}_k}\left[y_k - \mathbf{w}_k^T \mathbf{x}_k\right] = -\mathbf{x}_k \tag{2.15}$$

where y_k represents the measured data point at sampling instant k (figure 2.2 refers). From equation 2.15 follows:

$$\nabla f(\mathbf{w}_k) = -2E\{\varepsilon_k \mathbf{x}_k\} \tag{2.16}$$

From equation 2.16, a possible instantaneous estimate of the error surface gradient is evident. Substituting into the steepest descent equation 2.12:

$$\mathbf{w}_{k+1} = \mathbf{w}_k + 2\lambda\varepsilon_k\mathbf{x}_k \tag{2.17}$$

Equation 2.17 is the mathematical kernel of the least mean squares algorithm. It uses an instantaneous estimate of the gradient function in the adaptation of the weight vector. The algorithm has become widely used in many adaptive applications as a result of its simplicity and stability, in spite of weaknesses that it may have.

2.3.7 *Setting LMS Parameters*

Consider the LMS equation governing the updating of the filter weights, stated from a linear prediction viewpoint:

$$\mathbf{w}_k = \mathbf{w}_{k-1} + \lambda\varepsilon_{k-1}\mathbf{x}_{k-\Delta} \tag{2.18}$$

It is clear from equation 2.18 that given a weight vector $\mathbf{w}_{k-1}$ the convergence of the algorithm will be affected by 3 parameters:

1. Time delay Δ
2. Filter length L
3. Gradient search forgetting factor λ

Gradient search forgetting factor λ is also known as the prediction depth. Guidelines for setting the gradient search forgetting factor, or prediction depth λ, as extracted from available literature will be discussed here. Section 2.4 provides guidelines for setting the filter length and time delay, as these parameters are common to both adaptive implementations discussed in this work.

2.3.7.1 Forgetting Factor λ

Geometrical properties of the error performance surface of the LMS algorithm dictate that the algorithm will be convergent only if:

$$\frac{1}{\lambda_{\max}} \rangle \lambda \rangle 0 \tag{2.19}$$

where λ_{max} is the largest eigenvalue of the input correlation matrix **R** (Widrow & Stearns, 1985). Within these bounds, the forgetting factor λ determines the speed of adaptation as well as the noise in the weight vector solution. A further more restrictive bound is imposed on λ_{max}: λ_{max} cannot be greater than the trace of **R**, denoted tr[**R**]. In general then:

$$0 \langle \lambda \langle \frac{1}{tr[\mathbf{R}]} \tag{2.20}$$

Both prediction error and the noise estimate in the coefficients of the LMS algorithm remain proportional to λ as the adaptation time goes to infinity.

Use of the autocorrelation matrix to determine bounds for λ, as proposed by Antoni and Randall (2001), provides a method of using an autocorrelation matrix of decreased size, compared to the full autocorrelation matrix. The method specifies the computation of an autocorrelation matrix R of size dim(R), and computing the largest eigenvalue λ of this autocorrelation matrix. Plotting the λ / dim(R) curve then provides a guide as to the point where enlarging the autocorrelation matrix size does not result in a significantly larger eigenvalue. It is noted by the authors that the maximum eigenvalue may be estimated from a moderately sized autocorrelation matrix, smaller than the length L of the adaptive filter.

2.3.8 *Spherical Quadratic Steepest Descent*

The spherical quadratic steepest descent method was developed by Snyman and Hay (2001) at the University of Pretoria. This method effectively applies the steepest descent method to successive simple spherical quadratic approximations of the objective function in such a way that no explicit line searches are performed in solving the minimization problem.

This development of the spherical quadratic steepest descent adaptive algorithm follows the algorithmic development presented by Snyman and Hay (2001). Convergence tolerances for the gradient and step size, ε_g and ε_x respectively, as well as a step limit d>0 are usually chosen. For reasons similar to those used in the steepest descent formulation above, the gradient and step size tolerances are not used. The step limit d will however be defined.

Selection of a starting point $\mathbf{w}_0$ also determines the initial curvature c_0. In the calculation of the gradient $\nabla f(\mathbf{w})$ the same instantaneous approximation, equation 2.16, as was used for the LMS algorithm will be used:

$$\begin{aligned} c_0 &= \|\nabla f(\mathbf{w}_0)\|/d \\ &= \|2e_0\mathbf{x}_0\|/d \end{aligned} \tag{2.21}$$

Where the error signal e_0 is being calculated in analogous fashion to the LMS algorithm:

$$e_0 = y_0 - \mathbf{w}_0\mathbf{x}_0^T \tag{2.22}$$

It is to be noted that e_k denotes the exact error at iteration k, while ε_k denotes the expected value of the approximate error, as is later defined. Filter weights are updated according to:

$$\begin{aligned}\mathbf{w}_k &= \mathbf{w}_{k-1} - \frac{\nabla f(\mathbf{w}_{k-1})}{c_{k-1}} \\ &= \mathbf{w}_{k-1} + \frac{2e_{k-1}\mathbf{x}_{k-1}}{c_{k-1}}\end{aligned} \tag{2.23}$$

Step size is limited at this point to be smaller than the step limit d:

$$\begin{aligned}if\ \left\|\mathbf{w}_k - \mathbf{w}_{k-1}\right\| \rangle d:\ \mathbf{w}_k &= \mathbf{w}_{k-1} - d\frac{\nabla f(\mathbf{w}_{k-1})}{\left\|\nabla f(\mathbf{w}_{k-1})\right\|} \\ &= \mathbf{w}_{k-1} + d\frac{2e_{k-1}\mathbf{x}_{k-1}}{\left\|-2e_{k-1}\mathbf{x}_{k-1}\right\|}\end{aligned} \tag{2.24}$$

During successive steps, curvature c_k is chosen such that the approximation to f(**x**) interpolates f(**x**) at both $\mathbf{x}_k$ and $\mathbf{x}_{k-1}$.

$$\begin{aligned}c_k &= \frac{2\left[f(\mathbf{w}_{k-1}) - f(\mathbf{w}_k) - \nabla^T f(\mathbf{w}_k)(\mathbf{w}_{k-1} - \mathbf{w}_k)\right]}{\left\|\mathbf{w}_{k-1} - \mathbf{w}_k\right\|^2} \\ &= \frac{2\left[e_{k-1} - e_k + 2e_k\mathbf{x}_k^T(\mathbf{w}_{k-1} - \mathbf{w}_k)\right]}{\left\|\mathbf{w}_{k-1} - \mathbf{w}_k\right\|^2}\end{aligned} \tag{2.25}$$

It is ensured that the approximate objective function remains positive-definite by preventing curvature c_k from becoming smaller than zero:

$$c_k = 10^{-60} \forall c_k \langle 0 \tag{2.26}$$

The error signal e_k is calculated from the same equation used by the LMS algorithm:

$$e_k = y_k - \mathbf{w}_k\mathbf{x}_k^T \tag{2.27}$$

Importantly, it is remarked by Snyman and Hay (2001) that for quadratic functions, no step limit d is required. Numerous proofs by different authors have been presented that the error surface of an adaptive filter is a quadratic function of the weight vector. For the sake of reference, Widrow and Stearns (1985) is sited in this regard and discussed in the following section. Unconditional convergence, stability and economy are importantly pointed out by Snyman and Hay (2001) as being advantages of the SQSD method.

2.3.9 *Convergence of the SQSD based Adaptive Algorithm*

Proof of the quadratic nature of the error surface is provided by Widrow and Stearns (1985) as follows: Consider once more equation 2.27, the error signal:

$$e_k = y_k - \mathbf{w}_k^T\mathbf{x}_k \tag{2.28}$$

Obtain the instantaneous squared error:

$$e_k^2 = y_k^2 + \mathbf{w}_k^T \mathbf{x}_k \mathbf{x}_k^T \mathbf{w}_k - 2 y_k \mathbf{x}_k^T \mathbf{w}_k \tag{2.29}$$

Assuming e_k, y_k and $\mathbf{x}_k$ to be statistically stationary, and taking the statistical expected value over k:

$$E\{e_k^2\} = E\{y_k^2\} + \mathbf{w}_k^T E\{\mathbf{x}_k \mathbf{x}_k^T\} \mathbf{w}_k - 2E\{y_k \mathbf{x}_k^T\} \mathbf{w}_k \tag{2.30}$$

where E{·} denotes the expected value. An input correlation matrix **R** and a cross correlation vector between the desired response and the input components **p** is defined respectively as:

$$\begin{aligned} \mathbf{R} &= E\{\mathbf{x}_k \mathbf{x}_k^T\} \\ \mathbf{p} &= E\{y_k \mathbf{x}_k\} \end{aligned} \tag{2.31}$$

The elements of both **R** and **p** are constant second order statistics when $\mathbf{x}_k$ and y_k are stationary. Designating the expected value of the mean-square error by ε:

$$\varepsilon = E\{y_k^2\} + \mathbf{w}_k^T \mathbf{R} \mathbf{w}_k - 2\mathbf{p}^T \mathbf{w} \tag{2.32}$$

Clearly ε is a quadratic function of the components of **w**, when the input components and the desired response are stationary stochastic variables. Below in figure 2.3 is shown a sample mean square error surface for a two-weight system.

In their publication, Snyman and Hay (2001) prove convergence for the SQSD method in the general quadratic case. The following theorem is presented:

Theorem: The SQSD algorithm (without step size control) is convergent when applied to the general quadratic function of the form $f(\mathbf{x}) = (1/2)\mathbf{x}^T\mathbf{A}\mathbf{x} + \mathbf{b}^T\mathbf{x}$, where **A** is an n-by-n positive definite matrix and $\mathbf{b} \in E^n$.

Having presented the quadratic form of the objective function, or error signal, of the general adaptive filtering problem, and combining this with the theorem above, one may induce that the SQSD adaptive algorithm will be convergent in the general case. Herein lies a distinct advantage of the spherical quadratic steepest descent implementation: it is expected to be less sensitive to the step size parameter than the more conventional LMS algorithm.

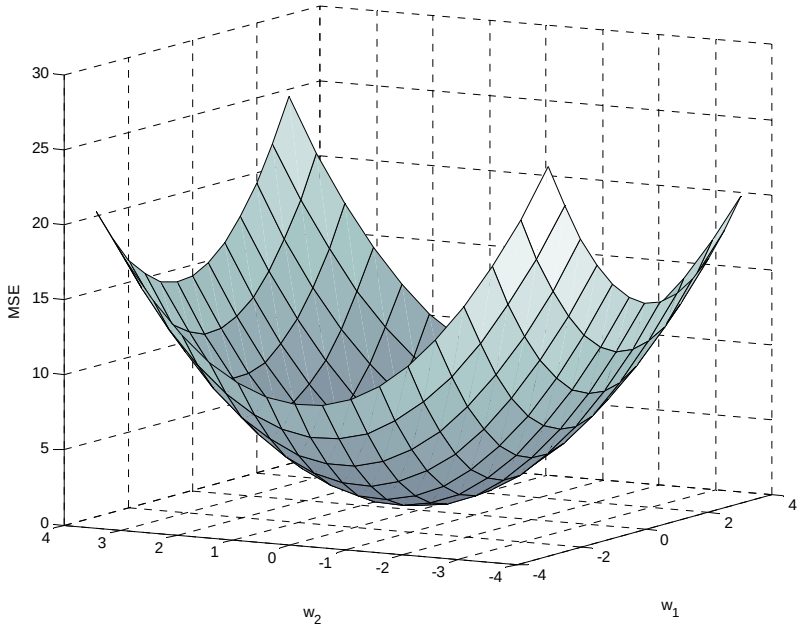

Figure 2.3: Sample MSE surface for two-weight system

2.3.10 Setting SQSD Parameters

Spherical quadratic steepest descent updates the filter weights from iteration to iteration according to:

$$\mathbf{w}_k = \mathbf{w}_{k-1} - \frac{\nabla f(\mathbf{w}_{k-1})}{c_{k-1}} \tag{2.33}$$

The curvature c_{k-1} is computed from the weight vectors **w** and error signal e of the current and previous iterations, as well as the gradient estimate $\nabla f(\mathbf{w})$ of the current iteration, according to equation 2.25. Its value is prevented from turning negative.

Step size is however limited by the parameter d:

$$if\ \left\|\mathbf{w}_k - \mathbf{w}_{k-1}\right\| \rangle d:\ \mathbf{w}_k = \mathbf{w}_{k-1} - d\frac{\nabla f(\mathbf{w}_{k-1})}{\left\|\nabla f(\mathbf{w}_{k-1})\right\|} \tag{2.34}$$

From the proof of convergence presented by Snyman and Hay (2001), convergence should be guaranteed without the use of the step size parameter d. Considering the continuous adaptation of the weights, it is evident that d will have considerable influence on the speed of adaptation and the amount of noise present in the weight vector solution. An interesting paradox is thus presented to the user of the algorithm: in spite of guaranteed convergence of the algorithm, the solution quality will be adversely affected by too large a

step size. Conversely, a high quality solution may be possible by setting d to a small value, but at the cost of slow convergence.

Upon considering the possibility of using the exponentially varying step size as suggested by Antoni and Randall (2001), a most promising possibility is realised: Start off with a large step size for speedy convergence while using a small step size to obtain a high quality solution later on. The fact that the SQSD method will converge with possibly much larger initial step size than LMS may in this way be utilised to obtain full advantage of the exponential decrease of the step size as suggested by Antoni and Randall (2001).

Computation of an autocorrelation matrix is a necessary step with the normal LMS method, in order to establish bounds for the forgetting factor λ. With the spherical quadratic steepest descent approach, this step may be discarded as convergence is almost guaranteed. It is expected that the SQSD method would be convergent with a step size d much larger than that of the LMS forgetting factor λ – possibly orders of magnitude larger.

2.4 Setting Adaptive Filter Parameters

For both implementations discussed, the filter length, or number of coefficients, and the time delay will influence the convergence behaviour and quality of the filtered signal. A brief discussion of guidelines for choosing these parameters, obtained from literature, follows.

2.4.1 *Filter Length L*

Choosing the filter length, L, equal to the number of coefficients used in the FIR realisation employed in the adaptive algorithm, necessitates a trade-off between the resolution in the frequency domain, and the amount of noise present in the filter coefficients.

A good approximation to the frequency response of a steady-state adaptive line enhancer operating on N sinusoids in white noise is proved by Zeidler, Satorius, Chabries and Wexler (1978) to be:

$$H^*(f) \cong \sum_{n=1}^{N} \frac{e^{-2\pi j(f_n\Delta+f)}}{L+2\sigma_0^2/\sigma_n^2} \frac{1-e^{-2\pi j(f_n+f)L}}{1-e^{-2\pi j(f_n+f)}} + \sum_{n=1}^{N} \frac{e^{-2\pi j(f_n\Delta-f)}}{L+2\sigma_0^2/\sigma_n^2} \frac{1-e^{-2\pi j(f_n-f)L}}{1-e^{-2\pi j(f_n-f)}} \qquad (2.35)$$

where: Δ : delay
L : filter length
f_n : frequency of n'th sinusoid

Equation 2.35 is valid only for long L, where the linear equations resulting from the Wiener-Hopf matrix equation tend to uncouple.

Widrow and Stearns (1985) have shown that noise in the weight vector increases proportionally to the length of the weight vector. By virtue of

assumptions made, Alexander (1986) arrives at simplified expression for the total noise in the weight vector. A similar conclusion is thus reached, albeit by a different route and under the restrictions of various assumptions.

By starting from the frequency response equation 2.35, as provided by Zeidler et al. (1978), whom also noted the increase in weight vector noise with increasing L, Antoni and Randall (2001) proposed that for two sinusoids separated by ΔB [Hz] and sampled at f_s [Hz], the filter length L should be:

$$L = \frac{f_s}{\Delta B} \tag{2.36}$$

As mentioned by the authors, the formula above depends on L to be quite large, in the order of a few hundreds, and at least $L \geq 2N$.

2.4.2 Time Delay Δ

Time delay used in the adaptive line enhancer is intended to cause decorrelation between the noise components, while causing a simple phase difference between the sinusoidal components. By forming a transfer function equivalent to that of narrow-band filters centred at the frequencies of the sinusoidal components, the noise component should accordingly be rejected, while the phase difference of the sinusoidal components is readjusted to cancel at the summing junction. The minimum error signal should thus be composed of only the noise component of the input data.

Prediction depth, or time delay Δ, should be chosen long enough so as to exceed the correlation length of the noise in the input signal, but not so long that it exceeds the correlation length of the periodic components. For pseudo-periodic signals, having a small distribution in periodicity, possibly encountered in vibration signals, this may place a limit on the maximum usable delay (Antoni & Randall, 2004). When off-line processing is carried out, available data is of finite length and excessive delay may limit the amount of data that may be processed.

2.4.3 Exponentially Decaying Step Size

Exponentially decaying the prediction depth λ and the step size d of the LMS and SQSD algorithms will be jointly discussed here. Similar cautionary remarks are applicable to both cases.

Statistical efficiency of a learning algorithm is defined by Widrow and Kamenetsky (2003) as the ratio of the quality of the converged solution to the amount of data used in training the weights. An efficient algorithm will minimize the usage of data while maximizing the quality of the solution. It is remarked by Widrow and Kamenetsky that minimizing data usage and maximizing the quality of the solution are generally antagonistic.

Fast convergence is desirable, and dictates a larger value for the step size or forgetting factor, within the limits as appropriate for the algorithm. High solution quality is equally desirable, but requires that the step size or forgetting factor be smaller. A good compromise is therefore to allow a decrease in the step size or forgetting factor. In this way faster convergence behaviour could be maintained in the transient adaptation phase, while a higher quality solution may be obtained in the steady state phase than may be possible with a single constant step size or forgetting factor.

Antoni and Randall (2001) suggested exponentially decreasing the forgetting factor λ of the LMS algorithm. Prediction error of the adaptive algorithm remains proportional to the forgetting factor λ as adaptation time goes to infinity. The amount of noise present in the weight vector solution is also proportional to λ (Widrow & Stearns, 1985). Similar arguments hold for the step size d of the SQSD algorithm.

Exponential decay fits the purpose of a fast initial decay in the coefficient, with asymptotic behaviour in the steady state phase. Antoni and Randall (2001) suggested a decay curve with signal dependant parameters A and α for the LMS algorithm:

$$\lambda(t) = Ae^{-\alpha t} \tag{2.37}$$

Choosing α is left to the good judgement of the user. This parameter determines the rate of decay, and has a pronounced effect on the shape of the decay curve.

Widrow and Stearns (1985) provide an upper bound for A by specifying the following necessary conditions for convergence of the LMS algorithm:

$$\begin{aligned} &\frac{1}{\lambda_{\max}} \rangle \lambda \rangle 0 \\ &0 \langle \lambda \langle \frac{1}{tr[\mathbf{R}]} \end{aligned} \tag{2.38}$$

Hence A may at best be as large as the reciprocal of the largest eigenvalue of the autocorrelation matrix **R**. More restrictively A may not exceed the reciprocal of the trace of the autocorrelation matrix.

3 Damage Detection Techniques

Vibration-based damage detection techniques have the goal of enhancing changes in a vibration signal caused by damage to gears while remaining invariant in the presence of changes caused by normal variations in the operating condition of the gears. Ultimately the goal of damage detection systems is toward the implementation of condition based maintenance strategies. Condition based maintenance requires that component replacement should only occur when there is objective evidence of an impending failure or fault condition, and as such is classified as a preventive maintenance strategy.

Dynamic machinery systems may constantly be exposed to dynamic loads; sustained vibratory and impulsive loads. Scheduled maintenance requires maintenance inspections, overhauls and part replacement to be frequently performed – an expensive and time consuming task. Performing maintenance on-condition reduces the frequency of maintenance inspections, and keeps healthy components in service until signs of failure or unacceptable deterioration in condition are detected.

Initial research in the area of transmission damage detection focussed on vibration signal analysis using various signal processing tools available. Statistical characteristics of vibration signals in the time domain were primarily used initially. The field has expanded to incorporate spectral analysis, time-frequency methods and wavelet analysis, and is continually expanding at present. A recent survey by Samuel and Pines (Article in press) gives an overview of techniques applicable to helicopter transmission diagnostics. Helicopter transmissions are often of the epicyclic kind, and are thus similar to the epicyclic transmissions studied in this work.

3.1 Gear Vibration Models

McFadden (1986) proposed a demodulation technique to obtain amplitude and phase modulation functions from a vibration signal. He proposed an analytical expression for the total vibration signal of the following form, assuming the shaft frequency f_r to be constant:

$$x(t) = \sum_{m=0}^{M} X_m \left(1 + a_m(t)\right) \cos\left(2\pi m T_g f_r t + \phi_m + b_m(t)\right) \tag{3.1}$$

The amplitude and phase modulation functions have the following analytical form:

$$a_m(t) = \sum_{l=0}^{L} A_{m,l} \cos\left(2\pi l f_r t + \alpha_{m,l}\right)$$
$$b_m(t) = \sum_{l=0}^{L} B_{m,l} \cos\left(2\pi l f_r t + \beta_{m,l}\right) \quad (3.2)$$

where:
- x(t) : continuous time domain amplitude and phase modulated gear meshing vibration
- t : continuous time variable
- m : index of harmonic number
- M : number of significant harmonics in x(t)
- X_m : amplitude of m-th harmonic
- a_m : amplitude modulation function of m-th harmonic
- b_m : phase modulation function of m-th harmonic
- $\alpha_{m,l}$: initial phase angle of amplitude modulation function
- $\beta_{m,l}$: initial phase angle of phase modulation function
- f_r : shaft rotation frequency
- T_g : number of gear teeth
- φ_m : original or initial phase angle of m-th harmonic
- l : index of harmonic number in amplitude or phase modulation functions
- L : number of significant harmonics in amplitude or phase modulation functions

In the general case, the shaft frequency f_r and modulation functions a_m and b_m are all functions of time. Equation 3.1 may be re-stated in the discrete domain, incorporating temporal variation of the shaft frequency (Bonnardot, El Badaoui, Randall, Daniere & Guillet, Article in Press):

$$x(n) = \sum_{m=0}^{M} X_m (1 + a_m(n)) \cos\left(2\pi m T_g f_r(n) n + \phi_m\right) \quad (3.3)$$

Consider also equations 3.2 in the discrete domain:

$$a_m(n) = \sum_{l=0}^{L} A_{m,l} \cos\left(2\pi l f_r(n) n + \alpha_{m,l}\right) \quad (3.4)$$

where:
- x(n) : discrete time domain amplitude and phase modulated gear meshing vibration
- $f_r(n)$: shaft rotation frequency as function of discrete time variable
- n : discrete time variable

Since the phase modulation function, b_m from equations 3.1 and 3.2, varies with time it is interpreted as a speed, or frequency fluctuation, and may be included in $f_r(n)$. Other variables remain as for equations 3.1 and 3.2.

Meshing error will also produce phase modulation of the gear mesh carrier signal, due to precession of the contact point about the perfect theoretical position. The frequency modulation produced by such errors will however be largely deterministic in the rotation domain, as the same meshing errors will be reproduced for each revolution of each gear. Meshing error is then also contained in the discrete time shaft rotation frequency $f_r(n)$.

Two primary contributors to the phase or frequency modulation of a gear mesh carrier signal are therefore identified: speed fluctuation and meshing error. The meshing error component will occur synchronous with the damaged gear's rotation frequency. Although the speed variation component of the modulation may also be synchronous with the rotation of some rotating component, possibly the damaged component, it may also be asynchronous to the rotation or even completely random in nature.

Brie, Tomczak, Oehlmann and Richard (1997) proposes the following signal model for amplitude and phase modulated signals, after modification for consistency of notation:

$$x_k(t) = \sum_{m=1}^{M} a_{k,m}(t)\cos\left(2\pi m T_g f_r t + \phi_{k,m}(t)\right) + e_{k,m}(t) \qquad (3.5)$$

where: $x_k(t)$: time domain amplitude and phase modulated gear meshing vibration at iteration k
$a_{k,m}(t)$: amplitude modulation law at iteration k
$\varphi_{k,m}(t)$: phase modulation law at iteration k
$e_{k,m}(t)$: additive noise at iteration k
k : iteration number

Variables not listed above remain as for equations 3.1 and 3.2. As the model employed by Brie, Tomczak, Oehlmann and Richard (1997) is used in an adaptive scheme, the iteration number k is introduced in equation 3.5.

Common to all three of the models presented is a periodic sinusoid, an amplitude modulation law and a phase or frequency modulation law. The phase or frequency modulation is included in the argument of the sinusoid, while the amplitude modulation requires a multiplication in the time domain of the sinusoid by the modulation law. Relating the different phase and frequency modulation laws to one another is a matter of algebraic manipulation of the argument of the sinusoid. Similarly, the amplitude modulations may be related by algebraic manipulation.

3.2 Time-Frequency Methods

Transmission vibration signatures in general consist of three significant components: a periodic component due to varying tooth load, a broad-band impulsive component due to local impact, and random noise. For

undamaged transmissions, the periodic components generally dominate. Although not generally strictly sinusoidal, the periodic portion of the vibration signal may be approximated to a good degree of accuracy by a sinusoid, is in equation 3.1.

With the progression of damage, sinusoidal components exhibit modulation phenomena and possibly changes in amplitude. Additionally both broad band impulsive components and random noise become more prevalent. Trends exhibited by the sinusoidal components are more visible in the frequency domain, while the trends exhibited by broad band impulsive components are more visible in the time domain (Samuel & Pines, 2004).

In the time-frequency domain, all components of non-stationary signals in the frequency range of interest, their sequences, causality and changes with time can be examined. Describing the energy density of a signal simultaneously in time and frequency is the basic objective of time-frequency analysis. Time-frequency analysis provides for better understanding of the transient signal components associated with damage (Dowling, 1993).

Fundamentally a joint function of time and frequency, P(t,ω), is sought that represents the energy or intensity per unit time per unit frequency of a signal, s(t) (Cohen, 1995). Ideally summing up the energy distribution for all frequencies at a particular time would give the instantaneous energy, and summing up over all times at a particular frequency would give the energy density spectrum. Marginals are derived from the joint distribution by integrating out the other variables. The instantaneous energy $|s(t)|^2$ and energy density spectrum $|S(\omega)|^2$ states the marginals of P(t,ω):

$$\begin{aligned} \int P(t,\omega)d\omega &= |s(t)|^2 \\ \int P(t,\omega)dt &= |S(\omega)|^2 \end{aligned} \tag{3.6}$$

Provided that the distribution satisfies the marginals of equation 3.6, the total energy in terms of the distribution will be equal to the total energy of the signal:

$$E = \int P(t,\omega)d\omega\, dt \tag{3.7}$$

Cohen (1989) proposes a general form of time-frequency distributions:

$$P(t,\omega) = \frac{1}{4\pi^2}\iiint s^*\left(u-\frac{1}{2}\tau\right)s\left(u+\frac{1}{2}\tau\right)\phi(\theta,\tau)e^{-j\theta t - j\tau\omega + j\theta u}du\, d\tau\, d\theta \tag{3.8}$$

where φ(θ,τ) is a two dimensional function called the kernel. Variables τ and θ denote the time and frequency shifts, respectively, used in the calculation

of the distribution. Cohen (1995) further states that all time-frequency distributions may be obtained from this general class of distribution. The kernel determines the distribution and its properties. In terms of the spectrum the general class may be stated as:

$$P(t,\omega)=\frac{1}{4\pi^2}\iiint S^*\left(u+\frac{1}{2}\theta\right)S\left(u-\frac{1}{2}\theta\right)\phi(\theta,\tau)e^{-j\theta t-j\tau\omega+j\tau u}du\ d\tau\ d\theta \tag{3.9}$$

An alternate form of this formulation may be obtained by denoting the symmetrical ambiguity function A(θ,τ) as:

$$\begin{aligned}A(\theta,\tau)&=\int s^*\left(u-\frac{1}{2}\tau\right)s\left(u+\frac{1}{2}\tau\right)e^{j\theta u}du\\ P(t,\omega)&=\frac{1}{4\pi^2}\iint\phi(\theta,\tau)A(\theta,\tau)e^{-j\theta t-j\tau\omega}d\theta\ d\tau\end{aligned} \tag{3.10}$$

This formulation is known as the characteristic function formulation.

3.2.1 Spectrogram

The spectrogram has been widely used in different fields for the analysis of time-varying spectra. A portion of a signal, centred on a particular point in time, is used to calculate an energy spectrum attributed to the time point, and the computation is repeated for each point in time (Cohen, 1989). In terms of the general class of equation 3.8, the kernel φ(θ,τ) of the spectrogram is:

$$\phi(\theta,\tau)=\int h^*\left(u-\frac{1}{2}\tau\right)e^{-j\theta u}h\left(u+\frac{1}{2}\tau\right)du \tag{3.11}$$

where h(t) is a suitable window function. This kernel may be expressed in the frequency domain in terms of the Fourier transform of the window:

$$\phi(\theta,\tau)=\int H^*\left(\omega-\frac{1}{2}\theta\right)H\left(\omega+\frac{1}{2}\theta\right)e^{j\tau\omega}d\omega \tag{3.12}$$

Cohen (1989) states that individual intensities of time and frequency are to be satisfied for the distribution to be a joint distribution for the intensity. This implies that when the frequency variable is integrated out, we should obtain the instantaneous power $|s(t)|^2$, and when the time variable is integrated out we should obtain the energy density spectrum $|S(\omega)|^2$. This in turn translates to the following constraints on the kernel:

$$\begin{aligned}\phi(\theta,0)&=1\\ \phi(0,\tau)&=1\end{aligned} \tag{3.13}$$

Considering the preservation of energy, we examine the kernel at θ,τ = 0:

$$\phi(0,0) = \int |h(t)|^2 \, dt \tag{3.14}$$

φ(0,0) should be equal to 1 if total energy is to be preserved, which implies that the window should be normalised to 1. This condition is known as the normalisation condition. It is weaker than the preceding two conditions of equation 3.6 in the sense that it is possible to have a joint distribution whose total energy is the same as that of the signal, but whose marginals are not identically satisfied. The spectrogram is an example of such a distribution.

Consider a window function h(t) centred at t, and calculate the spectrum $S_t(\omega)$ of the signal s(τ) multiplied by the window function:

$$S_t(\omega) = \frac{1}{\sqrt{2\pi}} \int e^{-j\omega\tau} s(\tau) h(\tau - t) d\tau \tag{3.15}$$

In terms of the Fourier transforms of the signal S(ω) and window H(ω), the spectrogram may be expressed as:

$$S_t(\omega) = \frac{1}{\sqrt{2\pi}} e^{-j\omega t} \int e^{jut} S(u) H(\omega - u) du \tag{3.16}$$

An energy density spectrum, that may be considered as the energy density at points t and ω, or the spectrogram is:

$$\begin{aligned} P_S(t,\omega) &= |S_t(\omega)|^2 \\ &= \left| \frac{1}{\sqrt{2\pi}} \int e^{-j\omega\tau} s(\tau) h(\tau - t) d\tau \right|^2 \end{aligned} \tag{3.17}$$

Different parts of the signal s(τ) are weighted according to the window function, h(τ-t).

By examining the equations of the spectrogram in the time and frequency domains, respectively, the following conclusions may be reached: The more peaked a window is made in the time or frequency domain respectively, the better the resolution obtained in the time or frequency domain. Considering the uncertainty principle (Cohen, 1994), both h(t) and H(ω) cannot be made arbitrarily narrow, and a compromise is made between time and frequency resolution in the spectrogram for a particular window.

Wang and McFadden (1993) remark in their publication that too narrow a peak suppresses part of the signal due to damage, and broadens the

spectrogram in the frequency domain, with consequent loss of resolution. At the other extreme, too wide a peak reduces sensitivity to the fault. Plotting the kernel of the spectrogram in the ambiguity plane illustrates this: narrower windows on the time axis broadens the window on the frequency axis. Figures 3.1 and 3.2 illustrate this for a narrow and a wider window, respectively, with respect to the time axis. The Gaussian window suggested by Wang and McFadden (1993) was used in generating these figures:

$$h(t) = ce^{-\sigma^2 t^2} \tag{3.18}$$

The value of c from equation 3.18 for the figures 3.1 and 3.2 was set to 1, while σ was set to 90 for the narrow window and 70 for the wider window. A relatively small difference in σ thus delivers a marked change in resolution.

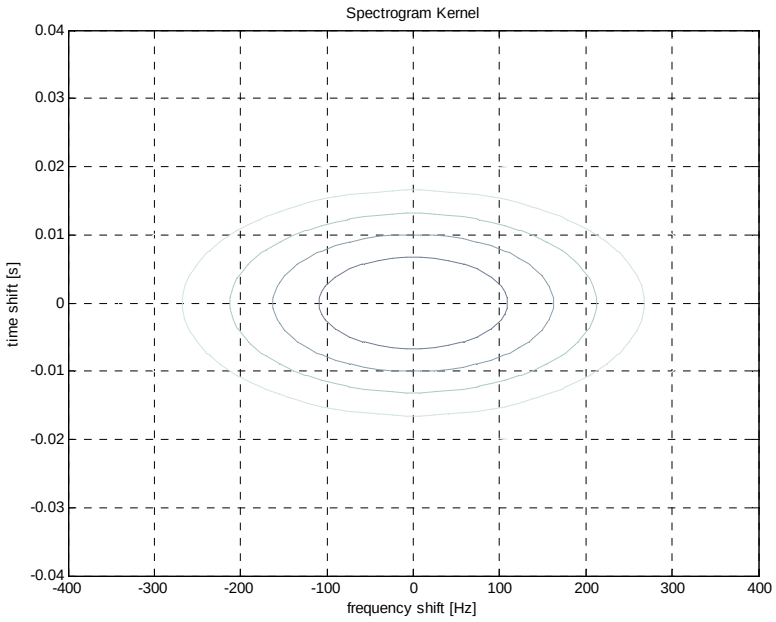

Figure 3.1: Narrow Gaussian window spectrogram kernel in ambiguity plane

3.2.2 Wigner-Ville Distribution

According to Cohen (1989) the Wigner distribution was the first to be proposed, and is the most widely studied and applied. The Wigner-Ville distribution, as it is also known when the computation is performed using the complex analytical signal, is obtained from Cohen's general class by setting the kernel equal to one: $\varphi(\theta,\tau) = 1$. Significant properties of the distribution is that it satisfies the marginals of equation 3.6, it is real and time and frequency shifts in the signal produce corresponding time and frequency shifts in the distribution.

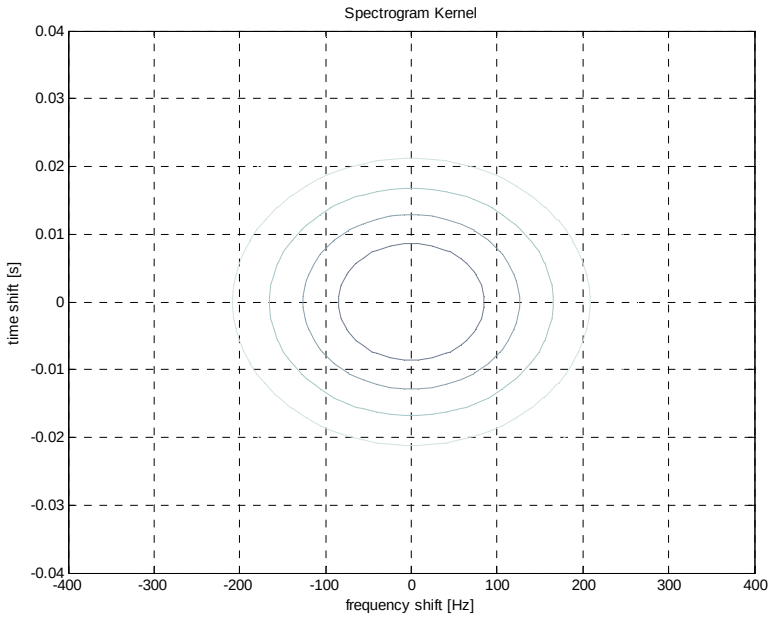

Figure 3.2: Wider Gaussian window spectrogram kernel in ambiguity plane

The Wigner distribution may be expressed in terms of the signal s(t) as (Cohen, 1989):

$$W(t,\omega)=\frac{1}{2\pi}\int s^{*}\left(t-\frac{\tau}{2}\right)e^{-j\tau\omega}s\left(t+\frac{\tau}{2}\right)d\tau \tag{3.19}$$

In terms of the spectrum, the Wigner distribution becomes:

$$W(t,\omega)=\frac{1}{2\pi}\int S^{*}\left(\omega+\frac{\theta}{2}\right)e^{-j\theta}S\left(\omega-\frac{\theta}{2}\right)d\theta \tag{3.20}$$

Narayanan and Prabhu (1989) provide an expression convenient for the implementation of the discrete Wigner-Ville distribution:

$$W(n,\omega)=2\sum_{p=-N}^{N}s(n+p)s^{*}(n-p)h(p)h^{*}(-p)e^{-j4\pi\omega p} \tag{3.21}$$

This discrete form of the Wigner-Ville distribution employs a window function, h(t). The windowed version of the Wigner-Ville distribution is also referred to as the pseudo-Wigner-Ville distribution.

Using the analytic form of the signal, conveniently computed by Hilbert transform, overcomes the well known issue surrounding the sampling frequency when using the Wigner distribution: a sampling frequency of four times the bandwidth is required if equation 3.21 is to be applied to real sampled data directly (Narayanan & Prabhu, 1989). The Wigner distribution

computed using the analytical form of the signal is known as the Wigner-Ville distribution.

Considering the range of the Wigner distribution in the time and frequency domains provides interesting insights into the occurrence of the so-called cross terms found in the distribution. A key point to remember in this regard is the fact that the Wigner distribution is computed as a sum of products of portions of a signal at past and future times, the time into the past being equal to the time into the future. For signals of infinite duration, the Wigner distribution will therefore be nonzero for all time. Finite support properties are satisfied by the Wigner distribution in time and frequency: $W(t,\omega) = 0$ for t outside (t_1, t_2) or for ω outside (ω_1, ω_2) if $s(t)$ is zero outside (t_1, t_2) or $S(\omega)$ is zero outside (ω_1, ω_2), respectively (Cohen, 1989).

Next consider the Wigner distribution for a portion of a signal in which there exists an interval over which the signal is zero. When computing the Wigner distribution on a focus point falling inside this zero interval, the distribution may not compute to zero even though the signal is equal to zero, due to the computation of the distribution as a sum of products of portions of the signal. Generally the Wigner distribution is not necessarily zero at times when the signal is zero and is not necessarily zero for frequencies that do not exist in the spectrum (Cohen, 1995). Manifestations of this phenomenon are often popularly referred to as cross terms or interference terms.

Discrete forms of the Wigner distribution often employ a window function, such as in equation 3.21. Window functions may be chosen such that local signal content surrounding the focus point is emphasized, and the locality of the distribution is hence improved. This is accomplished by specifying a window function that is peaked around the zero point of the lag variable, τ in equation 3.19. The Wigner distribution is highly nonlocal (Cohen, 1995). Application of the window function to obtain the pseudo-Wigner distribution makes the distribution less so. Cross terms are suppressed to a certain extent by the windowing of the Wigner distribution to obtain the pseudo-Wigner distribution.

Smoothing of the Wigner distribution in order to suppress some of the cross terms has been proposed and applied in various fields of time-frequency analysis. The smoothing process is a two dimensional convolution of the Wigner distribution with an appropriately chosen smoothing function $G(t, \omega)$. Smoothing functions may be chosen such that strictly positive Wigner distributions are obtained. Cohen (1989) warns that if the smoothing function $G(t, \omega)$ is taken independent of the signal, the only way to obtain a positive distribution is by sacrificing the time and frequency marginals of the distribution.

Garudadri, Beddoes, Benguerel and Gilbert (1987) provide a simple proof of the positivity of a smoothed Wigner distribution. Garudadri et al. further show that smoothing the Wigner distribution results in a Wigner distribution identical to a spectrogram computed using a Gaussian window. It is further shown that smoothing of the Wigner distribution causes a loss of the signal's phase information. It is argued that smoothing for positivity of the Wigner distribution eliminates all the phase information from the Wigner distribution. Partial smoothing may however be used to suppress negative regions and cross terms of the Wigner distribution, and retain the fine resolution in both time and frequency.

Both smoothing of the Wigner distribution and the application of a window function to obtain the pseudo Wigner-Ville distribution possibly causes the loss of time and/or frequency resolution. Though such deterioration in the quality of the distribution may be avoided by judicious choice of smoothing parameters, experimentation is likely to be required in order to obtain the best results. The application of the smoothing procedure further complicates the computations necessary to obtain the distribution, and makes the application of smoothing procedures less attractive from a computational viewpoint.

3.2.3 *Instantaneous Energy Density*

Consider the time marginal of a time-frequency distribution from equation 3.6:

$$\int P(t,\omega)d\omega = |s(t)|^2 \tag{3.22}$$

This integration over all frequencies present in the time-frequency distribution represents the instantaneous energy of the signal (Cohen, 1995). Loutridis (Article in Press) used this marginal condition to compute the instantaneous energy from the Wigner-Ville distribution, and applied his method to the gearbox diagnostic problem with success. He concludes that the energy feature based on Wigner-Ville distribution is a reliable means of detecting gearbox failure.

Generally the time marginal condition of equation 3.22 should hold for many of the members of Cohen's general class of time-frequency distributions. The possibility therefore exists of applying Loutridis' method to other members of the Cohen general class. For the Wigner-Ville distribution, Loutridis suggested computing the time marginal by taking the absolute value of the Wigner-Ville distribution:

$$E(t) = \int_{\omega_1}^{\omega_2} |W(t,\omega)|d\omega \tag{3.23}$$

In the discrete domain, Loutridis (Article in Press) suggests computing the instantaneous energy by summation over all frequency bins and dividing the result by the number of bins for normalisation.

For the spectrogram, which is a positive distribution, the instantaneous energy may be expressed in continuous form as:

$$E(t) = \int_{\omega_1}^{\omega_2} P_S(t,\omega) d\omega \tag{3.24}$$

A similar approach to that of the Wigner-Ville distribution may be followed in the discrete domain: summation over all frequency bins and dividing the result by the number of bins.

4 Experimental Work

Algorithm development involved testing by numerical simulation, as well as experimental testing. Numerical test cases were tailored to each algorithm's requirements. Three experimental test benches were used in the process of developing and testing the algorithms discussed: a simple cantilever beam experiment, an existing conventional gearbox test bench, and an epicyclic gearbox test bench that was developed for this work.

4.1 Experimental Test Benches

Three experimental test benches were used in development and verification of the algorithms discussed:

1. Cantilever Beam Simulator
2. Conventional Helical Gearbox Test Bench
3. Epicyclic Gearbox Test Bench

Each of the test benches were developed and used with particular purposes in mind.

4.2 Cantilever Beam Simulator

Structure borne noise and structural response to vibration signals may in certain cases drastically alter a vibration signal as it propagates through the structure, from its origin to the observation point. Observation point in this context is meant to imply the measurement position, i.e. the point where the transducer or sensor is applied to take its measurement from the structure.

Testing in an actual experimental environment is thus required to qualify the adaptive filter algorithms. With this goal in mind, and in absence of the larger gearbox test benches, it was deemed appropriate to carry out tests on a simple experimental bench that could be constructed quickly and inexpensively. A controlled environment that had some measure of structural response that would affect the vibration signals was required. Experience in the behaviour of the adaptive algorithms in a measured signal environment was required, before progressing to the more complex gear vibration signals.

Cantilever beam experiments that used electro-dynamic actuators to excite the beams were available in the laboratory. It was decided to modify one of these experiments to include a second source of excitation. This would provide a test bench that included a degree of structural response to the vibration signals, and would provide more than one source of vibration. The structural transfer function would modify the vibration signals as the signals propagated through the structure. The behaviour of the adaptive filter algorithms in a structurally-modified vibration environment with multiple sources of excitation could be studied and confirmed experimentally using this test bench.

4.2.1 Experimental Goal

After having tested the adaptive filters on numerical test cases, testing in an actual experimental environment was required. The behaviour of the filter algorithms when exposed to a signal originating from multiple sources and modified by a structural transfer function is of importance, considering the multi-machine environment on the aircraft from which this work is motivated. An environment containing at least 2 sources of vibration, and a structural transfer function was required.

Convergence behaviour of the algorithms needed to be studied. Various parameters of each algorithm, in a direct or indirect fashion, contribute to the convergence behaviour of the algorithm. The quality of the filtered solution obtained is of paramount importance. The purpose of this simple phase of experimental testing was principally to gain experience with the adjustment of convergence parameters for each algorithm. Secondly, a convenient platform with sufficient control over the input signals used was required to evaluate the convergence behaviour of the adaptive algorithms under various conditions. Thirdly, the effect of exponentially decreasing the step size parameter of the adaptive algorithms was investigated.

4.2.2 Experimental Setup

The cantilever beam simulator is shown in schematically in figure 4.1. Figure 4.2 displays a photograph of the cantilever beam simulator experiment, and the measurement hardware used. The measurement hardware consisted of two accelerometers, two load cells, a four-channel ICP amplifier for the accelerometers and load cells, a four-channel data acquisition unit and a personal computer. The Siglab® data acquisition unit incorporated anti-aliasing filters, and performed the analogue-to-digital conversion function. ICP accelerometers were used with sensitivities of 100 mV/g.

Electro-dynamic actuators provided excitation to the structure. The actuators were provided with control signals using the same Siglab® analyzer as with which the measurements were taken. The excitation signals consisted of various combinations of sinusoids, and in certain cases additive white noise. Starting with a single source of excitation, the experiments grew in complexity to dual source excitation with additive noise.

During each experiment, it was attempted to separate the deterministic parts from the noise. The experiments also provided the opportunity to become familiar with the reaction of the algorithms to changes in input parameters. Valuable experience was gained from these experiments with the adaptive filters' input parameters.

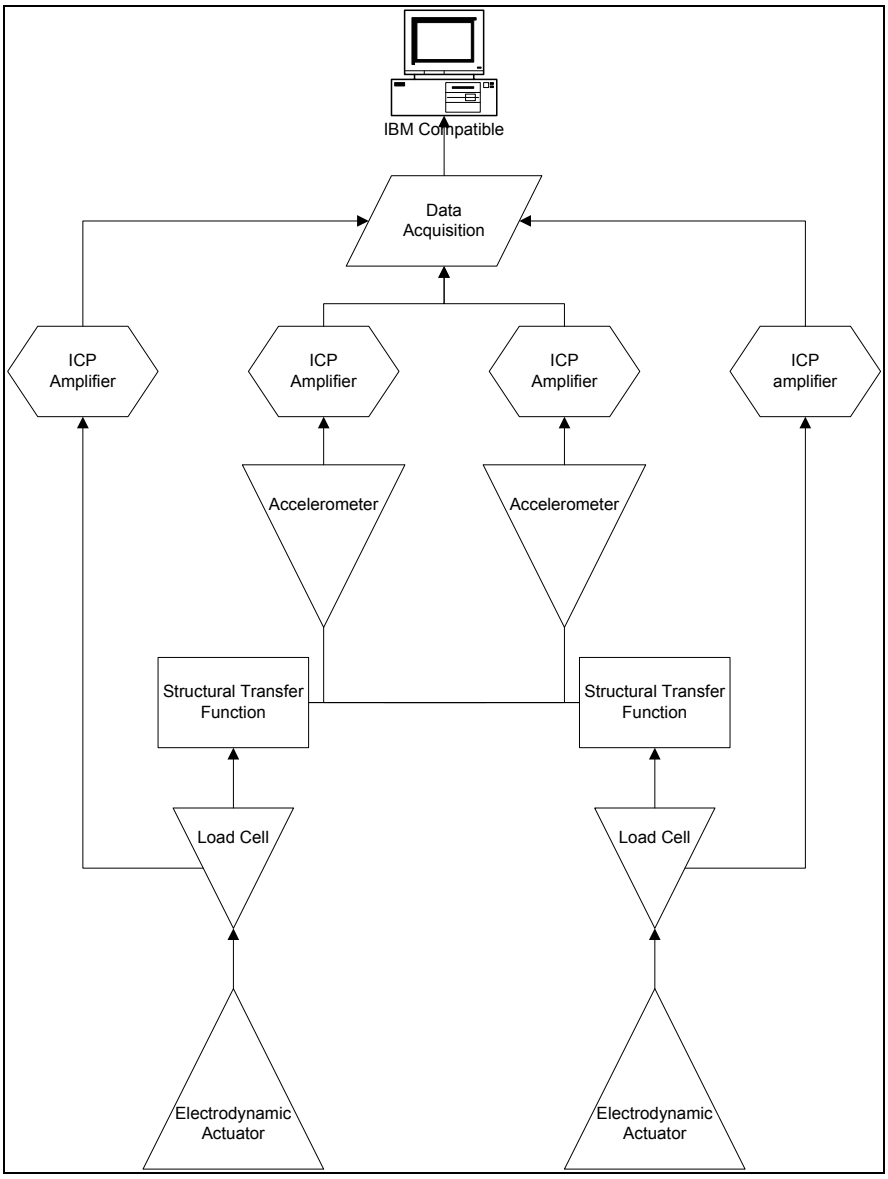

Figure 4.1: Cantilever Beam Simulator Schematic

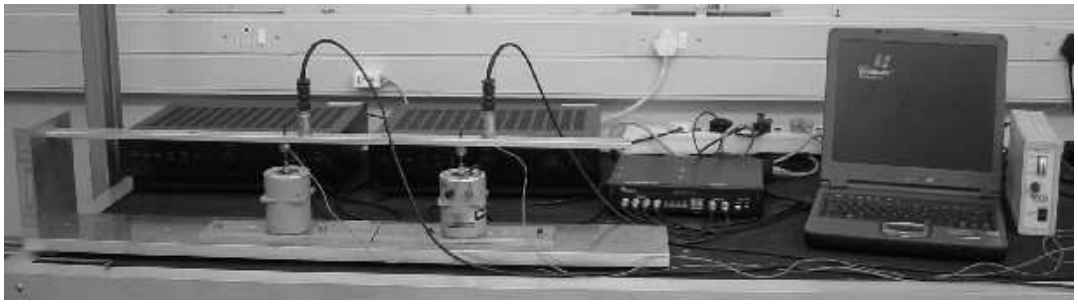

Figure 4.2: Cantilever Beam Simulator Experiment

4.2.3 *Experimental Procedure*

Experiments with the cantilever beam simulator involved various tests run at different excitation frequencies. The measured acceleration signal was found to be different from the pure sinusoidal input signals. This is attributed to the structure's response to the excitation, and some random measurement noise. It is assumed here that the noise is white in nature, with a Gaussian distribution. The source of this random noise is partly attributed to the structural response to the excitation, and partly to electric measurement equipment noise.

Different excitation frequencies and different sampling rates were used to record a number of signals from the accelerometers and load cells. Table 4.1 details the significant excitation parameters used. In each case the sinusoidal components were dominant in signals, in spite of the white noise that was added. It was expected that the structure and measurement hardware would contribute to the noise in the measured signals.

Table 4.1: Cantilever Beam Excitation

Channel 1	Channel 2	Channel 2 phase
40 Hz	40 Hz	0
40 Hz	40 Hz	random offset
45 Hz	45 Hz	30 deg
45 Hz	47 Hz	0

The recorded signals were then filtered using the adaptive line enhancer algorithms – the LMS and the SQSD based filters. Different step size parameters, λ for LMS and d for SQSD, were used to determine the effect of the step size parameter on the convergence of the algorithms. The feasibility of exponentially decreasing the step size was investigated by considering convergence with a constant step size as opposed to the convergence of exponentially decreasing step size.

Data presented are from the second accelerometer. The filter length N was determined from equation 2.36, with ΔB=2 Hz. Table 4.2 provides pertinent signal parameters for the data set under consideration.

Table 4.2: Cantilever Beam Signal Parameters

Description	Variable	Value	Units
Sampling frequency	f_s	2560	Hz
Excitation frequency 1		45.0	Hz
Excitation frequency 2		47.0	Hz
Frequency separation	ΔB	2.0	Hz
Filter Coefficients		1280	

4.2.4 *Experimental Findings*

Towards achieving the goal of gauging the sensitivity of the adaptive algorithms to changes in the step size parameters, data was filtered using different constant, as well as exponentially decreasing step sizes. The squared prediction error and Power Spectral Densities of the prediction error and filtered signals are presented. Figure 4.3 shows a power spectral density of the original data, in a frequency range from 30 Hz to 60 Hz where most of the activity was centred, plot on a decibel scale.

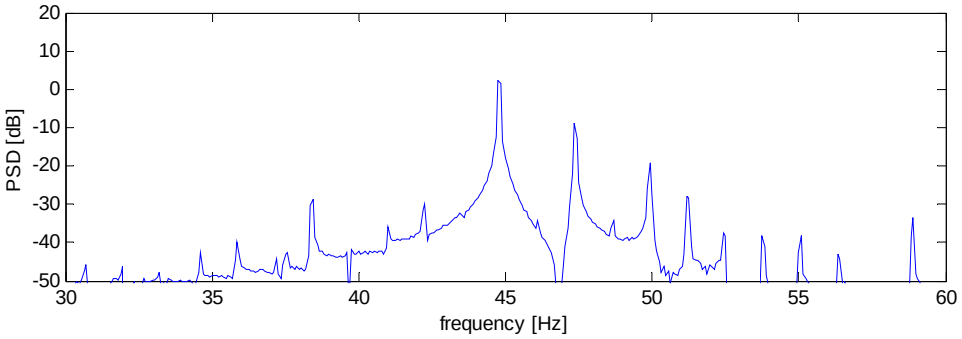

Figure 4.3: PSD of Original Acceleration

4.2.4.1 Least Mean Squares based Adaptive Line Enhancer

To gain an understanding of the convergence behaviour of the adaptive algorithms employed, the squared prediction error, the PSDs of the prediction error, as well as PSDs of the filtered signal will be considered. When computing the PSD of filtered data and squared prediction error, care has to be exercised that data points from the transient adaptation phase do not introduce spurious content into the computations' results. To this end, the transient parts of the signals were excluded from the PSD computations.

Figure 4.4 shows the squared prediction error of the LMS implementation for step sizes of a) λ=0.1, b) λ=0.01, c) λ=0.001 and d) λ=0.0001 respectively. The squared prediction error is the square of the difference between the prediction made by the filter algorithm, and the actual data point measured. Convergence of the filter algorithm, or prediction algorithm, is therefore indicated by a decrease in the squared prediction error. Fluctuation of the prediction error is to be expected as the signal is not identically stationary, due to its own properties and the properties of additive noise.

Note the faster convergence achieved for the larger step sizes during the transient initial phase. The smaller step size leads to slower convergence, but the fluctuation of the weight vector solution about the optimal solution in the steady state phase is also smaller. A higher quality solution is thus eventually obtained by the smaller step sizes, at the price of slower convergence.

Observe from figure 4.4 a) the activity over the first 8000 data points: the transient adaptation phase for λ=0.1. The bulk of the transient activity occurs over the first 5000 data points. Subsequent to this transient phase, there is

still some fluctuation over the rest of the data. These fluctuations in the steady phase are attributed to additive noise, and to the fact that the data may not be identically stationary.

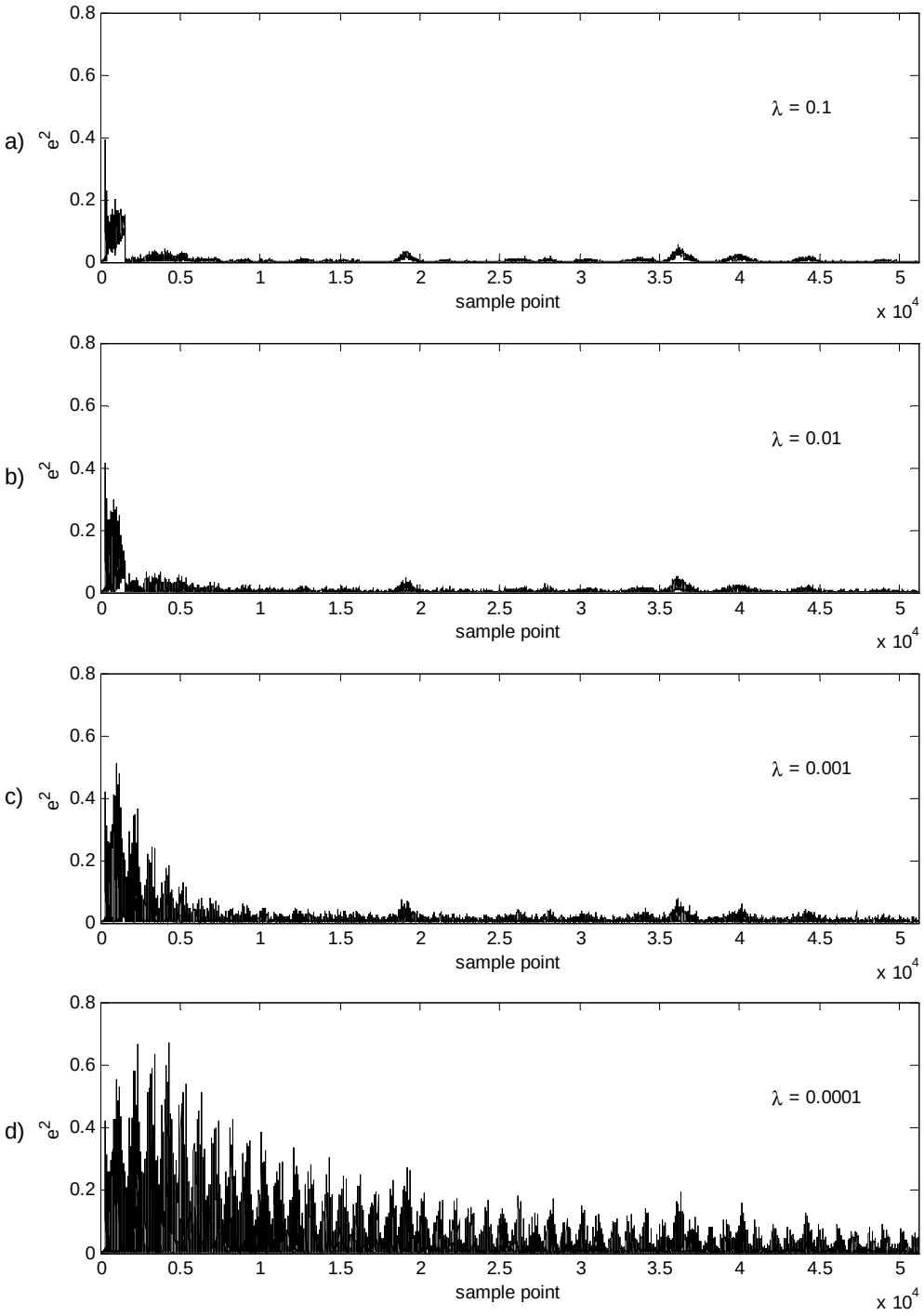

Figure 4.4: LMS Squared Prediction Error

For the step size parameter λ=0.01, the transient adaptation phase is still limited to the first 8000 points of data in figure 4.4 b). Transient activity is however more spread out over these 8000 data points than for the larger step

size of figure 4.4 a). Fluctuations in prediction error are still present over the rest of the data, as is to be expected.

In order to obtain a solution of higher quality, the step size was further reduced to λ=0.001, the squared prediction error of which is shown in figure 4.4 c). The transient adaptation phase still extends over the first 8000 data points. There is however a marked change during this phase when compared to figures 4.4 a) and 4.4 b): The squared prediction error decreases remarkably more smoothly over the transient adaptation phase. As before, variations in squared prediction error are still present over the rest of the data.

Slow convergence of the LMS algorithm is often mentioned in the literature as a complaint against the algorithm. Figure 4.4 d), where λ=0.0001, provides an example of such a case. The transient adaptation phase extends almost over the entire data record. Even though the squared prediction error seems more stable after 25 000 data points, there is still a decrease visible between the 25 000'th data point and the end of the record. Very little data would thus be available for further processing using a step size λ=0.0001. When generating the spectra presented here, data from sample point 20 000 onwards was used to eliminate the transient behaviour over the first 20 000 points.

Using the autocorrelation matrix to determine bounds for λ, as proposed by Antoni and Randall (2001) and discussed under section 2.5.3.1, could prevent the excessively slow convergence observed in figure 4.4 d). Examining the λ / dim(R) curve in figure 4.5 shows that the λ / dim(R) ratio stabilises for an autocorrelation matrix dimension, dim(R), of 200. The value of λ corresponding to this is around 0.05 – two orders of magnitude larger than λ=0.0001 used when figure 4.4 d) was generated.

Although it is remarked by Antoni and Randall (2001) that the autocorrelation matrix method is not infallible, it does in this case prove to provide a guide for choosing the step size parameter λ. Throughout processing the data recorded during the cantilever beam experiments, the autocorrelation matrix method was used to determine an initial step size parameter λ. Although this method does not in any way guarantee convergence of the LMS based adaptive filter, it proved to be a valuable means of selecting a starting point in as far as the step size parameter is concerned.

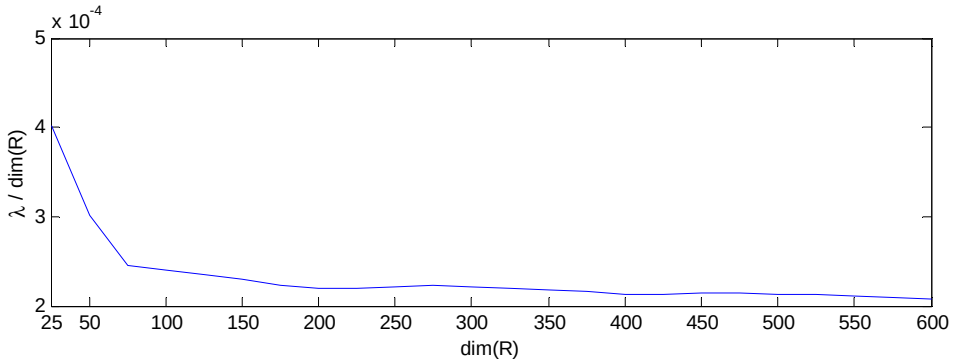

Figure 4.5: Step Size vs. Autocorrelation Matrix Dimension

Considering the squared prediction error in isolation neglects the quality of the weight vector solution obtained. A measure of the conformance of the filtered signal to the requirement set for the adaptive algorithm should also be considered. In this work, energy and its distribution at certain frequencies are of interest. Hence spectra generated by FFT, PSD or time-frequency methods will be used in order to assess the quality of the solution obtained from the adaptive filtering operations.

From table 4.2 the excitation frequencies of 45 Hz and 47 Hz may be extracted. Observe also the peaks at 45 Hz and 47 Hz on the PSD of the original unfiltered acceleration signal, figure 4.3. Ideally the prediction error will not include components of the deterministic excitation signal, i.e. significant activity at the excitation frequencies of 45 Hz and 47 Hz. It is desirable for the filtered signal to not only contain peaks at the excitation frequencies, but also that the level of these elements should be enhanced when compared to the unfiltered signal.

Power spectral densities of the prediction error are shown in figure 4.6 for step sizes of a) λ=0.1, b) λ=0.01, c) λ=0.001 and d) λ=0.0001 respectively. There is present in the power spectral density of the prediction error peaks at 47 Hz for all four of the step size parameters λ, in figure 4.6. The level of this peak rises from approximately -20 dB to +10 dB as the step size parameter decreases from λ=0.1 to λ=0.0001. Peaks at 45 Hz only become prominently visible for step sizes smaller than λ=0.001.

Filtered signals' power spectral densities are shown in figure 4.7 for step sizes of a) λ=0.1, b) λ=0.01, c) λ=0.001 and d) λ=0.0001 respectively. Prominent peaks are present at the excitation frequencies for all four of the step size parameters employed.

Prominent peaks at 45 Hz and 47 Hz are present on the PSD of figure 4.7 a) for λ=0.1. Surrounding peaks attributable to noise are however more prominent than for the unfiltered case of figure 4.3. Although the level of the excitation related peaks are unaltered, the levels of the surrounding peaks have increased, and it may be concluded that the effect of the filtering

operation has been limited to the introduction of additional noise. Clearly, although it may be argued that the filter successfully converged to a stable solution, the quality of this solution is not as high as desired. The large step size of λ=0.1 does however converge, in spite of being larger than λ=0.05 as suggested by the method of Antoni and Randall (2001).

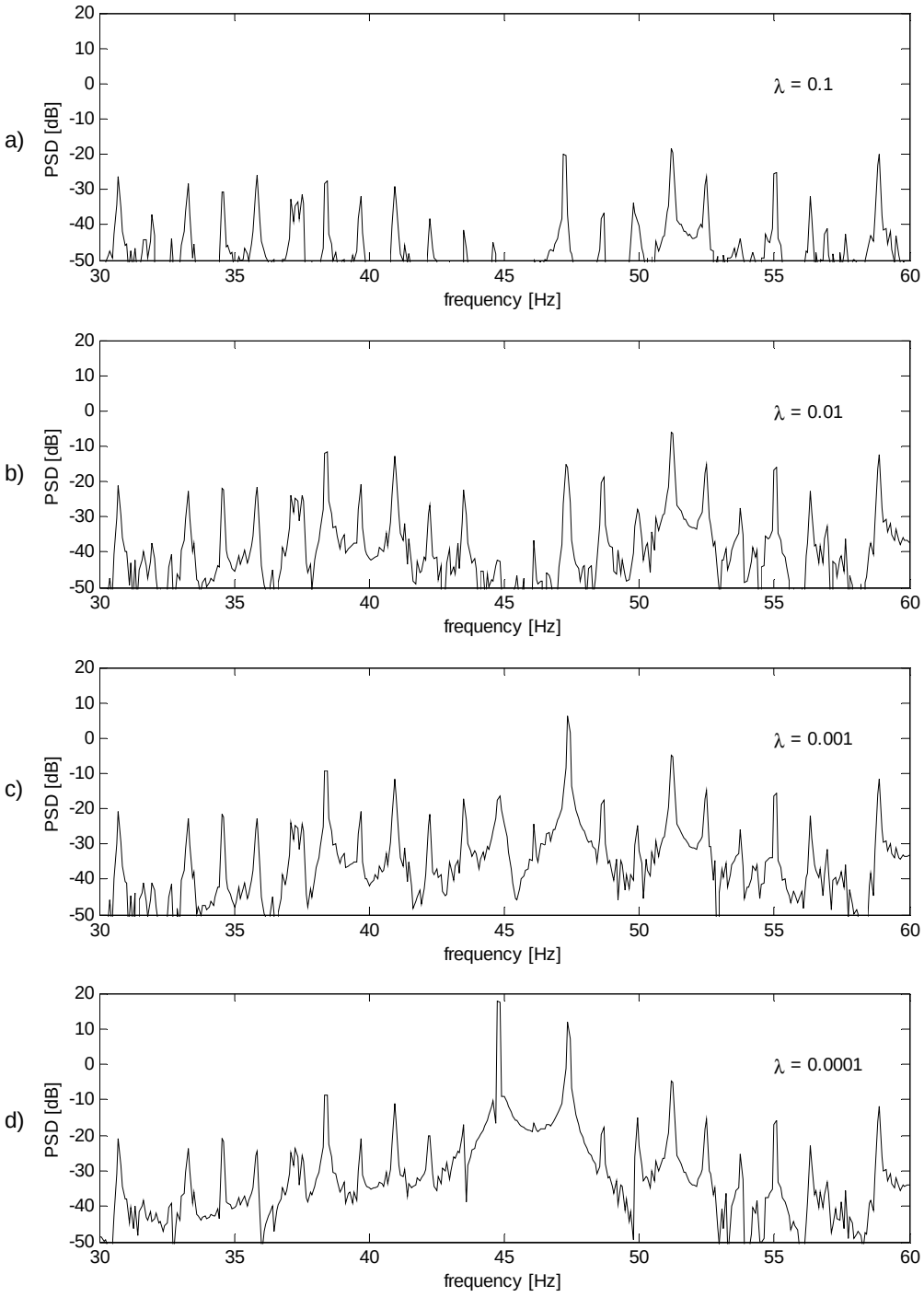

Figure 4.6: PSD of LMS Prediction Error

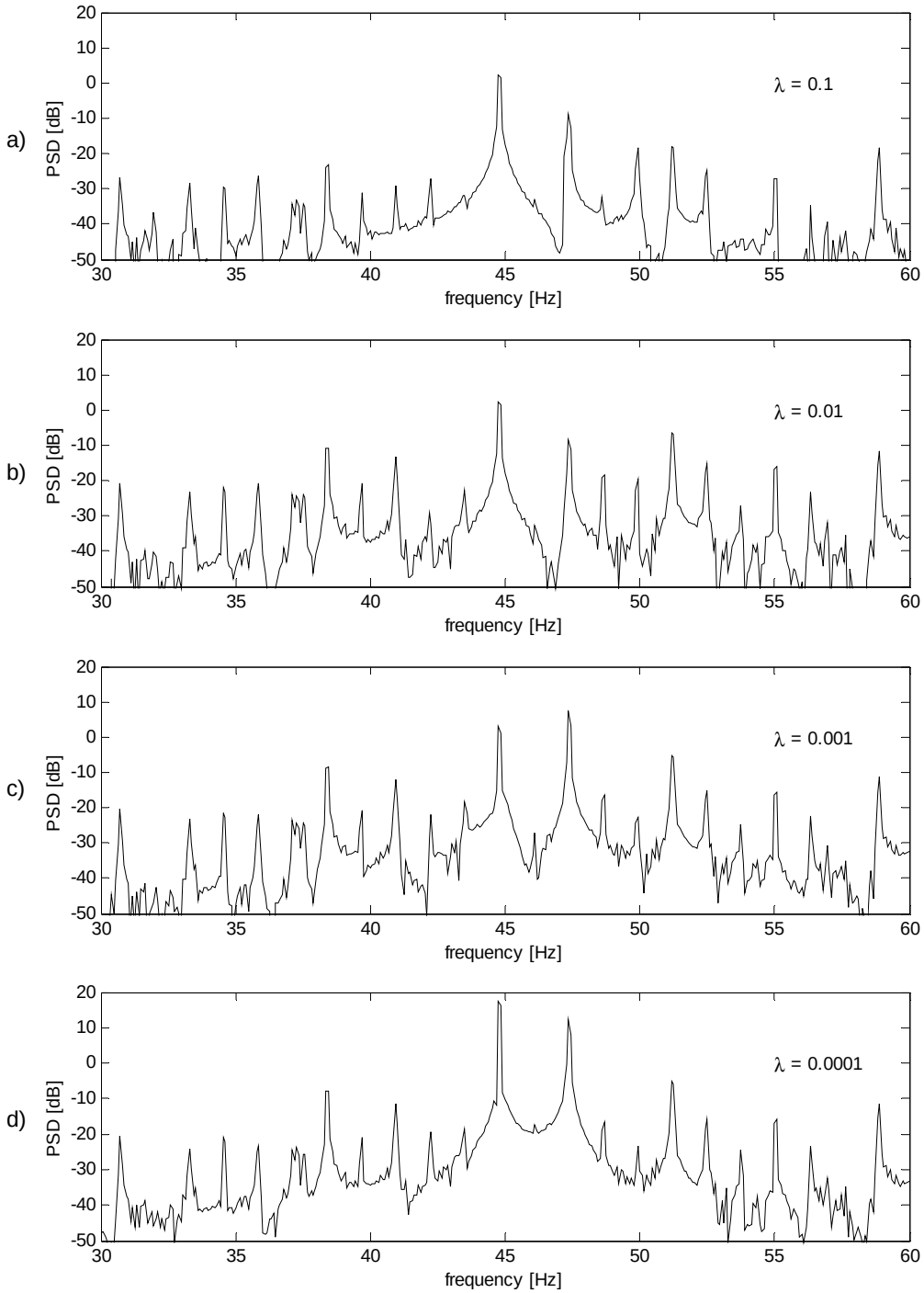

Figure 4.7: PSD of LMS Filtered Signal

Using λ=0.01 does not improve the situation: The peaks at 45 Hz and 47 Hz on figure 4.7 b) stays at the same level as for the unfiltered case, while the surrounding peaks are emphasised even more than for the larger step size parameter λ=0.1. Note that λ=0.01 is smaller than the step size recommended from the method of Antoni and Randall (2001) of λ=0.05, and it would therefore be expected that a superior solution would be obtained in this case.

Again convergence to a stable solution has been attained. The prediction error seems to contain mostly data from sources other than the excitation, from consideration of the PSD of the prediction error, figure 4.6 b). The quality of the solution is however still less than desired, because of the additional peaks present in the PSD of the filtered data, figure 4.7 b).

Although the PSD of the prediction error for a step size parameter λ=0.001 does contain a prominent peak at 47 Hz on figure 4.6 c) , the peaks associated with the excitation at 45 Hz and 47 Hz are more prominent on the PSD of the filtered signal of figure 4.7 c). Peaks not stemming from the excitation frequencies are present in the PSD of the filtered signal presented in figure 4.7 c), but are smaller relative to the peaks associated with the excitation, than for the larger step sizes. A solution of better quality has thus been obtained, with an acceptable rate of convergence. Comparing this solution to the PSD of the unfiltered signal, figure 4.3, the unfiltered signal still makes a clearer case for the purpose of identification of the driving excitation frequencies.

Peaks attributable to the excitation, at 45 Hz and 47 Hz, are clearly the most significant features of the PSDs of the prediction error and filtered signal, figures 4.6 d) and 4.7 d), respectively. A substantial component of the error is thus made up of deterministic signal components which do not belong to the error category. This, together with the excessively slow convergence may lead to the rejection of the filtered data when λ=0.0001. It has to be noted that the most significant features of the filtered signal's PSD are the peaks associated with the excitation frequencies.

These results are in agreement with existing adaptive filter literature. A conclusion that may be reached from these constant step size parameter experiments is that the prediction error may be used as a measure or indication of convergence for the algorithms. In cases where convergence or lack thereof, needs to be confirmed, the squared prediction error may be used as an indication. The converged case shows a decrease in prediction error when convergence is achieved. Considering prediction error in isolation may however lead to unexpected results. It is pointed out that the filtered signal, or some of its properties or characteristics, should also be considered to gauge the quality of the solution obtained and ensure satisfaction.

4.2.4.2 Spherical Quadratic Steepest Descent based Adaptive Line Enhancer

As for the LMS algorithm's case, the squared prediction error, the PSDs of the prediction error, as well as PSDs of the filtered signal will be considered in order to asses the SQSD algorithm's behaviour. When computing the PSDs of filtered data and squared prediction error, the transient parts of the signals were excluded from the PSD computations in order to prevent the transient parts from influencing the computations.

Figure 4.8 shows the squared prediction error of the SQSD based adaptive line enhancer implementation for step sizes of a) d=0.1, b) d=0.01, c) d=0.001 and d) d=0.0001 respectively. The squared prediction error is the square of the difference between the prediction made by the filter algorithm, and the actual data point measured, and a decrease in the squared prediction error may indicate convergence of the algorithm. As for the LMS filter, fluctuation of the prediction error is to be expected due to non-stationarity of the signal.

Larger step sizes still achieve faster convergence during the transient initial phase. As for the LMS algorithm, the smaller step size leads to slower convergence, but the fluctuation of the weight vector solution about the optimal solution in the steady state phase is also smaller. Based on the squared prediction error it may therefore be concluded that a higher quality prediction is eventually obtained by the smaller step sizes, at the price of slower convergence.

Using a step size parameter d=0.1 resulted in the squared prediction error graph of figure 4.8 a). The transient adaptation phase is harder to distinguish than was the case with the LMS based filter using the same step size. It appears that most of the adaptation occurred over the first 8000 data points. The fluctuation in the prediction error is much larger than that of the LMS case of figure 4.4 a). From considering the squared prediction error only, it would thus appear that the SQSD based algorithm has not fared as well as the LMS algorithm for the same step size parameter of 0.1.

Proceeding to attempt to enhance the effect of the adaptive filter, a smaller step size of d=0.01 was applied, the squared prediction error of which is shown in figure 4.8 b). There is much similarity between figures 4.8 b) and 4.4 b). It is noteworthy that the fluctuation present in the prediction error is slightly larger for the SQSD case than for the LMS case. Transient adaptation behaviour occurs over the first 8000 points, while the expected fluctuation in the mean square error persists over the remainder of the data.

Using yet smaller step size parameter, d=0.001, yields slower adaptation over the first 8000 data points, but marginally better fluctuation in prediction error in the steady state phase over the rest of the data record as shown in figure 4.8 c). Fluctuation in the prediction error after the transient adaptation phase compares well with that of the LMS case.

For the new SQSD adaptive filter, it is also possible to demonstrate a case of slow convergence by selecting a small step size parameter d=0.0001. Convergence has not strictly been attained over the entire data record: figure 4.8 d). As for the LMS case, although convergence seems likely, very little useable filtered data will result from using such a small step size.

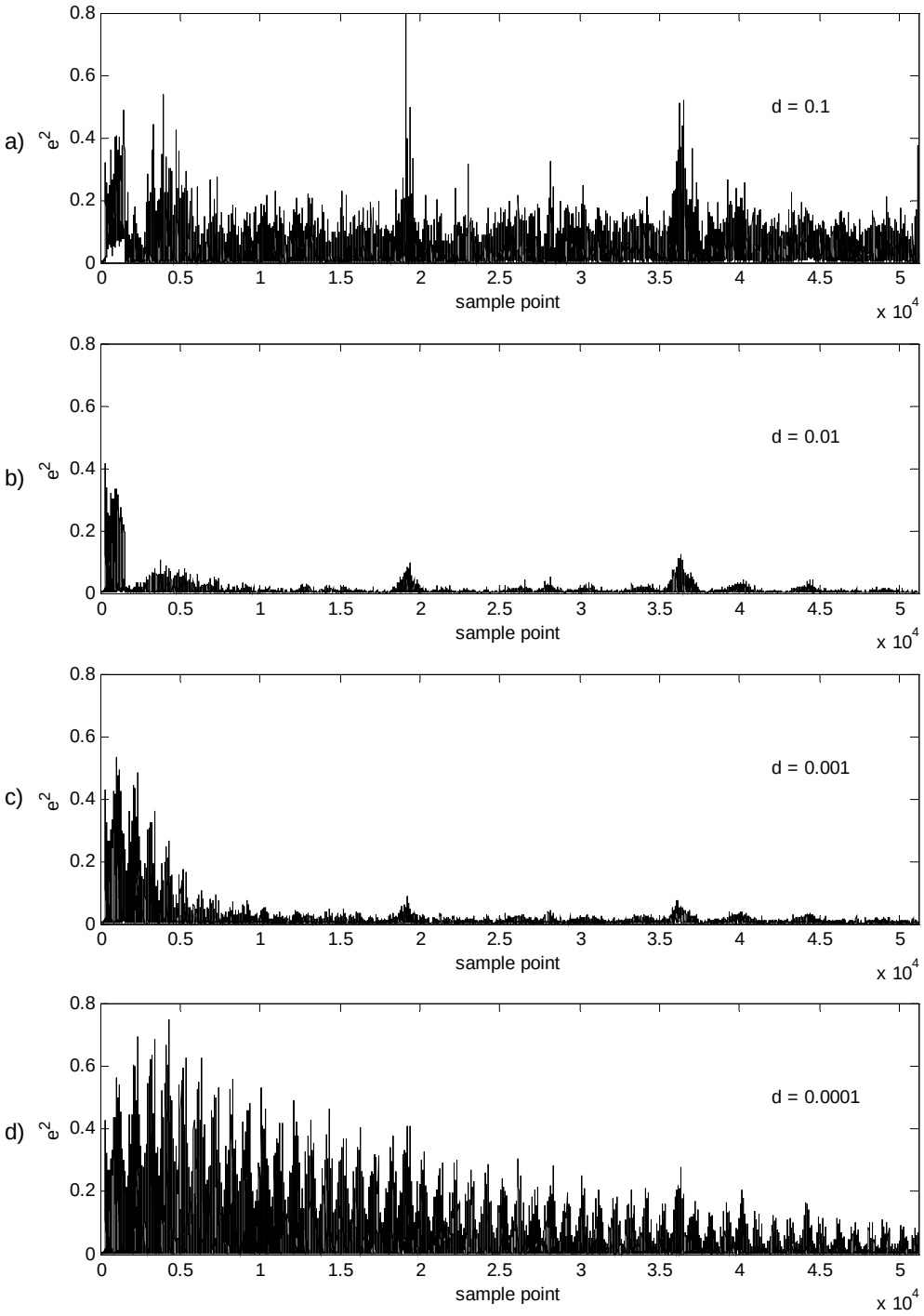

Figure 4.8: SQSD Squared Prediction Error

Excitation frequencies as listed in table 4.2 still apply, as does the PSD of the unfiltered signal from figure 4.3. It is desirable that the prediction error will not include components of the deterministic excitation signal, and for the filtered signal to not only contain peaks at the excitation frequencies, but also that the level of these elements should be enhanced when compared to the unfiltered signal.

Power spectral densities of the prediction error are shown in figure 4.9 for step sizes of a) d=0.1, b) d=0.01, c) d=0.001 and d) d=0.0001 respectively. Peaks at the excitation frequencies are identifiable for the smaller two step sizes, d=0.001 and d=0.0001, but not for the larger step sizes.

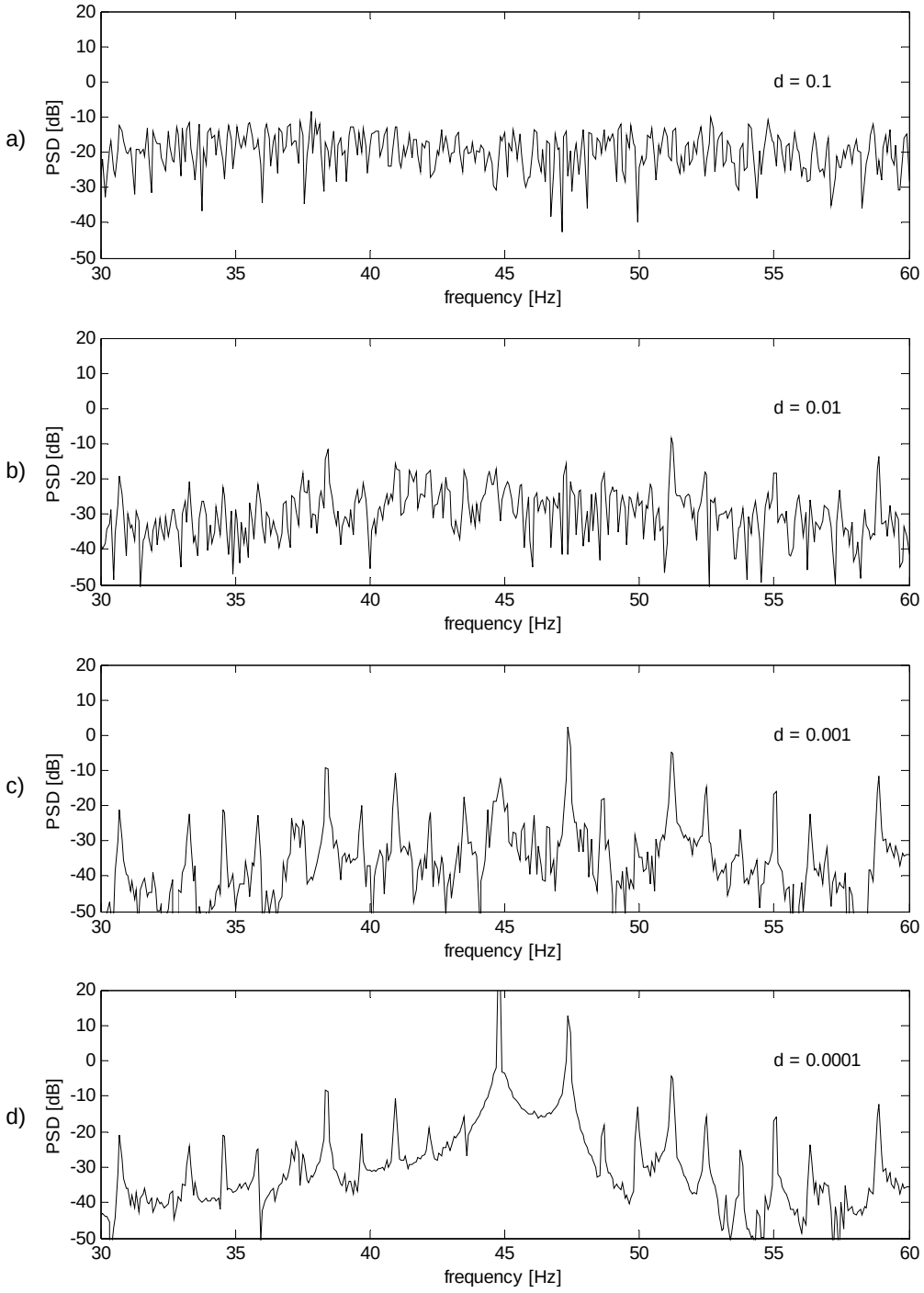

Figure 4.9: PSD of SQSD Prediction Error

SQSD based filtered signals' power spectral densities are shown in figure 4.10 for step sizes of a) d=0.1, b) d=0.01, c) d=0.001 and d) d=0.0001 respectively. Peaks are present at the excitation frequencies for all four of the step size parameters employed, although the peak at 47 Hz for the largest step size parameter of d=0.1 is small.

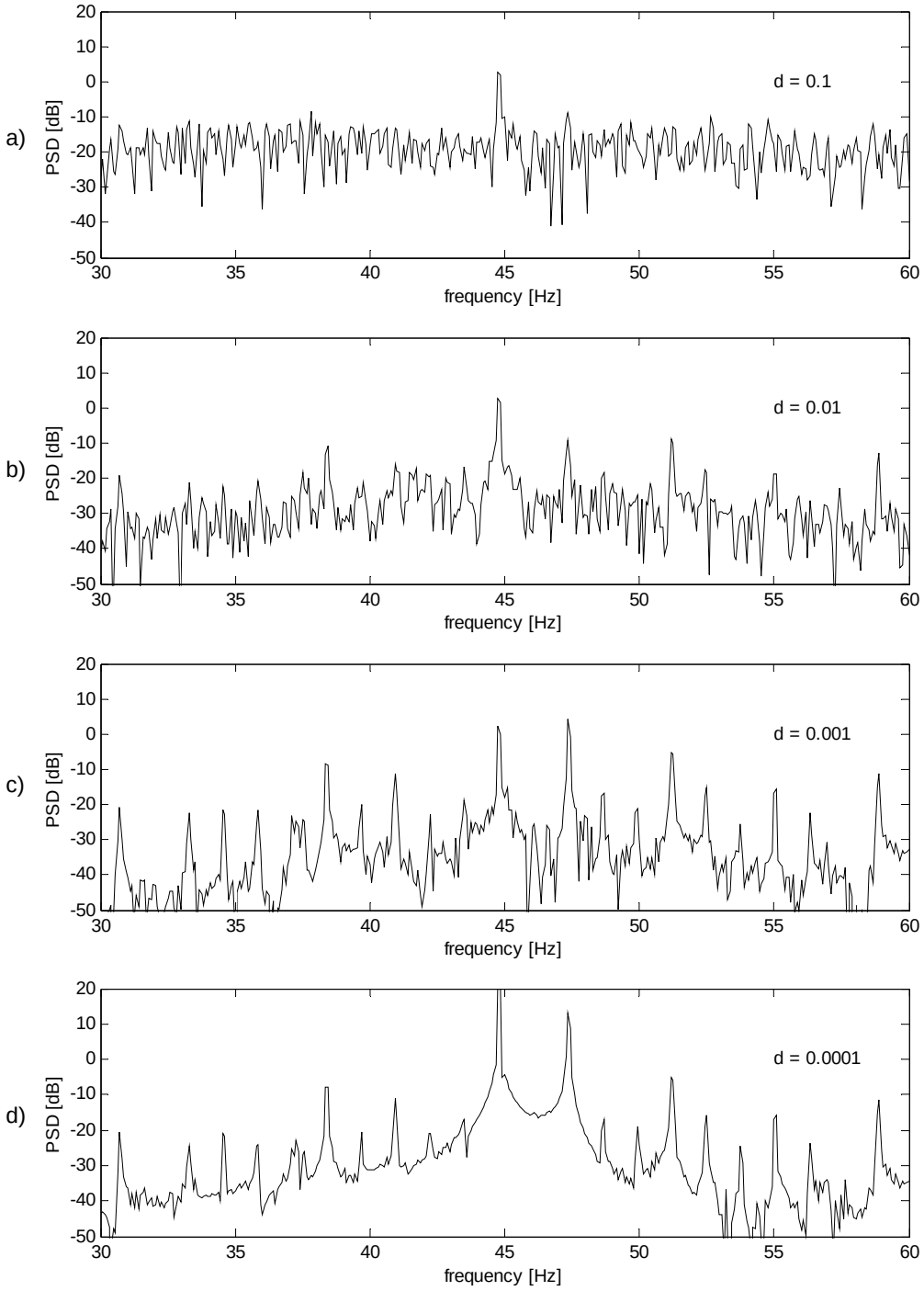

Figure 4.10: PSD of SQSD Filtered Signal

No peaks are discernable at 45 Hz or 47 Hz on the PSD of the squared prediction error for the largest step size, d=0.1 of figure 4.9 a). As the squared prediction error, shown in figure 4.8 a), in this case does not provide clear and concise evidence of convergence, little may be concluded from these figures, apart from the apparent lack of proper convergence. The PSD of the filtered signal, shown in figure 4.10 a), contains a clear peak at 45 Hz, but only a small peak at 47 Hz. This compares poorly with the PSD of the unfiltered signal of figure 4.3. Although the PSD of the filtered signal of figure 4.10 a) contains fewer peaks, the noise floor around the 45Hz peak has been raised. The prediction error of the SQSD based filter in figure 4.8 a) is also much noisier than with the LMS case of figure 4.4 a), although no distinct peaks are observable on the PSD of the squared prediction error at the 45Hz and 47Hz excitation frequencies – figure 4.9 a).

Prediction error frequency content on the PSD of figure 4.9 b) appears devoid of significant content at the excitation frequencies of 45 and 47 Hz. A small artefact does exist at 47Hz though. The filtered signal exhibits peaks at 45 Hz and 47 Hz, although the peak at 47 Hz is not as significant as one would like. The decreasing squared prediction error indicates convergence for this case of d=0.01. It is clear that the filter is converging to an acceptable solution for enhancement of the deterministic signal components. It is however desirable to achieve a solution with less noise present in the filtered signal.

For the step size parameter d=0.001, the PSD of the prediction error, shown in figure 4.9 c), exhibits peaks at 45 Hz and 47 Hz – the excitation frequencies. Corresponding peaks at 45 Hz and 47 Hz are however more prominent than for the larger step sizes on the PSD of the filtered signal in figure 4.10 c). Especially the peak at 47 Hz has been enhanced. Although the prediction error does contain elements from the excitation, there has been clear improvement in the filtered signal's PSD.

Prominent peaks are visible at 45 Hz and 47 Hz in both the PSD graphs of the prediction error and the filtered signal, figures 4.9 d) and 4.10 d), for the step size parameter d=0.0001. The prediction error hence contains a significant part of the deterministic signal. Such results are not useful for the purpose of signal enhancement. During the calculation of the PSDs, only the second part of the data record from the 20 000th sample point was used in an attempt to minimise the effect of the transient adaptation phase. The slow adaptation rate exhibited by the squared prediction error of figure 4.8 d) clearly implies that adequate convergence has not been attained with this small step size parameter.

4.2.4.3 Exponential Decrease of the Step Size Parameter

Exponentially decreasing the step size parameter of the adaptive algorithm offers the fast convergence advantage of larger step sizes, as well as the higher solution quality obtained from a smaller step size parameter, as discussed under 2.7.3. The step size parameters λ and d were decreased

exponentially from 0.01 to 0.001 and from 0.005 to 0.0005, respectively, in order to asses the feasibility of this approach. Figure 4.11 a) shows the squared prediction error for the LMS case, while figure 4.11 b) shows the squared prediction error for the SQSD based algorithm.

From the squared prediction error depicted in figure 4.11 a) it can be seen that the transient adaptation phase occurs over the first 8000 points, approximately. A much lower prediction error is attained quicker than for the case of a constant λ=0.001 though: compare figures 4.4 c) and 4.11 a). The prediction error in the steady state phase compares well with that of the case λ=0.001, figure 4.4 c).

The step size parameter d was decrease exponentially from 0.005 to 0.0005 to investigate the feasibility of this technique, considering the SQSD method. Figure 4.11 b) shows the squared prediction error obtained. The transient adaptation phase extends approximately over the first 8000 points. The low fluctuation of prediction error in the steady state portion indicates high prediction accuracy.

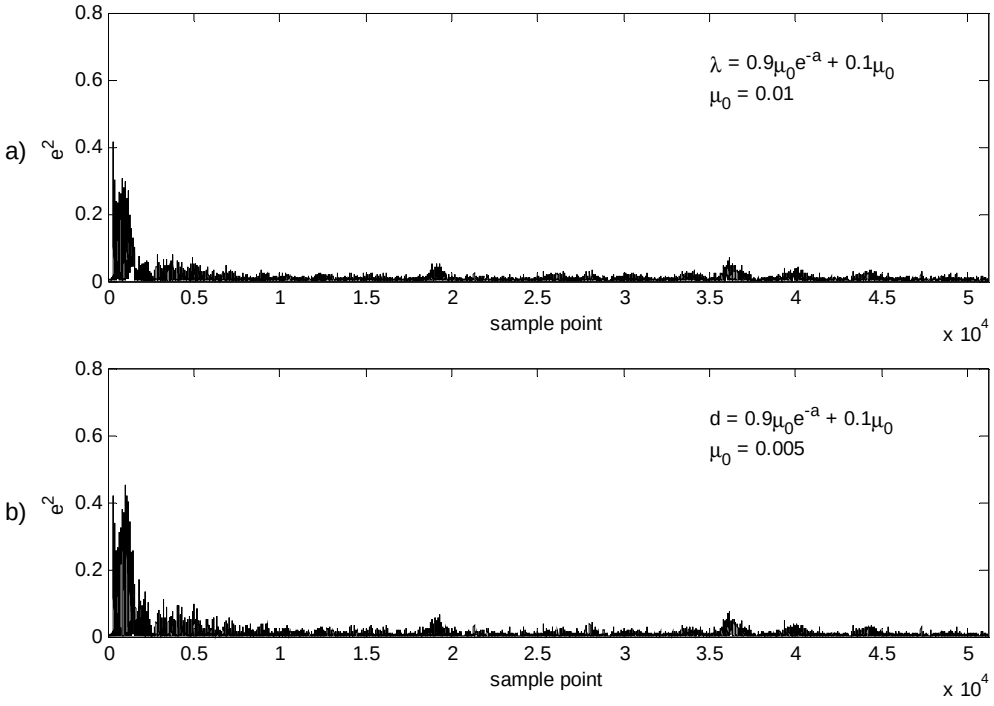

Figure 4.11: Squared Prediction Errors, Exponentially Decaying Step Size

In both cases, judging only from the squared prediction error, it seems that the fast rate of convergence of the larger factor is indeed maintained, as is the higher solution quality of the smaller forgetting factor. The exponential decrease curve was chosen such that most of the decay would occur over the first 10 percent of the data. Figure 4.12 shows the decay curve of λ – the LMS forgetting factor. The SQSD algorithm's decay curve looks similar to that of the LMS algorithm.

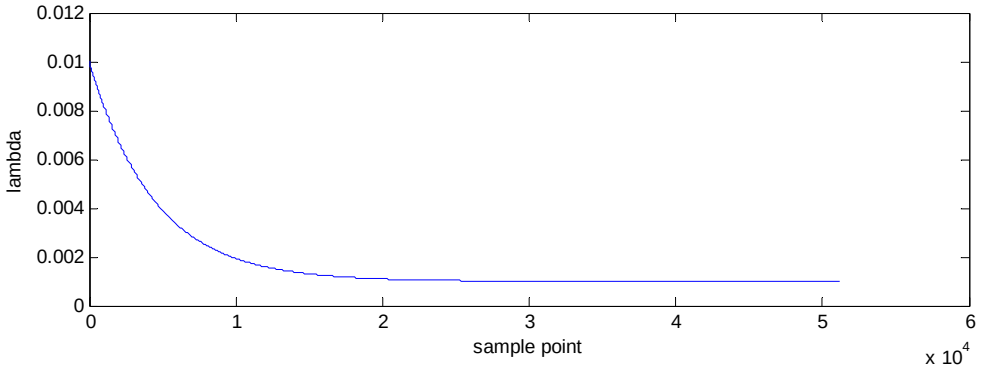

Figure 4.12: Exponentially Decaying Forgetting Factor, λ=0.01 to 0.001

PSDs of the squared prediction errors for the LMS and SQSD cases, and PSDs of the signals filtered by the LMS and SQSD based adaptive line enhancers are shown as figure 4.13 a) and b), and c) and d), respectively. Both the PSDs of the prediction errors, figures 4.13 a) and b), exhibit peaks at 45 Hz and 47 Hz: peaks stemming from the impending structural excitation. The peaks at 45 Hz are poorly defined, and not clearly distinguishable from the surrounding activity. It is therefore concluded that the prediction error, in both cases, contains at least some of the deterministic signal content.

PSDs generated from the filtered signals contain significant peaks at 45 Hz and 47 Hz. In both the case of the LMS adaptive line enhancer, figure 4.13 c), and that of the SQSD adaptive line enhancer, figure 4.13 d), the peaks at 45 Hz and 47 Hz are the most prominent components of the spectrum. Considering the dominance of the peaks concurrently with the spectral symmetry about 45 Hz, a diagnosis can be made as to the driving excitation frequencies impending on the structure. As in the preceding cases, the transient adaptation phase was not included in the calculations of the PSDs.

Use of the exponentially decreasing step size has in this case provided for fast convergence while maintaining good solution quality. The SQSD filtered signals PSD of figure 4.13 d) appears spikier than that of the LMS case of figure 4.13 c). The peaks in the SQSD case are however slightly better defined, as the surrounding noise has been suppressed. There is still a lot of noise present on the PSDs in both cases though. In both cases however, the use of the exponentially decreasing step size parameters has resulted in PSDs that present the signal frequency content more clearly than for the constant step sizes: compare figures 4.7, 4.10 and 4.13.

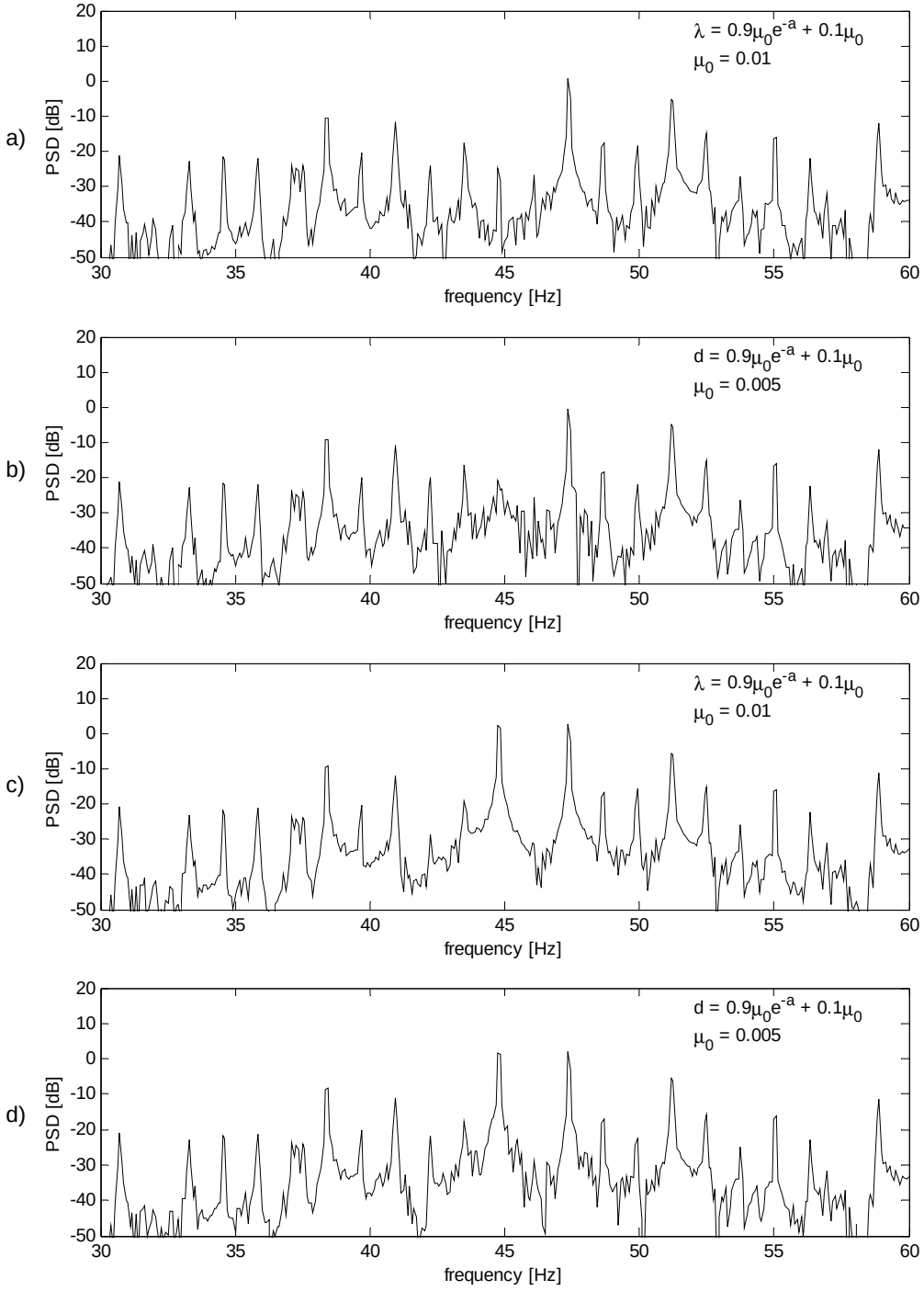

Figure 4.13: Exponentially Decreasing Step Size Parameter PSDs

4.3 Conventional Gearbox Test Bench

Gear vibration signals are generally not pure sinusoids (Randall, 1982). Amplitude and phase modulations, that give rise to the occurrence of side bands in the signal spectrum, are present in these signals. Though theoretical models exist that simulate the measured gear vibration signals, actual measured signals are preferable from an application point of view.

4.3.1 Expected Conventional Gear Vibration

Gear vibration signals are characterized by a periodic signal at the tooth meshing rate which is due to deviations from the ideal tooth profile, either from tooth deflection under load or geometrical profile errors. The following discussion draws on Randall (1982).

Tooth deflection under load tends to give a sinusoidal waveform of stepped nature because of periodically varying compliance as the load is shared between different numbers of teeth. The signal hence includes several harmonics of basic tooth meshing frequency. Tooth deflection is however largely dependant on load. Tooth deflection will fluctuate with load, and cause amplitude modulation of the resulting vibration signal. A possible source of load variation, in spite of constant system load, is eccentricity of one of the gears. Amplitude modulation of a signal gives rise to symmetric sidebands about that signal's carrier frequency, spaced on either side of the carrier frequency by the modulation frequency.

Localized tooth faults result in modulation by a short pulse of length of the order of the tooth meshing period, repeated every revolution, and giving rise to a large number of side bands of almost uniform low level. For more distributed faults, as the fault envelope in the time domain widens, the corresponding envelope in the frequency domain becomes narrower and higher, and the resulting modulation products become more prominently grouped around the tooth meshing harmonics.

Frequency modulation will occur when the rotational speed of the gear is not constant or the tooth spacing is not perfectly uniform. Fluctuations in the tooth contact pressure which give rise to amplitude modulation must simultaneously result in fluctuating torque applied to the gears, and hence result in angular velocity fluctuations at the same frequency. Frequency modulation of a carrier signal, even by a pure tone, gives rise to a whole family of sidebands with spacing equal to the modulation frequency.

Amplitude or phase modulation, in isolation, produces symmetrical families of sidebands about the carrier frequency. The phase relationships on either side of the carrier frequency are different though, and the combination can give reinforcement on one side and cancellation on the other side of the carrier frequency. The manner in which this happens is very sensitive to the initial phase relationships of the amplitude and frequency modulations.

4.3.2 Experimental Goal

Having confirmed the convergence behaviour of the adaptive algorithms in a simplified vibration signal environment, exposure to gear vibration signals was required. This phase of testing was meant to be a transitory testing ground: it would provide conventional gear vibration signals that were less complex than those from epicyclic gearboxes.

Damage was already present on the test setup: a tooth had been removed from the input gear. As testing on the conventional gearbox test bench was regarded as a transition from the very simple cantilever beam to the more complicated epicyclic gear vibration signals, it was not considered worth while to generate undamaged condition data on this test bench.

4.3.3 Experimental Setup

An existing conventional gearbox test bench provided the opportunity to study the behaviour and applicability of the adaptive algorithms in a measured gear vibration environment. A conventional single stage helical gearbox is used on the test bench, mounted between two larger gearboxes. Vibration was measured on the casing of the gearbox by means of stud mounted accelerometers. The test bench was driven by a synchronous motor controlled by a frequency drive, and load was provided by a generator combined with a resistance bench. Figure 4.14 shows the experimental setup.

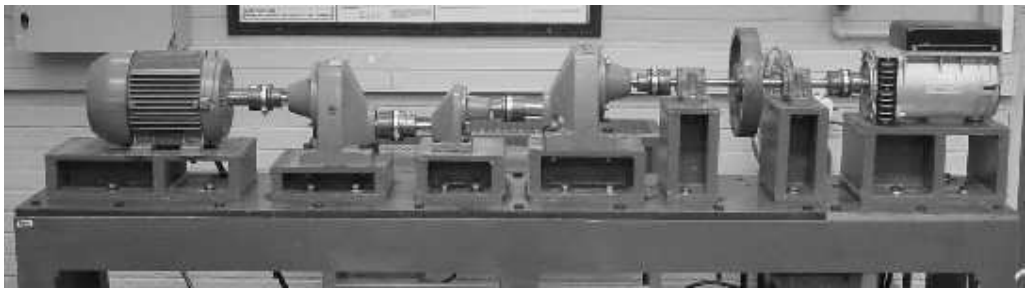

Figure 4.14: Conventional Helical Gearbox Test Bench

Measurement hardware consisted of three accelerometers, a four-channel ICP amplifier for the accelerometers, a four-channel data acquisition unit and a personal computer. As before the Siglab® data acquisition unit incorporated anti-aliasing filters, and performed the analogue-to-digital conversion function.

Accelerometers with nominal sensitivities of 500mV/g were used. The primary accelerometer was mounted in the vertical plane on the central gearbox. A second accelerometer was mounted in the horizontal plane, also on the central gearbox. The third accelerometer was mounted on the third gearbox, in the vertical plane, and was intended as a redundant reference.

Damage was seeded on the central smallest gearbox by removal of one of the teeth from the driving gear. Figure 4.15 shows a photograph of the damaged drive gear mounted in the gearbox, with one of the teeth removed towards the top of the gear. Data was recorded at various sampling frequencies and running speeds. In each case the gear mesh frequency and its harmonics were the dominant elements of the spectrum in the appropriate frequency band.

Figure 4.15: Damaged Drive Gear

4.3.4 *Experimental Procedure*

Damage detection techniques were combined with the adaptive filters to process the data for enhanced diagnostic capability during the experiment. Both the spherical quadratic steepest descent and the steepest descent based LMS filter algorithms were used. Spectral analyses, as well as time-frequency methods (spectrogram and Wigner-Ville distribution) were used to judge the effectiveness of the filtering algorithms. Although it is possible to attempt diagnosis of damage, judged by the prominence of the sidebands surrounding the meshing frequency, this was not attempted during the course of these experiments; the reason for this simply being the absence of data from the undamaged condition to form a basis for objective judgement. Evidence of damage is however pointed out on the time-frequency diagrams.

Data was recorded from the three accelerometers mounted on the test bench. The primary vibration data source was the accelerometer mounted in the vertical plane on the central gearbox, and assigned to channel 1 on the analyzer. No additional filtering was performed, apart from the built-in anti-aliasing filters incorporated in the analyzer. As for the cantilever beam experiment, different sampling frequencies were used for different batches of test runs.

DC offsets from zero mean was removed by computing a least-square fit of a straight line to the data, and subtracting the resulting function from the data. Band-pass filtering of the signals about the meshing harmonics of interest was carried out in an attempt to narrow the spectral content of the signal, and "focus" the diagnostic methods on a particular portion of the spectra. Digital FIR filters were used, and the non-causal filtering approach discussed by Gustafsson (1996) was implemented to produce filtered signals with minimal phase distortion.

Succeeding the initial preparation of the signals – digitization, de-trending and band-pass filtering – adaptive filtering algorithms were applied. The purpose of the adaptive filtering phase was to remove some of the random noise present in the signals. Effectiveness of the adaptive filtering is best judged by examining the spectra or time-frequency graphs of the signals. Convergence of the adaptive algorithms may be assessed by examining the squared prediction error.

4.3.5 *Experimental Findings*

Experimentally measured gear vibration signals were found to be in excellent agreement with models such as those published by Randall (1982) and McFadden (1986). Though noise and interfering elements were present in the spectra observed, the gear vibration signatures were clearly observable. Various strong periodic interference terms may however be observed in the spectra. These are caused by all the other machines and components on the test bench, each a source of its own vibration signature.

Data discussed hereunder was sampled at 2560 Hz. For the input shaft speed of 280 rpm, the gear mesh frequency is expected at 200.7 Hz. Table 4.3 summarises the properties of the gear set under consideration, denoted as the test gearbox, as well as the other two gearboxes used on the test bench.

Although not apparent when examining the time domain data, any possible DC offset was removed by computing a least-square fit of a straight line to the data, and subtracting the resulting function from the data. This procedure ensures that the data is spread about a mean value of zero.

Band-pass filtering about the gear mesh frequency between 150 Hz and 250 Hz removed frequency content too far away from the gear mesh frequency to be of interest to gear fault diagnostics. A finite impulse response filter with 140 coefficients was used, designed to have -60dB attenuation in the stop bands, less than 0.1dB ripple in the pass band and 50 Hz roll-off bands. Phase distortion of the filtering process was reduced by using the non-causal forward-backward filtering approach described by Gustafsson (1996).

Table 4.3: Gear Set Parameters

	Description	Variable	Value	Units
Test Gearbox	Input Shaft Speed		280.0	rpm
	Input Shaft Frequency		4.67	Hz
	Input Gear Teeth		43	
	Output Gear Teeth		22	
	Gear Ratio		1.95	
	Gear Mesh Frequency		200.67	Hz
First Gearbox	Motor Shaft Frequency		22.04	Hz
	Input Gear Teeth		18	
	Output Gear Teeth		85	
	Gear Ratio		0.21	
	Gear Mesh Frequency		396.67	Hz
Third Gearbox	Test Gearbox Output Shaft Frequency		9.12	Hz
	Input Gear Teeth		85	
	Output Gear Teeth		18	
	Gear Ratio		4.72	
	Gear Mesh Frequency		775.30	Hz
	Sampling Frequency	f_s	2560	
	Frequency Separation	ΔB	2	Hz
	Filter Coefficients		1280	
	Filter Delay	Δ	256	

Band-pass filtering resulted in most of the activity above 290 Hz and below 110 Hz being suppressed in the filtered signal. Figure 4.16 shows the power spectral density of the band-pass filtered signal in the vicinity of the first harmonic. Note that in spite of the symmetry of the filter about 200 Hz, the upper roll-off region, between 250 Hz and 300 Hz, contained a lot of activity before filtering, and hence the filtered signals' PSD may appear unsymmetrical.

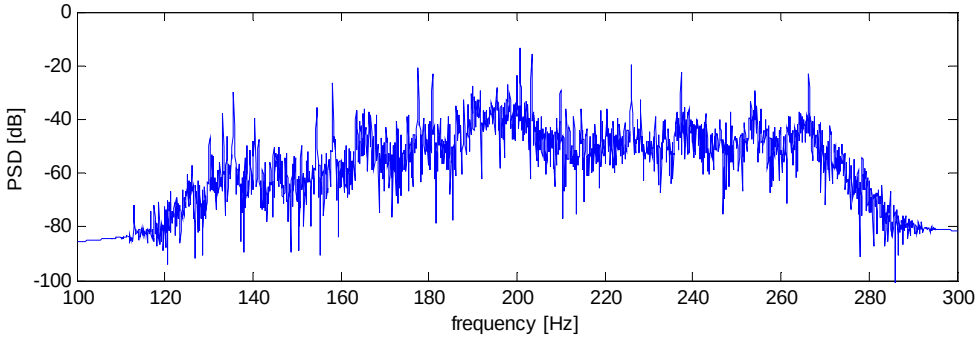

Figure 4.16: PSD of Band-Pass Filtered Signal

Examining the frequencies where sidebands would be expected around the first harmonic, displayed in figure 4.17 as dashed lines, reveals that although the gear mesh frequency at 200.7 Hz is the dominant element in the spectrum, the sidebands are not necessarily dominant in their respective

areas. Reliable diagnostics from this graph will hence be problematic, and an alternative method to pure spectral analysis may be appropriate.

Other peak pairs, symmetric about the gear mesh frequency, are visible around the gear mesh frequency in figure 4.17. Table 4.4 summarises the frequencies of these peak pairs, as picked manually from the graph. Figure 4.18 presents these symmetric peak pairs, indicated as short dashed lines, as graphically picked from the graph. Lack of precision in the frequencies of the peaks may be explained by considering the manual methodology employed in picking the peaks from the graphs.

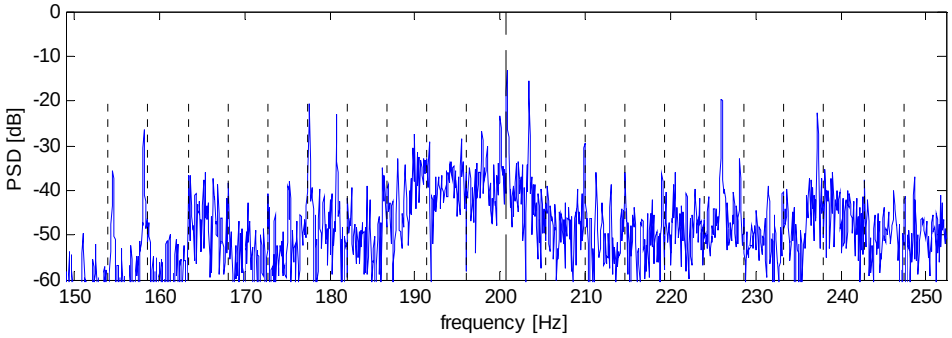

Figure 4.17: GMF and Sidebands, First Harmonic Band-Pass Filtered Signal

Table 4.4: Symmetric Peak Pairs

Lower freq.	higher freq.	lower spacing	higher spacing	multiple of 9.1
191.6	209.9	9.2	9.1	1
182.6	219.0	18.2	18.2	2
173.4	228.1	27.4	27.3	3

Comparing the spacing above and below the gear mesh frequency on figure 4.18 reveals that all are divisible by 9.1 Hz, from which we may conclude that the signal is being modulated at a rate of 9.1 Hz in addition to the modulation at the damaged gear's shaft frequency. The rotation frequency of the driven gear is 9.1 Hz, as indicated in table 4.3 as "Test Gearbox Output Shaft Frequency". Modulation of the gear mesh carrier signal at frequencies of both gears making up the gear pair is to be expected from gear vibration signals, and is hence considered as normal.

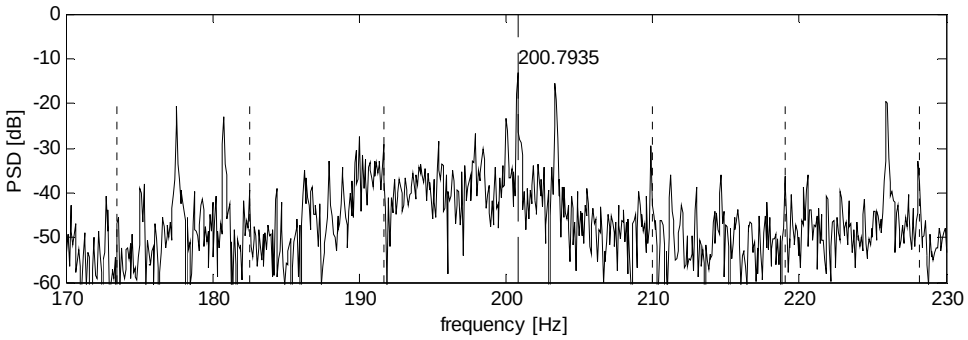

Figure 4.18: Symmetric Peak Pairs, First Harmonic

Using the autocorrelation matrix method suggested by Antoni and Randall (2001) to compute an upper bound for the LMS forgetting factor λ, figure 4.19 may be generated for the band-pass filtered signal about the first harmonic of the gear mesh frequency.

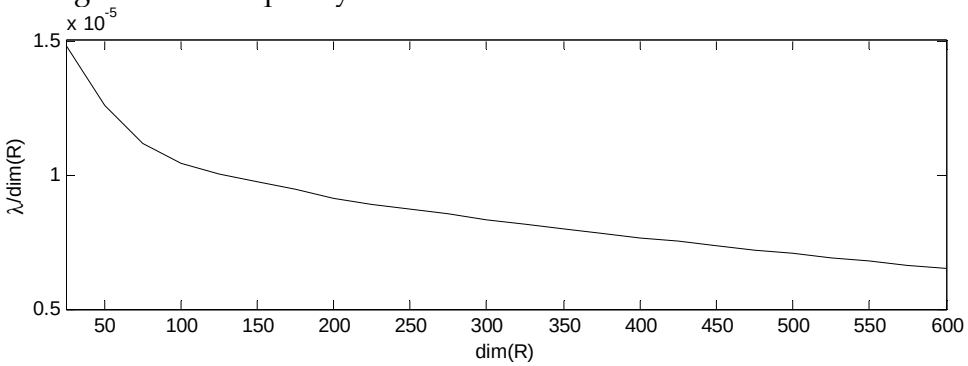

Figure 4.19: λ / dim(R), First Harmonic Band-Pass Filtered Signal

From figure 4.19, λ is chosen as 0.003, corresponding to an autocorrelation matrix dimension of 600. Although the λ / dim(R) curve has not clearly reached a plateau at this point, an autocorrelation matrix with dimension of 600 x 600 was the largest that could conveniently be calculated. To choose the adaptive filters' length, with ΔB=2Hz and f_s the sampling frequency of 2560 Hz, use the formula provided by Antoni and Randall (2001):

$$L = \frac{f_s}{\Delta B} \tag{4.1}$$

Using the parameters as specified, the filter length works out to 1280 coefficients. It was decided to use a filter length of 1024 coefficients. The time delay Δ is chosen so as to decorrelate the noise component of the signal, but not so long as to decorrelate the deterministic component. In this case a delay of 100 sample points was chosen.

First, adaptive filtering was attempted using the steepest descent based LMS adaptive line enhancer. In addition to the filter length and delay, an initial weight value of one and exponentially decreasing forgetting factor of

μ_0=0.003 were used. For these parameters the squared prediction error of figure 4.20 a) does not indicate appreciable decrease with convergence of the algorithm. Various smaller and larger values of the forgetting factor were experimented with, but convergence could not clearly be judged from the squared prediction error in any of the cases.

Having failed to achieve convergence convincingly with the LMS algorithm, the SQSD based adaptive filter is used with similar parameters. In this case the convergence behaviour of the SQSD based adaptive algorithm, as judged from the squared prediction error, appears superior to that of the LMS based algorithm. Figure 4.20 b) shows the squared prediction error for step size parameter d=0.003. It was found during experimentation with the value of d that when d is set to too large a value, the coefficients would tend toward unity, and the signal would pass through the filter largely unaffected.

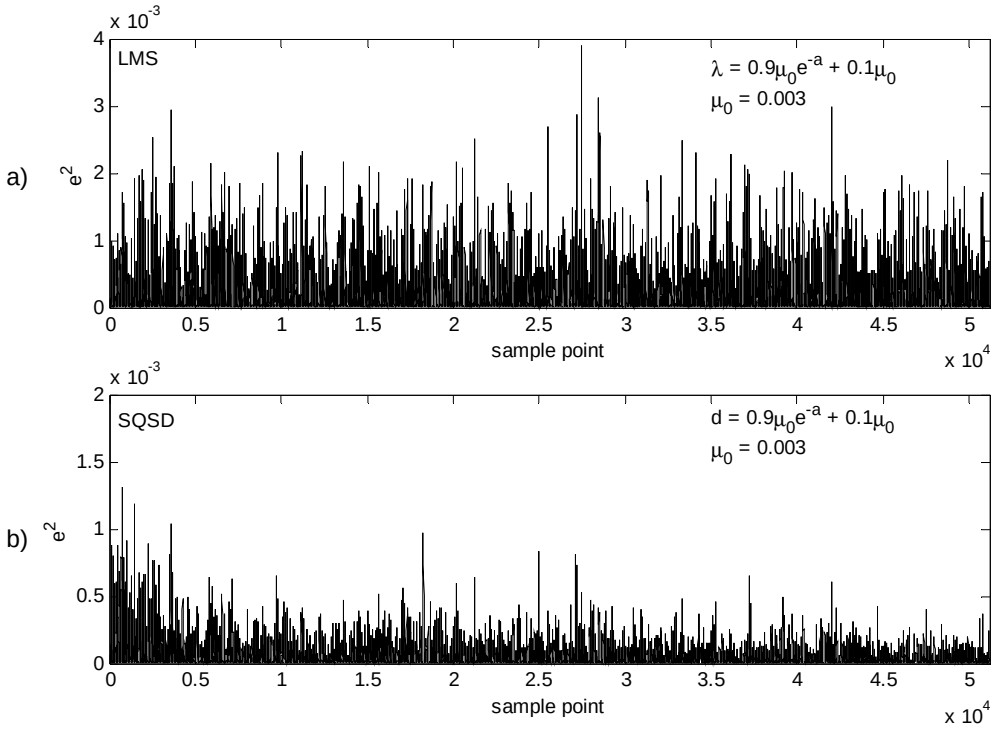

Figure 4.20: LMS and SQSD Squared Prediction Errors

It is thus considered necessary by this researcher to examine not only the squared prediction error, but also the filtered signal, and possibly the filter coefficients from the weight vector. Figures 4.21 a), b) and c) present, respectively, the PSD of the band-pass filtered signal, the PSD of the LMS adaptively filtered signal and the PSD of the SQSD based adaptively filtered signal, all between 150 Hz and 250 Hz and 0 dB to -60 dB.

LMS based adaptive filtering seems to have raised the level of some of the most prominent peaks in the spectrum. It is however also clear that the noise floor between prominent peaks has been raised. Taking into account the lack

of evidence of convergence in the squared prediction error, no clear diagnosis of gear damage can be made from examining the PSD of the LMS filtered signal. It would appear that the LMS filtering operation did indeed fail to converge satisfactorily.

Spherical quadratic steepest descent based adaptive filtering has left the most prominent peaks in the PSD of figure 4.21 c) largely unaffected; specifically the peaks immediately surrounding the gear mesh frequency of 200.7 Hz. It has to be noted that the overall noise floor has however been slightly raised, comparing the band-pass filtered only signal of figure 4.21 a) to the SQSD filtered signal of figure 4.21 c). Certain components surrounding the gear mesh frequency have been emphasized. The noise floor in the immediate vicinity of the gear mesh frequency has been lowered somewhat or left unchanged at worst. The change in the PSD is however small, and inconclusive. Clear damage identification from this PSD may still be considered hazardous.

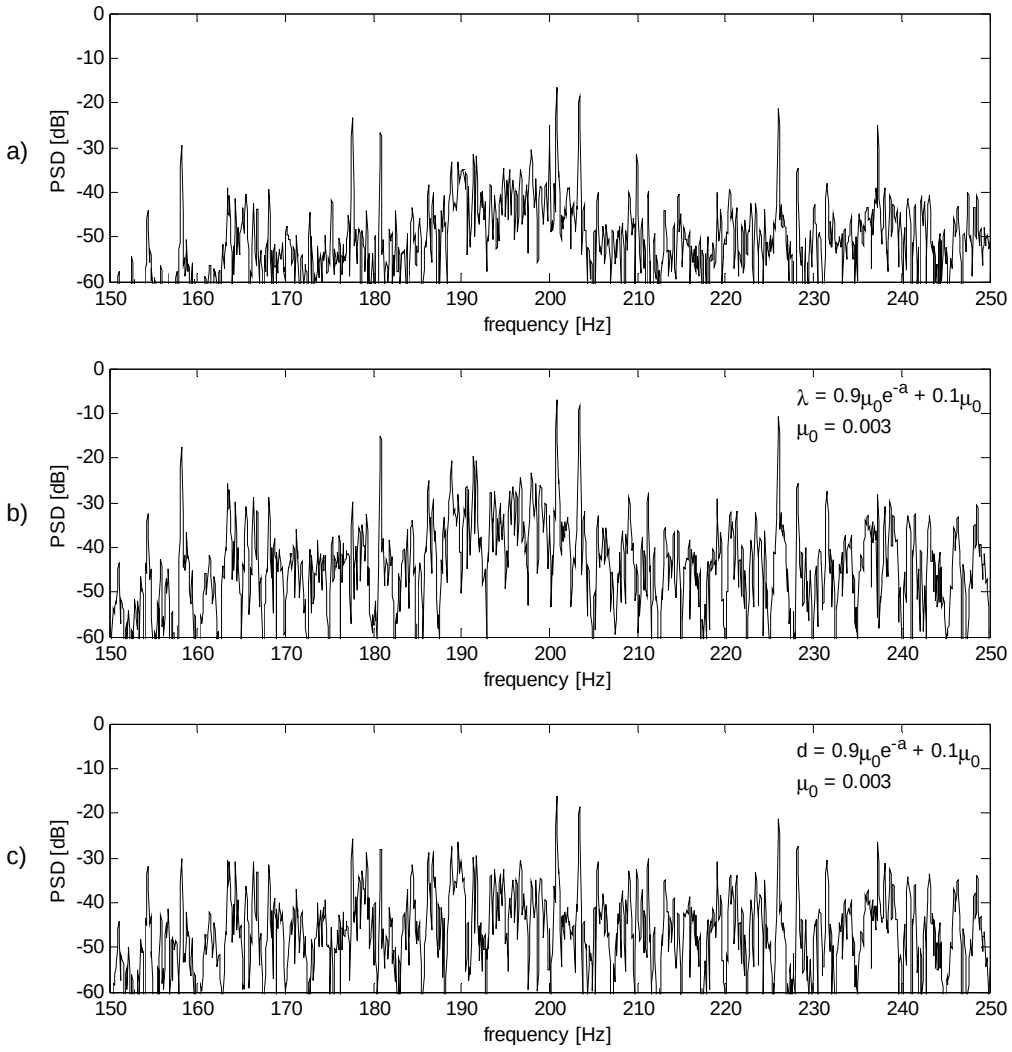

Figure 4.21: PSD of Band-Pass Filtered Signal, 150 Hz – 250Hz, 0 – 60dB

Time frequency methods, and the associated energy method of Loutridis (Article in Press), may still provide a viable alternative to spectrum analysis for the purpose of damage identification. As the data analysed here has not been order tracked or averaged in any way, evidence of speed and load variations should be observable when examining the data in the time domain.

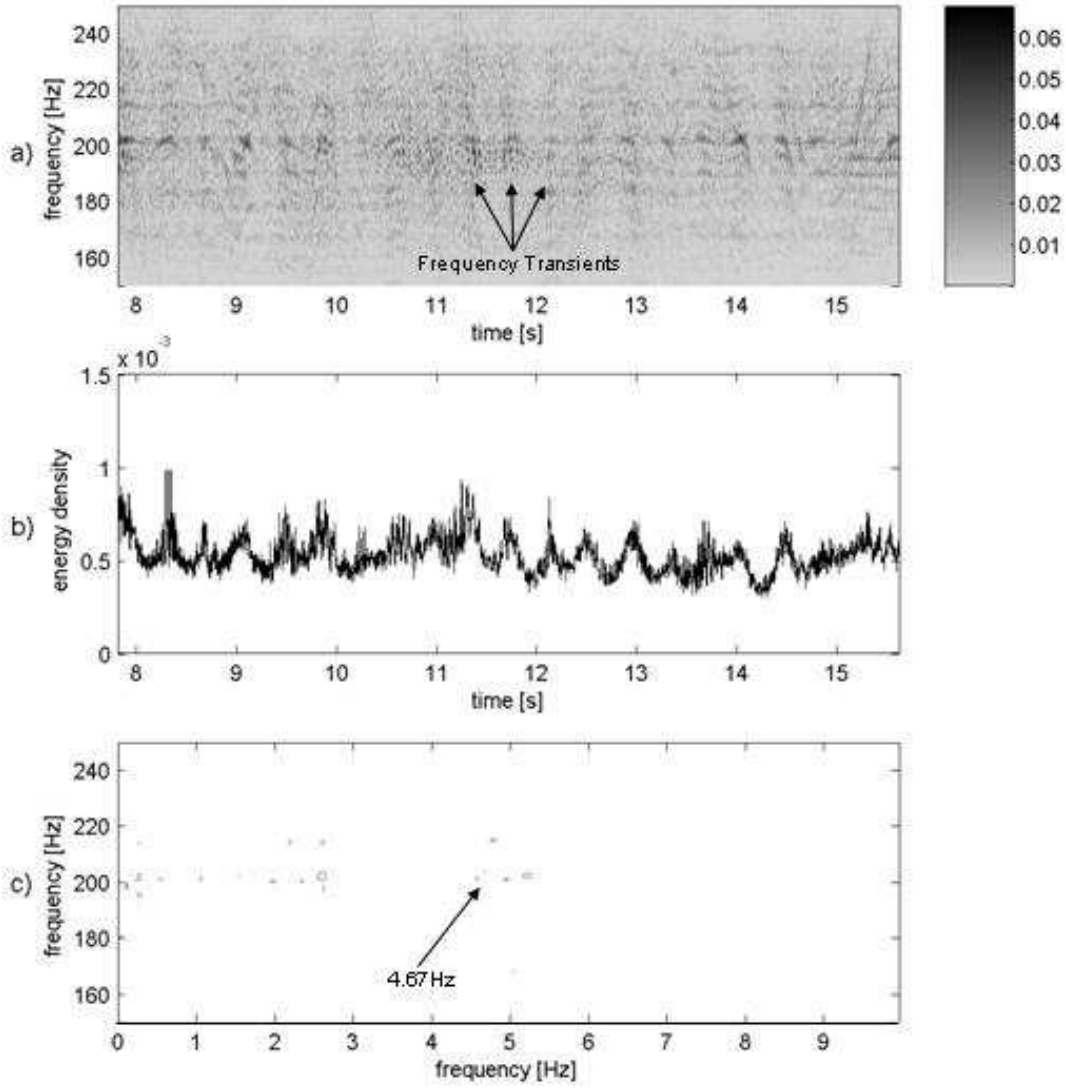

Figure 4.22: Pseudo Wigner-Ville Distribution, SQSD Filtered signal

End effects may be present in the signal as a result of the conventional and adaptive filtering operations undertaken. To overcome this difficulty, a portion of data in the middle of the total record will first be examined. This will ensure that possible end effects, associated with the filtering operations, are eliminated from the portion of data under consideration. Figure 4.22 a) displays the pseudo Wigner-Ville distribution computed from the band-pass filtered data, between 7.8 s and 15.6 s. This time interval is contained within the interval between the 20 000th and 40 000th sample points, which is the

interval that was used for computing all the PSDs previously presented. Figure 4.22 b) and c) display respectively the instantaneous energy density and the results of a frequency analysis performed along the time axis of each frequency of the Wigner-Ville distribution.

In the portion of the Wigner-Ville distribution between 11 and 12 seconds there seems to be evidence of wide-band transient frequency content, possibly associated with the transient events characteristic of gear failure phenomena. In the case under consideration, a gear tooth was removed from one of the gear wheels, and one would expect to see evidence of a shock as this tooth moves through the meshing region. Although evidence of wide-band frequency transients is present at other time intervals as well, specifically the 11 to 12 second interval will be considered here.

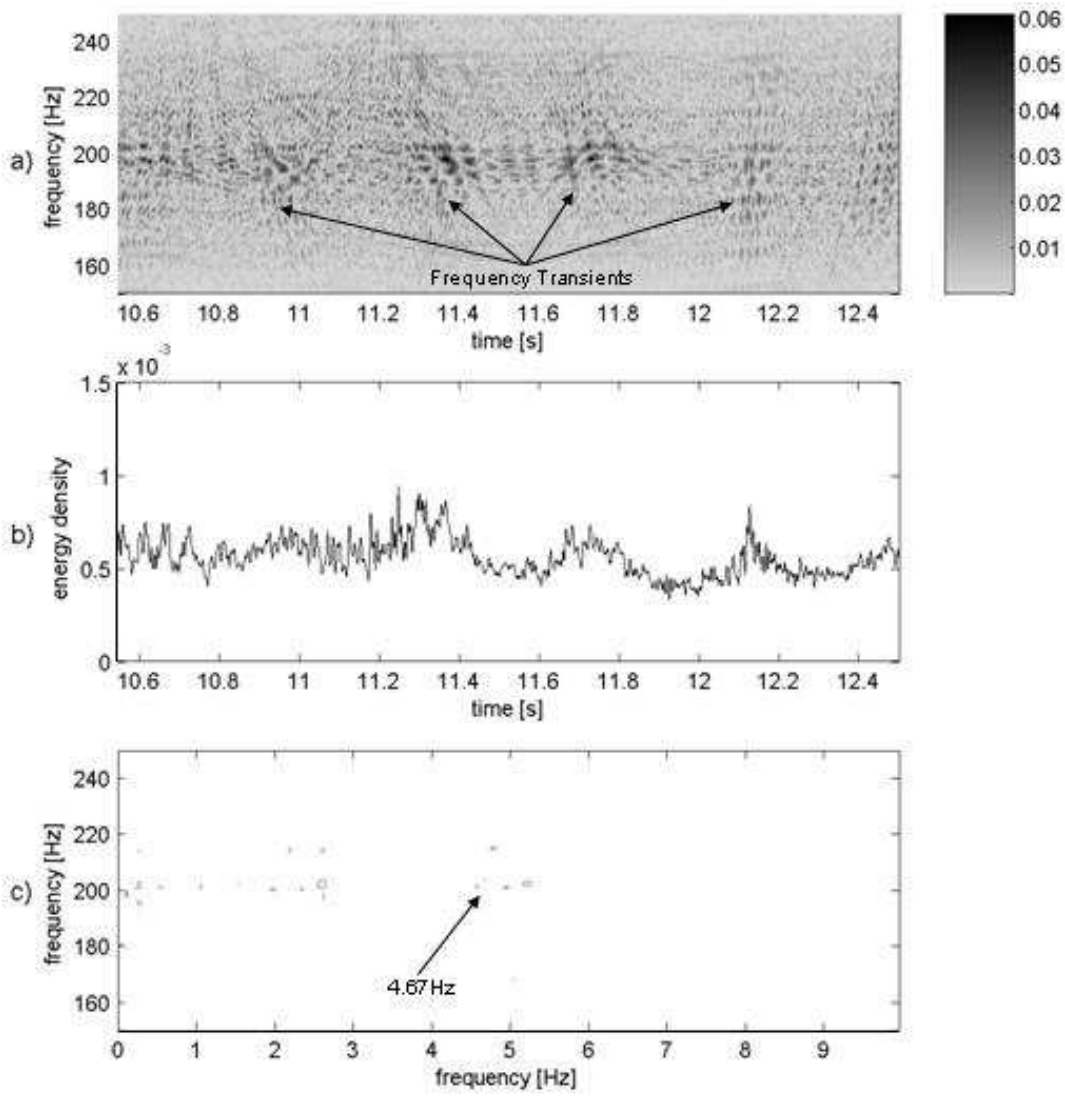

Figure 4.23: Pseudo Wigner-Ville Distribution, SQSD Filtered Signal

Figure 4.23 a) presents the pseudo Wigner-Ville distribution surrounding the 11 to 12 second interval identified. Evidence of transient events are observable at time of 10.95 s, 11.38 s and 11.7 s. From the input shaft frequency of 4.7 Hz (table 4.3), the period expected between successive events associated with damage to a single gear tooth can be computed as the reciprocal of the shaft frequency, equal to 0.213 s.

The separation between the two events at 10.95 s and 11.38 s is equal to twice the shaft rotation period, while the separation between 10.95 and 11.7 s is approximately equal to four times the shaft rotation period of 0.213 s. Considering also the speed variation over this period, evident on the pseudo Wigner-Ville distribution as the variation of the high energy band with time around 200 Hz, it seems feasible that the transients identified are indeed related to damage to one of the gear teeth.

Frequency analysis of the pseudo Wigner-Ville distribution along the time axis reveals that in the meshing frequency range there is indeed activity around the shaft rotation frequency of 4.67 Hz (approximately 4.7Hz). The frequency analysis results are shown in figure 4.23 c). The analysis entails FFT analysis of each frequency band, over the time axis, to resulting in the graph showing frequency on both axes.

Considering the instantaneous energy density criterion suggested by Loutridis (Article in Press), shown in figure 4.23 b), peaks are observed at 11.38 s and 11.7 s. It is however hard to clearly distinguish a prominent peak at 10.95 s. In this case it is then evident that the energy criterion in isolation will not provide a firm basis for reliable fault diagnosis.

4.4 Epicyclic Gearbox Test Bench

In addition to the amplitude and phase modulations found in conventional gear spectra, epicyclic gearboxes exhibit modulations of the carrier wave related to the motion of the planetary gears relative to the stationary observer location, termed planet-pass modulation by Forrester and Blunt (2003). Complex, multi-stage epicyclic gearboxes are common in the aerospace industry, in both aeroplane and helicopter transmissions. In order to develop a strategy for the monitoring of time domain gear vibration data of epicyclic gearboxes, an experimental bench was designed and constructed for the purpose of this work.

4.4.1 *Expected Vibration from Epicyclic Gearboxes*

Numerous publications detail vibration measurements obtained from epicyclic gearboxes. Notable contributions were made by McFadden and Smith (1985) and McFadden (1991).

McFadden and Smith (1985) propose an explanation for the asymmetry of the modulation sidebands about the tooth meshing frequency of epicyclic gearbox vibration signals. The principal component of the observed spectrum of the epicyclic gearbox vibration may be somewhat removed from the meshing frequency. Complete suppression of the vibration component at the tooth meshing frequency has been observed. Different planet gears in the same system result in different phase angles relative to the first planet gear. The relationships between the different phases produced by the planets were shown to account for the asymmetry of the observed spectrum.

The phasor sum of the different phase spectra is given by:

$$Q_{mr} = \sum_{i=1}^{N} P_i\left(mZ_a + r\right) \tag{4.2}$$

where: P_i : phase angle of planet gear i
m : harmonic number
r : sideband number
Z_a : number of teeth on annular gear

The frequency at which the sidebands may be observed is given by:

$$f_{mn} = \left(mZ_a + n\right)f_c$$
$$\because f_c = \frac{Z_s}{Z_s + Z_a} f_{sg} \tag{4.3}$$
$$\therefore f_{mn} = \left(mZ_a + n\right)\frac{Z_s}{Z_s + Z_a} f_{sg}$$

where: f_c : carrier rotation frequency
f_{sg} : sun gear rotation frequency
Z_s : number of teeth on sun gear
Z_a : number of teeth on annular gear

Sidebands hence occur at some multiple of the planet carrier rotation frequency away from the tooth meshing frequency.

Modulation of the signal from a single planet gear occurs as a result of the motion of the planet gear relative to the measurement position. This occurrence is purely a result of the motion of the planetary gears relative to the measurement position, and is not a characteristic of the pure meshing signal of the planetary gears. As the planet gear moves toward the vibration transducer the signal increases, reaches a peak when the gear is closest to the transducer position and then decreases as the planet recedes. Modulation of the individual planet gear signal hence occurs at the frequency of the carrier rotation (McFadden, 1991). When examining a vibration signal obtained from a planetary gearbox, modulation of the carrier signal will thus appear at the planet pass frequency, equal to the product of the planet carrier rotation frequency and the number of planetary gears, assuming equal spacing of the planetary gears.

Defects on a single tooth will show up at a fault frequency equal to the rate at which the faulted tooth contacts the annular gear, or sun gear. Transmission path effects are however more likely to mask the fault showing up from contact with the sun gear, assuming that the measurement position is on the annular gear. The rate at which a faulted tooth will contact the annular gear can be computed as the product of the carrier rotation frequency and the ratio of planet gear teeth to annular gear teeth, or as the sum of the planet gear rotation frequency and the planet carrier rotation frequency (McFadden 1991; Forrester & Blunt 2003):

$$\begin{aligned} f_a &= \frac{Z_a}{Z_p} f_c \\ &= f_c + f_p \\ &= \frac{f_{sg}}{Z_a/Z_s + 1} \cdot \left(\frac{Z_a}{Z_p} \right) \end{aligned} \tag{4.4}$$

where: f_a : planet to annulus gear corresponding tooth mesh frequency
f_c : carrier rotation frequency
f_{sg} : sun gear rotation frequency
Z_s : number of teeth on sun gear
Z_a : number of teeth on annular gear
Z_p : number of teeth on planetary gear

The meshing frequency f_m can be computed as follows:

$$f_m = Z_s\left(f_{sg} - f_c\right) = Z_s f_{sg}\left(1 - \frac{1}{Z_a/Z_s + 1}\right) \tag{4.5}$$

Mechanical unbalance, misalignment and other defects show up in the vibration spectrum at the shaft frequency of rotating components. Shaft frequencies in an epicyclic gearbox are related to the input shaft, the output shaft – usually connected to the planet carrier, and the planetary gear rotation frequency.

In summary, for an epicyclic gearbox one expects to see a vibration signal centred about the meshing frequency, amplitude and phase modulated by functions synchronised to the planet gear rotation frequency. As a result of the fixed observer position, the measured signal will be further modulated at the planet pass frequency.

4.4.2 Experimental Goal

Damage detection on epicyclic gearboxes is the ultimate goal of the algorithms developed during the course of this work. Exposure to an epicyclic gear vibration environment is thus essential. A multi-machine environment is further required in order to more closely simulate the application environment on aircraft.

Both undamaged and damaged condition data were generated during these tests. Undamaged condition testing established a base for the identification of damage later on. The damaged condition tests were run at comparable load and shaft frequency to the undamaged condition's tests.

Only the constant load and constant speed cases were considered. Although different speed and load combinations were considered, the load was always applied such that it would produce significant vibration signals.

Time frequency methods, specifically the spectrogram and Wigner-Ville distribution, as well as the instantaneous energy density computed from the time-frequency methods, were used in attempts to identify damage. The effect of the adaptive filtering algorithms on the effectiveness of the damage identification methods was investigated.

4.4.3 Experimental Setup

A new Epicyclic Gearbox Test Bench was designed and built for the purpose of the experimental portion of this work. A multi-gearbox, epicyclic gearbox test facility, with load and speed control was constructed. Speed control is achieved through a 3kW DC motor with control circuitry. Load is provided

on the system by a hydraulic gear pump, combined with an electro-hydraulic pressure control valve.

The system was designed using a modular approach, since it would be necessary to remove components from the system to seed damage, or monitor wear. The design allows for the easy removal and re-insertion of any system component, with features that simplify mechanical alignment of the system modules. Alignment in the vertical plane is obtained by the use of pre-cut shims. In the horizontal plane, a mechanism was designed which allows the components to be securely oriented by means of set screws.

The motor and gearboxes are mounted on a horizontal surface, parallel to the axes of the shafts. The gear pump's design intends mounting on a vertical surface, perpendicular to the axis of the input shaft. The mounting fixture of the gear pump is designed such that horizontal and vertical translation of the pump is achieved by adjustment of set screws, to simplify and speed up the alignment process. Torque transmission between each system module is achieved through rigid spider couplings.

During the design process, various conceptual designs were evaluated. The best design was chosen using criteria of versatility, simplicity and cost. Manufacturing of components and assembly all took place in house, except for the hydraulic sub-system. In-house manufacturing included the mounting fixtures of the gearboxes, motor and hydraulic pump, and the vibration isolation table on which the test bench is secured. The hydraulic sub-system was conceptually designed by the author, but detail design and manufacturing were contracted out to a regular and trusted supplier.

Assembly of the 3kW DC machine and associated control circuitry was entrusted to an external supplier. The machine is equipped with a forced ventilation system. Control circuitry consists of a sophisticated reconfigurable feedback control drive system, capable of using a shaft encoder mounted on the motor for feedback.

Load and speed control were required for the test bench. Although it was intended that load and speed would remain constant for the purpose of this work, future work will focus on variable speed and variable load scenarios. Speed control is achieved by the DC machine and associated drive system. By varying the pressure in the hydraulic system, the torque required to turn the hydraulic gear pump is varied and load control is achieved. Pressure variation in the hydraulic system is achieved by a proportional pressure relief control valve, with integrated control electronics. Both motor and gear pump are capable of accepting external control signals, so that load and speed control can be actuated from an external control source.

The working surface was defined by the motor's power surface, and the hydraulic components' operational ranges. The valve activation pressure was a limiting factor on the one hand, while the maximum system pressure limited operation at the opposite end. Figure 4.24 displays the working surface of the test rig, ignoring individual component efficiencies.

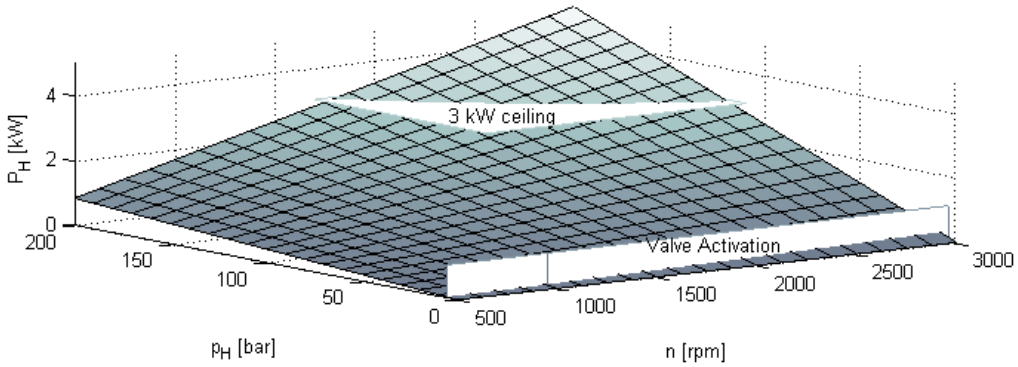

Figure 4.24: Hydraulic Performance Surface

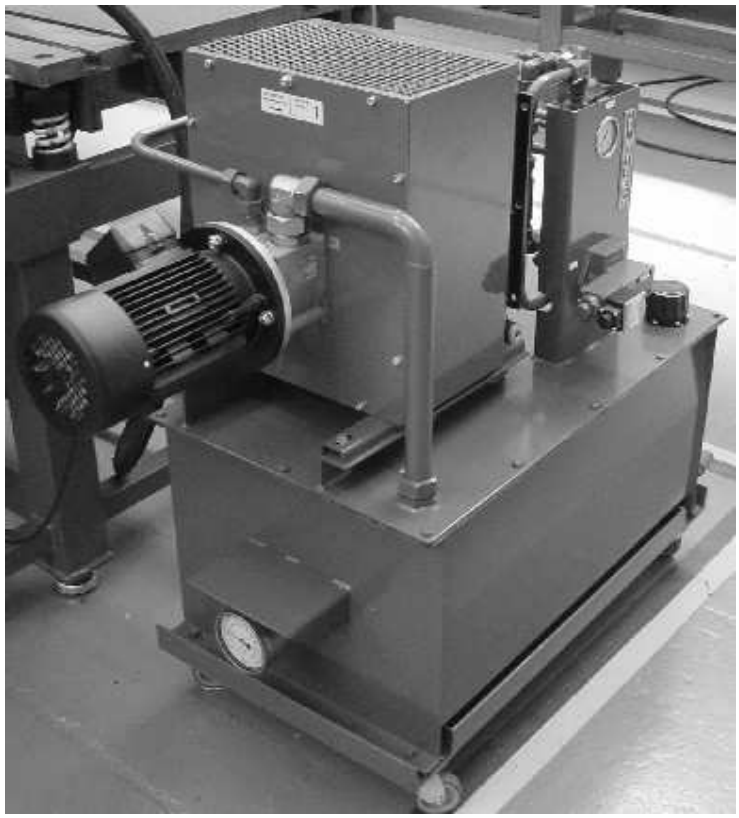

Figure 4.25: Hydraulic Power-Pack Module

Hydraulic components, with exception of the hydraulic gear pump, were assembled in a hydraulic power-pack module. The proportional pressure relief control valve was included in this module. The module includes a forced draught cooling system, capable of dissipating 3 kW by cooling the

hydraulic fluid. Connection between the power-pack and the gear pump is by quick-connect flexible high pressure hydraulic hosing. The power-pack module is shown in figure 4.25.

The test bench was constructed on an inverted T-slot base, suspended on springs to isolate it from ambient vibrations. Figure 4.26 shows a photograph of the test bench set up in the Sasol laboratory, at the University of Pretoria. The T-slot base allows for quick approximate alignment of the system modules. Thereafter, precise alignment is achieved by using the various mechanisms designed into each module. The T-slot tables were mounted on a newly constructed table, purpose designed.

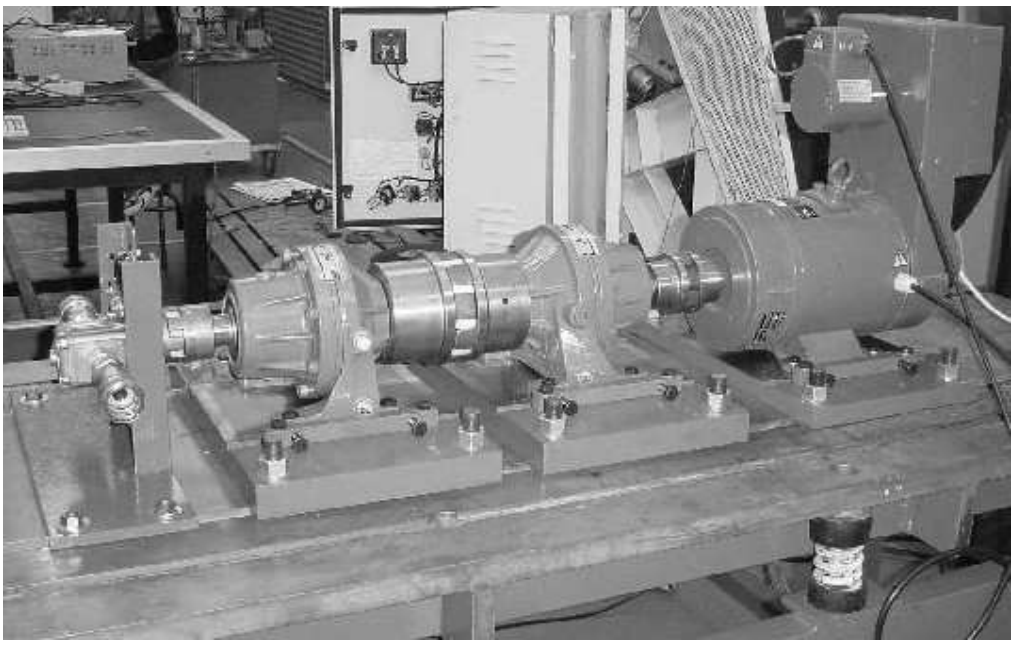

Figure 4.26: Epicyclic Gearbox Test Bench

Figure 4.27 displays a schematic representation of the test system, along with measurement equipment. Notably in this case analogue low-pass filters were employed before digitization took place. It was intended that over sampling of data would be undertaken, and hence it was necessary to eliminate unwanted frequency content from the vibration signals by low-pass filtering.

Measurement hardware consisted of three accelerometers, a four-channel ICP amplifier for the accelerometers, a four-channel data acquisition unit and a personal computer. The accelerometers used were of the piezo-electric type, with a nominal sensitivity of 500mV/g. As before the Siglab® data acquisition unit incorporated anti-aliasing filters, and performed the analogue-to-digital conversion function. Higher frequency content was removed from the accelerometer signals by using eighth order Butterworth analogue low-pass filters with cut-off frequency of 300Hz – well below that of the anti-aliasing filters employed in the data acquisition hardware.

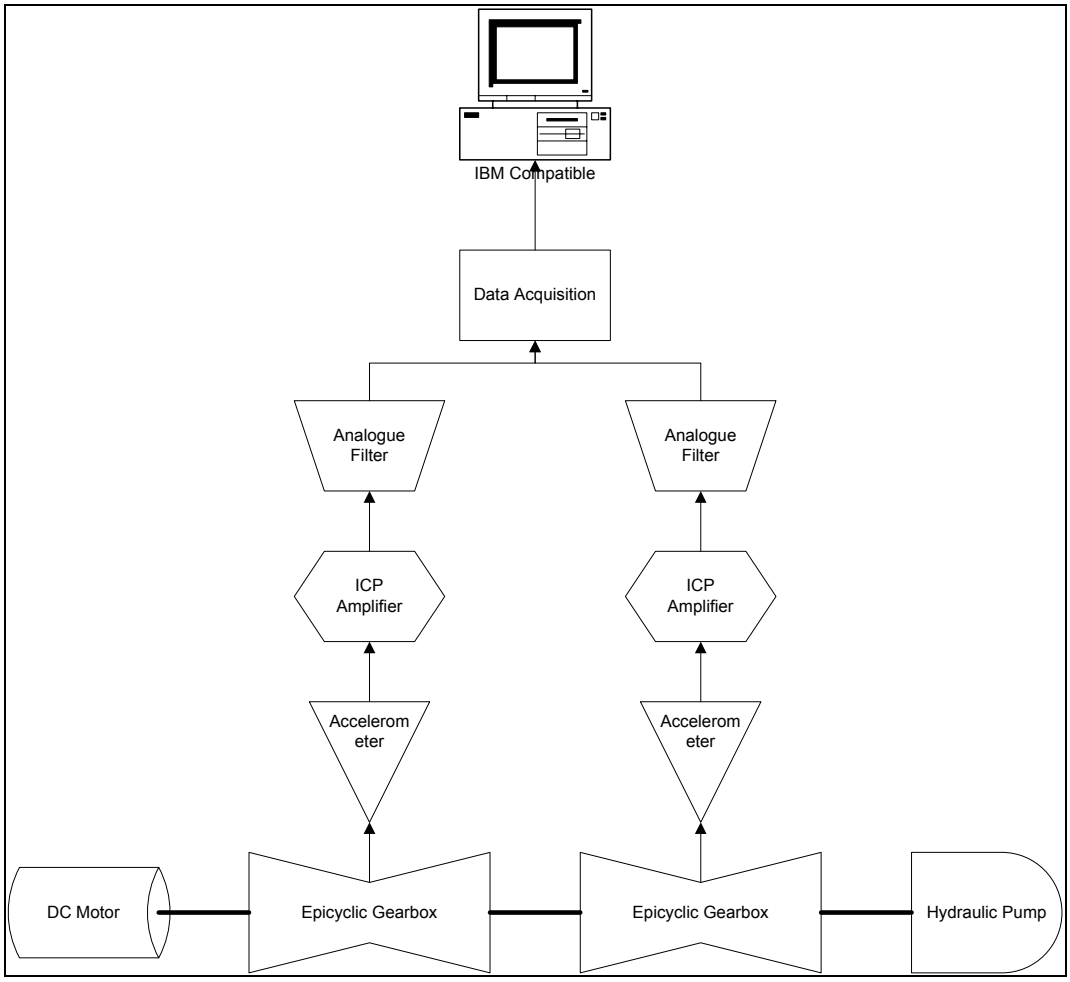

Figure 4.27: Epicyclic Gearbox Test Bench Schematic

The primary accelerometer was mounted in the vertical plane on the second gearbox, and connected to channel 3 on the analyzer. A second accelerometer, connected to channel 2 on the analyzer, was mounted in the horizontal plane, also on the second gearbox. Data from this accelerometer was not used. The third accelerometer was mounted on the first gearbox, in the vertical plane, and connected to channel 1 on the analyzer.

Damage was seeded on a single tooth of one of the planetary gears. A small amount of material was removed from both sides of the tooth by filing away the flank of the tooth. Figure 4.28 shows the damaged gear tooth. A small notch was inserted on the edge of this tooth to ensure ease of identification.

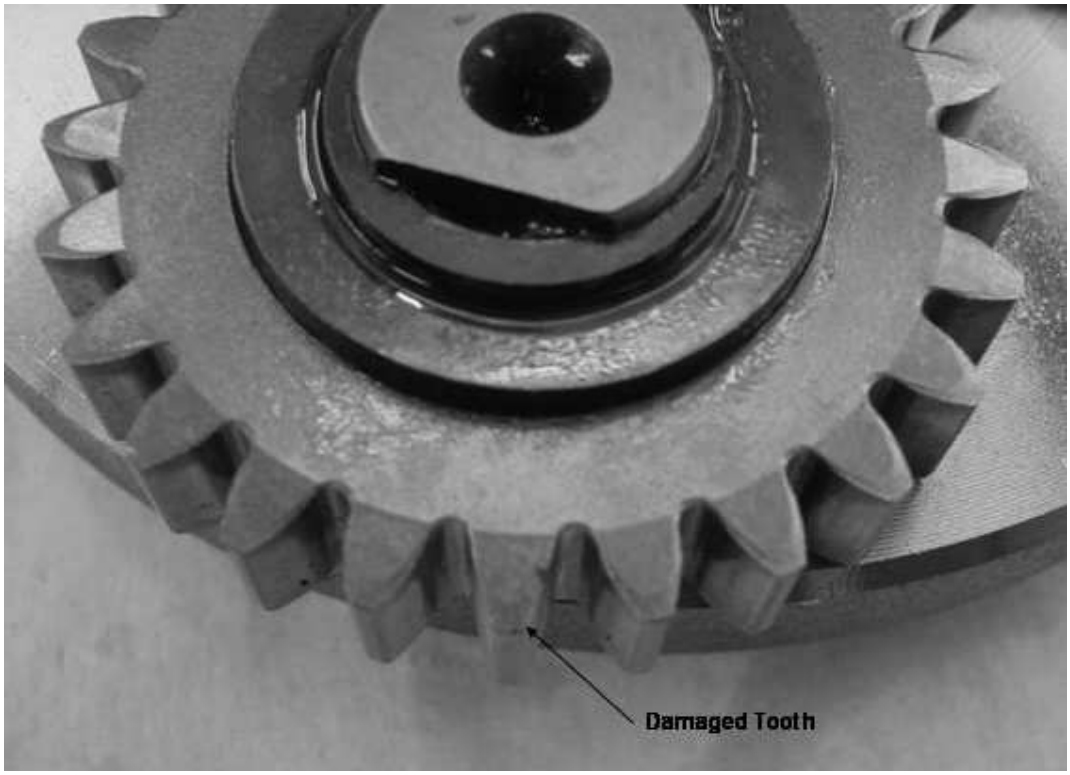

Figure 4.28: Damaged Planetary Gear

4.4.4 *Experimental Procedure*

Damage identification on epicyclic gearboxes is the main aim of this experimental phase. Adaptive algorithms are used to de-noise the vibration data. Time-frequency techniques form the basis of the damage identification methodology applied.

Data was recorded from 3 accelerometers, as discussed under section 4.4.3. Data from the primary data channel – accelerometer mounted in the vertical plane on the second gearbox, was sampled at different sampling frequencies. Irrespective of the sampling frequency, analogue filters were employed to remove higher frequency content from the data. The eighth order Butterworth analogue filters used had cut-off frequencies of 300Hz, well below the cut-off frequency of the built-in anti-aliasing filters of the Siglab® analyzer.

DC offset from zero mean was removed as before by computing a least-square fit of a straight line to the data, and subtracting the resulting function from the data. In an attempt to narrow the spectral content of the signals and "focus" the diagnostic methods on relevant portions of the spectra, band-pass filtering of the signals about the meshing harmonics of interest was carried out. Phase distortion resulting from the digital filtering operations was once again minimized by employing the forward-backward filtering technique of Gustafsson (1996).

After digitization, de-trending and band-pass filtering, adaptive filtering algorithms were applied in order to remove some of the random noise present in the signals. Effectiveness of the adaptive filtering is best judged by examining the time-frequency distributions of the signals. The time-frequency distributions may also at this point be used for the purpose of damage identification.

4.4.5 *Experimental Findings*

Vibration data was collected at different sampling frequencies, and different shaft speed combinations for an undamaged gearbox, as well as a gearbox on which damage had been seeded. The discussion here follows specific data records from the undamaged and damaged conditions, which were judged to be representative of the findings after having examined and processed an ensemble of several data records. Similarity of operating parameters such as load and speed were further considered.

Accelerometer signals were sampled at 5120 Hz, after having been low-pass filtered through an eighth order Butter filter with cutoff frequency of 300Hz. To remove phase distortion introduced by the analogue filter, an LMS based adaptive system identification algorithm was developed. Random data sampled at 5120 Hz and with bandwidth of 2 kHz was used to characterize the filter. A suitable frequency response was obtained from an FIR filter with 4096 coefficients.

Figure 4.29 displays a one second portion of a random signal filtered with the analogue Butter filter, as well as the 4096 coefficient FIR implementation. The curves are not appreciably discernible from each other. In figure 4.30 is shown the first tenth of a second of the same signal. The two signals overlie each other almost exactly.

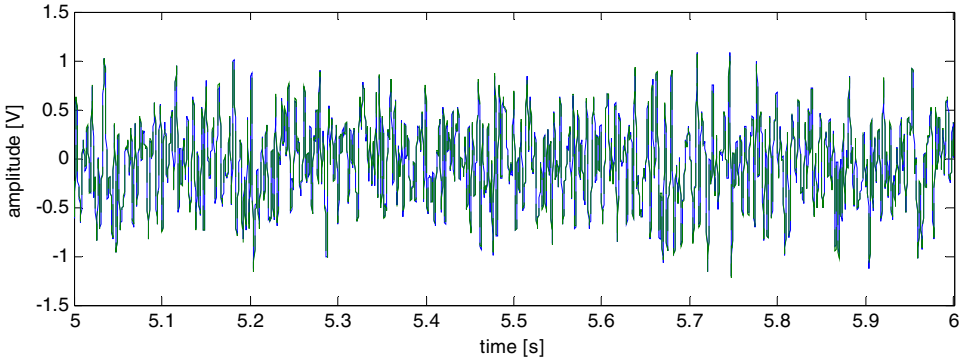

Figure 4.29: Filtered Random Data, 1 s

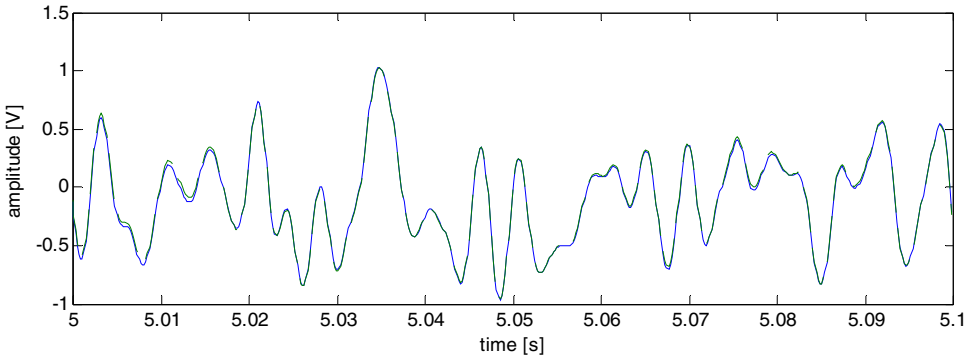

Figure 4.30: Filtered Random Data, 0.1 s

Using the FIR filter obtained, it is possible to employ the forward-backward filtering process described by Gustafsson (1996) in an attempt to remove some of the phase distortion introduced by the analogue filtering operation. The analogue filtered sequence has to be reversed, filtered by the FIR digital filter, and reversed again to complete the non-causal filtering operation.

For the input shaft speeds of 1040 rpm and 1037 rpm for the undamaged and the damaged conditions, the gear mesh frequencies are expected at 186.3 Hz and 185.7 Hz, respectively. Table 4.5 summarizes relevant parameters.

Table 4.5: Epicyclic Gearbox Parameters

	Description	Variable	Value	Units
Gear Set	Sun Gear Teeth	N_s	13	
	Planetary Gear Teeth	N_p	24	
	Annular Gear Teeth	N_r	62	
Undamaged Condition	Sun Gear Shaft Speed		1040	rpm
	Sun Gear Shaft Frequency	f_{sg}	17.33	Hz
	Gear Meshing Frequency	f_m	186.28	Hz
	Planet Carrier Rotation Frequency	f_c	3.00	Hz
	Planet Gear Corresponding Tooth Mesh Frequency with Annulus	f_a	7.76	Hz
	Planet Pass Modulation Frequency	f_{ppm}	9.01	Hz
Damaged Condition	Sun Gear Shaft Speed		1037	rpm
	Sun Gear Shaft Frequency	f_{sg}	17.28	Hz
	Gear Meshing Frequency	f_m	185.74	Hz
	Planet Carrier Rotation Frequency	f_c	3.00	Hz
	Planet Gear Corresponding Tooth Mesh Frequency with Annulus	f_a	7.74	Hz
	Planet Pass Modulation Frequency	f_{ppm}	8.99	Hz

The raw data was found to contain a DC offset. This may be due to leakage currents resulting from induced currents on the test bench, or as a result of imperfections in the driving circuitry of the accelerometer. A further plausible explanation may be the lack of a common electrical earth point

between the measurement equipment. The offset was removed by de-trending the data by computing a least-square fit of a straight line to the data, and subtracting the resulting function from the data. The piezo-electric type accelerometers used are incapable of measuring down to zero frequency associated with direct current operation.

At this point the signals contained data in the frequency range from 0 Hz to just above the cutoff frequency of the analogue low-pass filter at 300 Hz. The data was band-pass filtered about the gear mesh frequency between 150 Hz and 250 Hz. An FIR filter with 280 coefficients was used, designed to have -60dB attenuation in the stop bands, less than 0.1dB ripple in the pass band and 50 Hz roll-off bands. The forward-backward filtering implementation discussed by Gustafsson (1996) was employed to minimize phase distortion resulting from the filtering operation.

The band-pass filtered signals' power spectral densities, shown in figure 4.31, show that frequency content in the signal above 290 Hz and below 110 Hz have largely been attenuated by the filtering process. The spectra are however still relatively noisy and reliable diagnosis of possible fault conditions seems unlikely. Figure 4.31 a) shows the undamaged condition's data, while figure 4.31 b) shows the damaged condition's data.

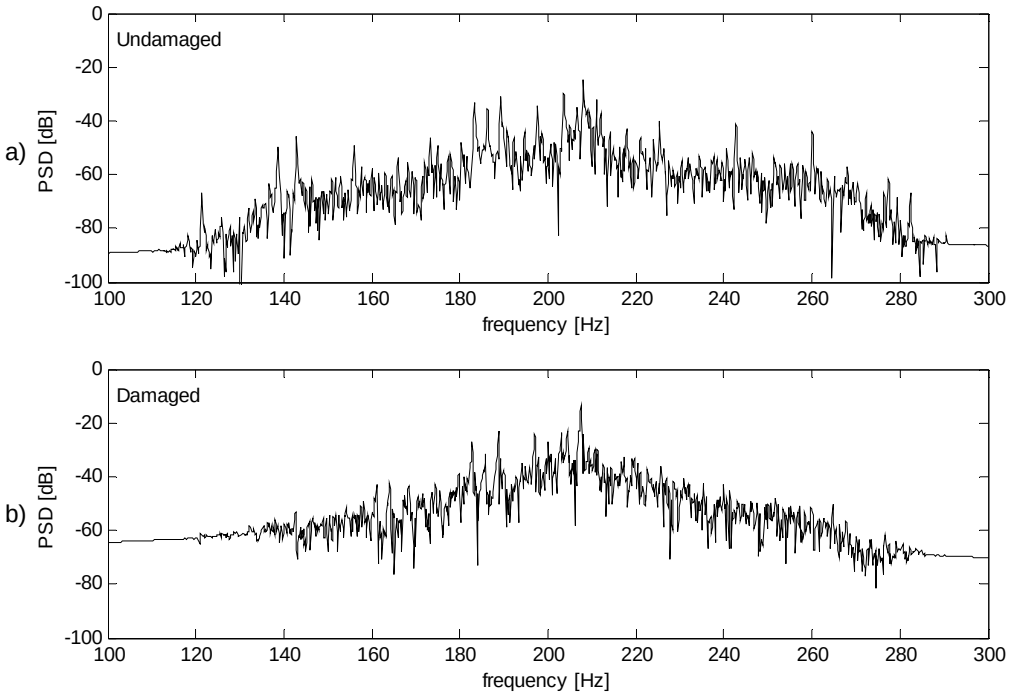

Figure 4.31: PSD of Band-Pass Filtered Signals

Examining the power spectral densities of the band-pass filtered signal computed over the entire signal length for spectral components associated with gear meshing confirms that diagnosis will be difficult. Figure 4.32 shows the PSDs of the signal, with the frequency ranges selected around the first harmonic of the gear mesh frequency to aid interpretation. Solid lines

from -60 dB to -20 dB indicate positions on the frequency axis where activity would be expected, considering arguments laid by McFadden and Smith (1985). The long-short dashed line indicates the epicyclic gear meshing frequency, which is not expected to be visible. Short dashed lines show sideband frequencies where no activity is expected. The solid line from -60 dB to 0 dB indicates the gear meshing frequency of the gear pump used to apply load to the system, and the long dashed lines indicate the positions of its expected sidebands.

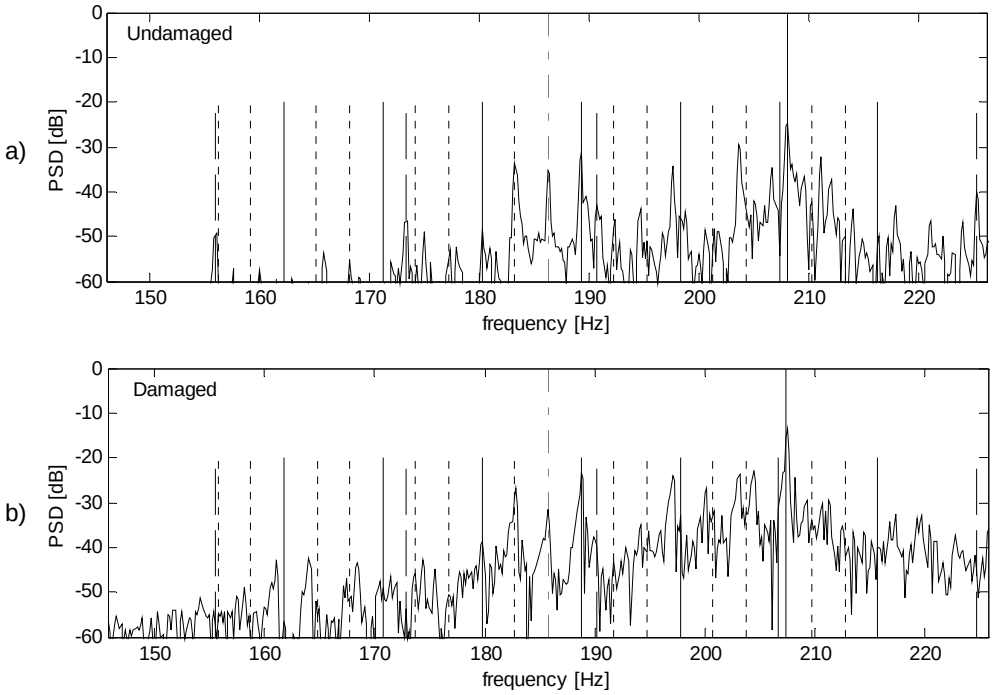

Figure 4.32: PSD of Band-Pass Filtered Signals, First Harmonic

Table 4.6 lists the gear mesh frequencies of the epicyclic gearbox and the gear pump, as well as the frequencies of the sidebands that are expected. The most prominent peak in both cases is that associated with the meshing frequency of the hydraulic gear pump. Activity at the gear pump's sideband frequencies is clearly discernible in the undamaged case of figure 4.32a), but less so in the damaged case of figure 4.32 b).

For the purpose of adaptive filtering, the value of the step size parameter of the LMS algorithm, known also as the forgetting factor λ, may be determined from an autocorrelation matrix of the data. Considering graphs of the step size, denoted as λ in the figures, divided by the autocorrelation matrix dimension dim(R), shown in figure 4.33, indicated that step sizes λ may be estimated from moderately sized autocorrelation matrices R. The step size was selected as λ=0.005 at dim(R) = 500 for the undamaged case, and λ=0.05 at dim(R) = 500 for the damaged case.

Table 4.6: Gear Mesh and Sideband Frequencies

	Epicyclic		Conventional Gear Pump		
	Undamaged	Damaged	Undamaged	Damaged	Units
Gear Mesh Frequency	186.3	185.7	208.0	207.4	Hz
Visible Sidebands	162.2	161.7	156.0	155.6	Hz
	171.3	170.8	173.3	172.8	Hz
	180.3	179.7	190.7	190.1	Hz
	189.3	188.7	225.3	224.7	Hz
	198.3	197.7			Hz
	207.3	206.7			Hz
	216.3	215.7			Hz

Even though the ratios of λ / dim(R) had not clearly stabilized at these points, the computational burden of enlarging the dimension of the autocorrelation matrix becomes excessive for dim(R)>500. It was also observed that the size of the largest eigenvalues of the autocorrelation matrix tended to increase with the dimension of the autocorrelation matrix. Choosing the step size parameter from a smaller autocorrelation matrix would thus tend to err on the conservative side.

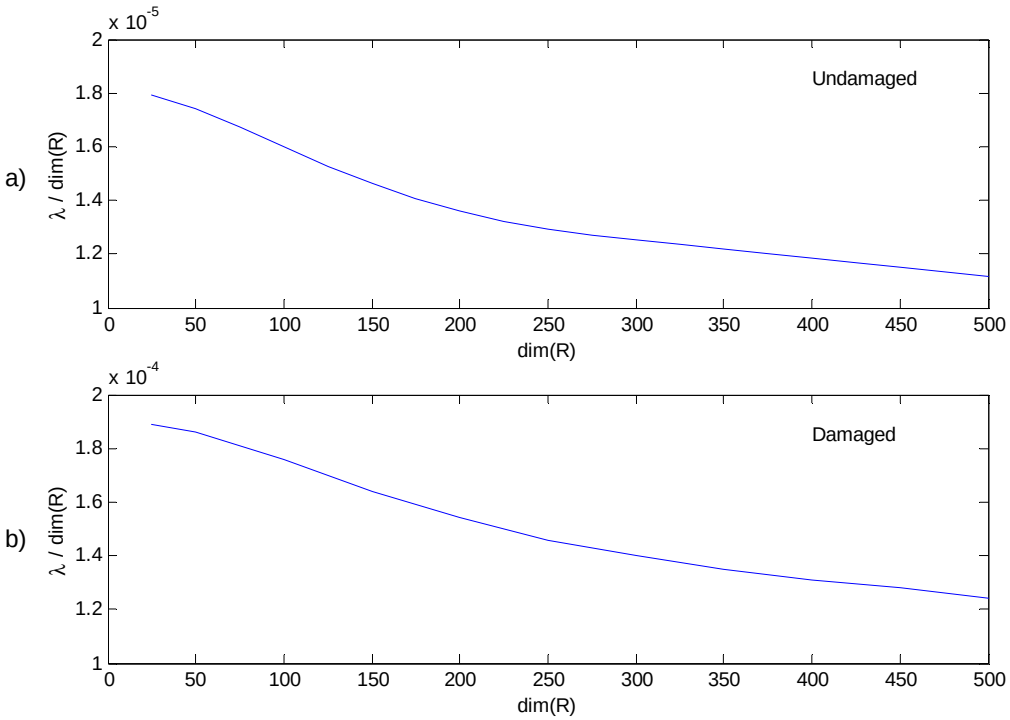

Figure 4.33: Forgetting Factor λ vs. Autocorrelation Matrix Dimension

Using the chosen values for the step size parameters, an LMS based adaptive line enhancer was used in attempts to remove the noise component from the measured data. Examining the squared prediction errors depicted in figures

4.34 a) and c) for the undamaged and damaged cases respectively, it is not clearly evident that the LMS algorithm converged in either case.

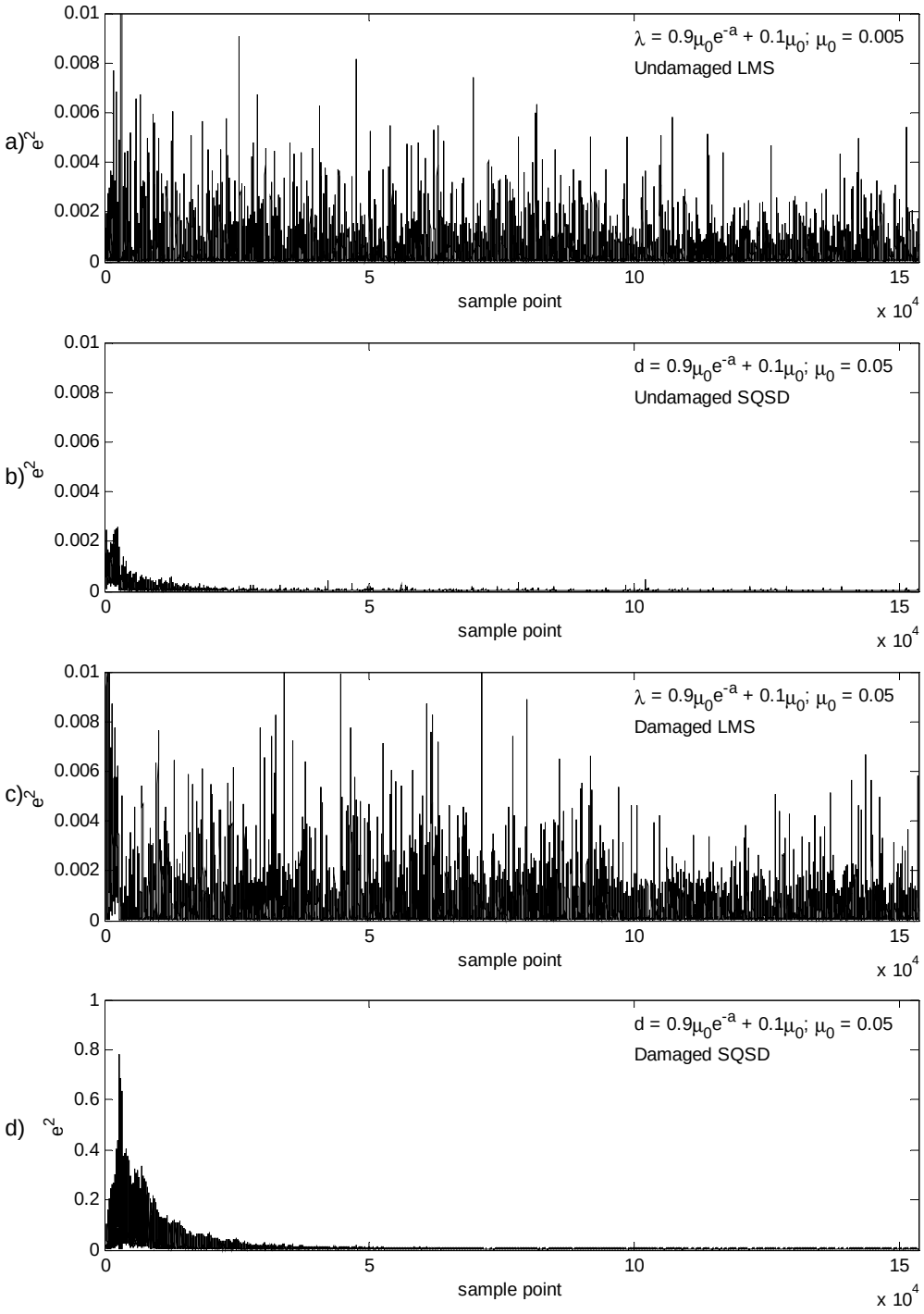

Figure 4.34: Squared Prediction Errors

Although there appears to be a slight decrease in prediction errors over the signal lengths, this is not convincing evidence of convergence. This may indicate excessively slow convergence however; where the step size parameter was chosen so small that appreciable convergence will take a very

long time to manifest. To disprove this notion, forgetting factors of a single order of magnitude larger for both the damaged and undamaged case, as well as two orders of magnitude larger for the undamaged case were used. The algorithm persisted in showing no appreciable decrease in prediction error.

As an alternative to the LMS based adaptive line enhancer, a Spherical-Quadratic Steepest Descent based algorithm was used for the same purpose of de-noising the data. The squared prediction errors for the step size parameter d=0.05 is shown in figures 4.34 b) and d) for the undamaged and damaged conditions, respectively. With d=0.05 there is a very clear decrease in the prediction error of the algorithm in both cases. Using the squared prediction error, it can be concluded from figure 4.34 that the SQSD based ALE did indeed converge in both cases. As before however, convergence should be confirmed by alternative methods, i.e. examination of spectra or time-frequency distributions.

Once more it seems that the SQSD based algorithm has outperformed the LMS based algorithm. The SQSD based algorithm has been found to converge much easier than its LMS counterpart. Some discretion is however still required when choosing the algorithm's parameters. For none of the results presented in this work did the first choice of the step size parameter d yield the best results. Although convergence is easy to attain, a good solution quality is not. Experimentation is still required to fine tune the parameters and obtain a solution of acceptable quality.

From examination of the PSDs of the prediction errors it seems that the LMS algorithm's prediction error contains much of the periodic gear vibration signals from both the epicyclic gearboxes, as well as the gear pump. Figure 4.35 shows the PSDs of: a) the undamaged condition LMS filtered prediction error; b) the undamaged condition SQSD filtered prediction error; c) the damaged condition LMS filtered prediction error and d) the damaged condition SQSD filtered prediction error. The long-short dashed line indicates the meshing harmonic which should be unobservable, the short dashed lines indicate sidebands which should be unobservable and the solid lines from -60 dB to -20 dB indicate sidebands which should be observable, according to McFadden and Smith (1985). The solid line from -60 dB to 0 dB indicates the gear meshing frequency of the gear pump used to apply load to the system, and the long dashed lines indicate the positions of its expected sidebands.

Although the PSDs of the SQSD prediction errors, figures 4.35 b) and d), do in places contain peaks at gear mesh or sideband frequencies, these peaks are smaller than in the case of the LMS algorithm. Less energy from the gear vibration components of interest are therefore present in the SQSD filter's error signal than in that of the LMS filter algorithm.

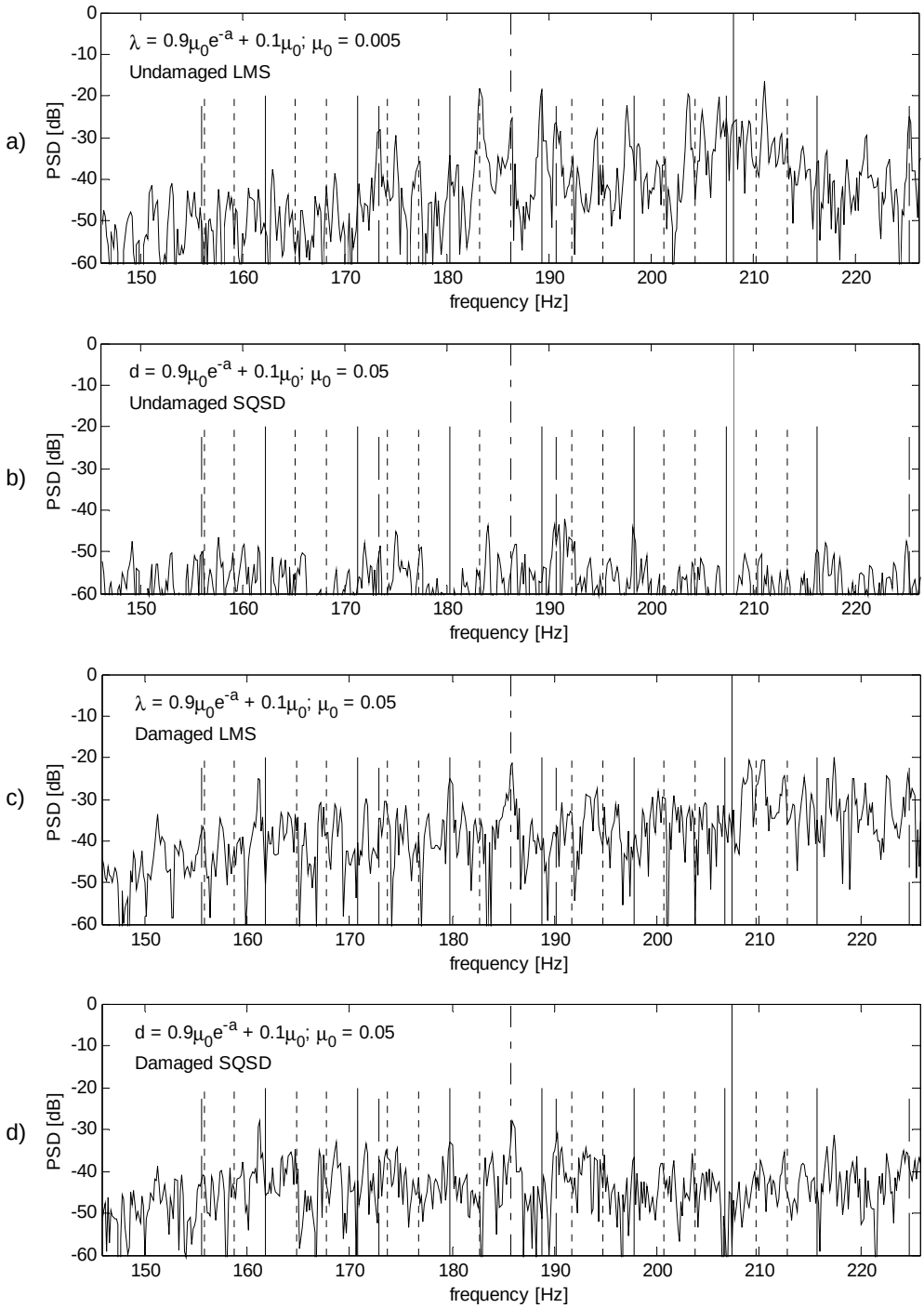

Figure 4.35: ALE Prediction Error PSDs

Comparing the PSD of the LMS filtered undamaged condition signal in figure 4.36 a), with the band-pass filtered signal's PSD from figure 4.32 a), it is evident that the level of the entire signal's PSD has been raised. Although peaks coinciding with gear mesh and sideband frequencies have been raised, the noise floor between prominent peaks has also been raised relative to the peaks. Even though sidebands are observable at some of the frequencies

where they were expected, diagnosis of the gearbox's condition may be hazardous from figure 4.36 a). Many other peaks are visible between the frequencies where sidebands were expected, and strong peaks are visible at frequencies associated with the gear pump gear mesh and sidebands.

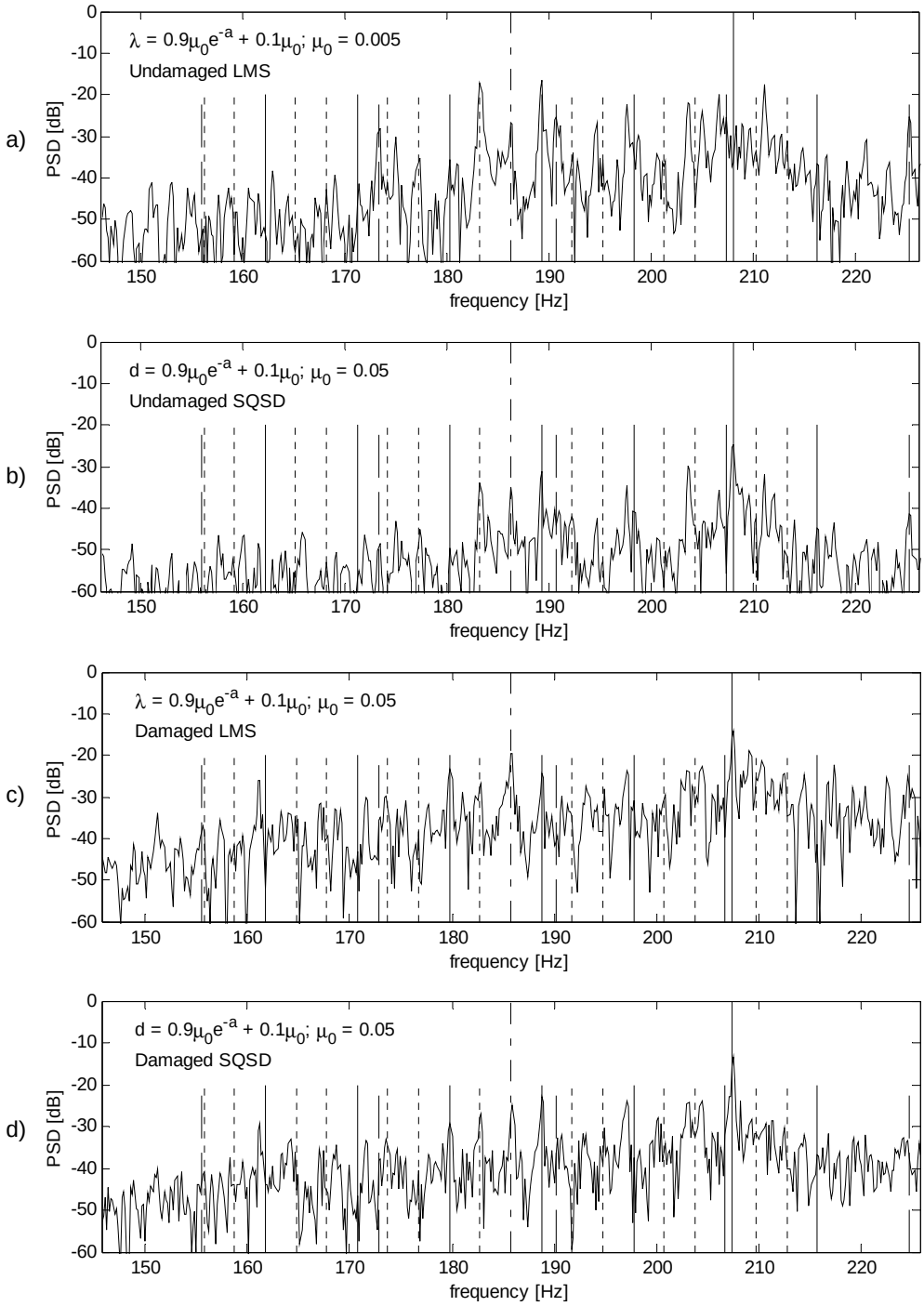

Figure 4.36: ALE Filtered Signal PSDs

LMS based filtering of the damaged condition's signal has similarly resulted in a rise over the entire bandwidth presented in figure 4.36 c), when comparing with figure 4.32 b). The effect is especially evident in the portion

of the PSD below 180 Hz. The gain in signal level has however occurred to the detriment of the diagnostic capacity. Many of the frequencies where activity would be expected show no such activity. Diagnosis of the gearbox's condition from the PSD of figure 4.36 c) would therefore be hazardous. The poor quality of the PSD enforces the conclusion reached from examining the squared prediction error: the LMS adaptive line enhancer has failed to converge.

From a comparison between the PSD of the undamaged condition SQSD adaptive line enhancer filtered signal, displayed as figure 4.36 b), and the undamaged condition band-pass filtered signal's PSD in figure 4.32 a), once again it appears that the level of the entire signal has been raised. In contrast to the LMS filtered case of figure 4.36 a) though, the noise floor has not been raised as substantially, relative to prominent peaks on the PSD associated with meshing phenomena. Although overall there has been a lift in the level of the noise floor, around the meshing frequency of 186.3 Hz the noise floor has stayed low, compared to the peak at the gear mesh frequency. Sidebands of the epicyclic gear mesh frequency at 180.3 Hz and 189.3 Hz have been emphasized somewhat, and are larger relative to the gear pump meshing peak at 208 Hz. The changes are however subtle.

In the lower half of the frequency band shown in figure 4.36 b), peaks associated with sideband frequencies have been emphasized slightly. Considering the sidebands expected around the first harmonic, these are clearly visible at some of the expected frequencies indicated on figure 4.36 b), more so than on the band-pass filtered signal's PSD of figure 4.32 a). In this particular case, judged from the spectra presented here, the SQSD based adaptive line enhancer seems to have delivered superior performance to the conventional LMS based adaptive line enhancer.

SQSD based filtering of the damaged condition's data also indicates a slight advantage. Peaks associated with gear meshing phenomena have been slightly emphasised on the PSD of figure 4.36 d) relative to the band-pass filtered signal of figure 4.32 b). The noise floor has however also been raised slightly. Comparison between the graphs of figure 4.32 and 4.36 once more emphasises the difficulty that would result from attempting to diagnose the gearbox's condition by methods of spectral analysis only. The differences in the spectra are too small to provide any appreciable indication that the machine has experienced damage or deterioration of its condition.

Time-frequency representations, like the spectrogram and Wigner-Ville distribution, are useful when studying time varying spectra. Figure 4.37 shows spectrograms of the band-pass filtered undamaged and damaged condition's signals as a) and c), respectively Figure 4.37 e) shows the instantaneous energy density, as suggested by Loutridis (Article in press). Frequency analyses were performed on the time-frequency representation,

by taking the Fourier transform along the time axis for each discrete frequency. The results are displayed in figure 4.37 b) and d) for undamaged and damaged cases, respectively.

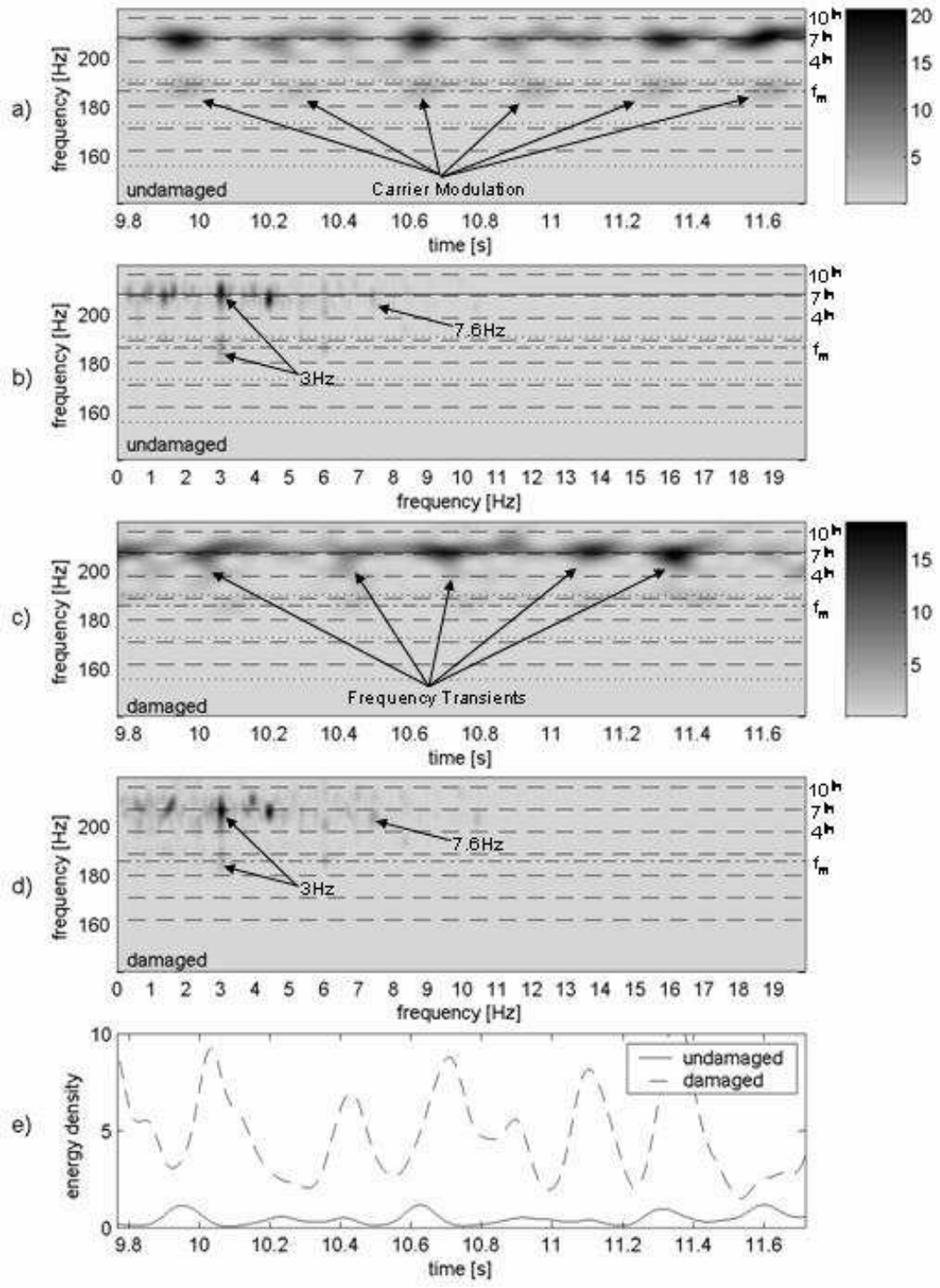

Figure 4.37: Spectrograms of Band-Pass Filtered Signals

The energy band most prominent on the spectrograms is that between the fourth and the tenth sideband of the first harmonic of the epicyclic meshing

frequency, the centre of which lies on the seventh sideband of the epicyclic meshing frequency and on the meshing frequency of the hydraulic gear pump. McFadden and Smith (1985) provide an explanation for the asymmetric spectra often observed from epicyclic gearboxes. In this particular case however, it is the meshing frequency of the hydraulic gear pump that dominates the spectrum.

Darker patches are visible between the first sideband above and second sideband below the epicyclic gear mesh frequency, f_m, on figure 4.37 a) and c), although more clearly in the case of figure 4.37 a). These patches coincide with the planet carrier rotation frequency (table 4.5), and show up in the frequency analyses of the spectrograms, figures 4.37 b) and 4.37 d), at 3 Hz. Darker patches are visible in the band between the first sideband above and second sideband below the epicyclic meshing frequency, as well as on the gear pump mesh frequency of figure 4.37 b) and d).

Meshing of a particular tooth on one of the planetary gears with the annular gear takes place at the "planet to annular gear corresponding tooth mesh frequency", f_a=7.6 Hz. Small darker regions are visible at this frequency between the fourth and seventh sidebands above the epicyclic meshing frequency on the frequency analyses of figure 4.37 b) and d), being slightly more prominent in the damaged case of figure 4.37 d).

The damaged condition's spectrogram, figure 4.37 c), does show evidence of frequency transients, as indicated. These events are however not as clear as is desirable, and damage identification based on their existence can not be performed with confidence. The events are best reflected in the 3 Hz darker region of the frequency analysis of figure 4.37 d).

Though the spectrogram clearly indicates the frequencies and times where the energy in the frequency band under consideration occurs, the resolution is fairly poor. Higher frequency resolution, as well as higher time resolution is desirable. The Wigner-Ville distribution provides for better resolution, albeit at the price of interference in the form of so called cross terms. The spectrograms presented in figure 4.37 do not provide a clear indication of damage to the transmission under consideration.

Pseudo Wigner-Ville distributions of the same undamaged and damaged condition signal portions of the band-pass filtered signals are presented in figure 4.38 a) and c), respectively. The instantaneous energy density is presented as figure 4.38 e) (Loutridis, Article in Press). The frequency resolution as well as the time resolution of the Wigner-Ville distribution is much better than that of the spectrogram. The underlying structures of the events on the graphs are clearer in the Wigner-Ville distributions of figure 4.38 than on the spectrograms of figure 4.37. The first meshing harmonic of the hydraulic gear pump shows up as a horizontal dark line at 208 Hz, and

the small speed fluctuations to which the system was subjected are visible as fluctuations in this dark band.

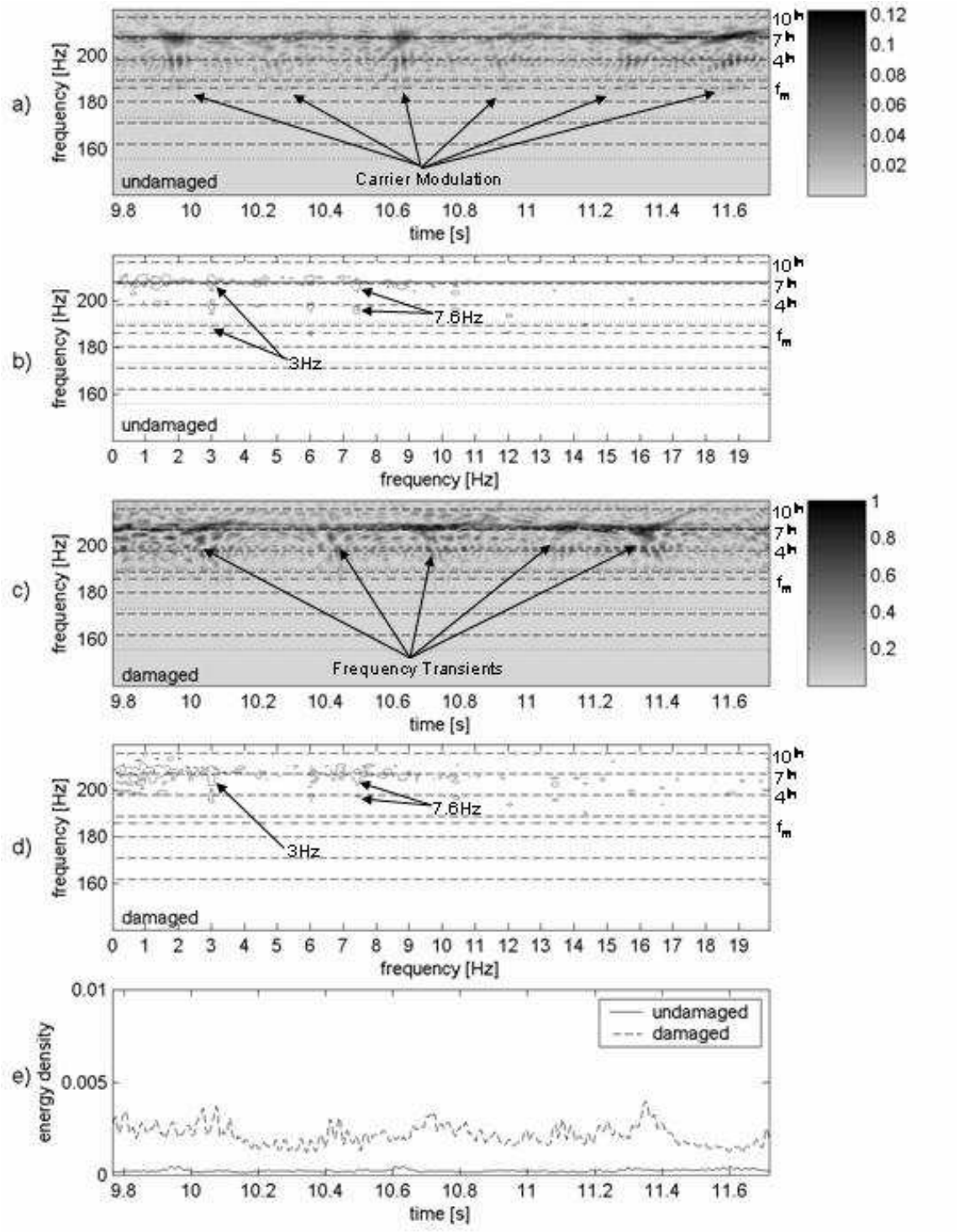

Figure 4.38: Pseudo Wigner-Ville Distributions, Band-Pass Filtered Signals

Modulation synchronous with the planet carrier rotation (table 4.5) are visible as darker patches are between the first sideband above and second sideband below the epicyclic gear mesh frequency, f_m, on figure 4.38 a) and

c). Again, as for the spectrograms of figure 4.37, these modulations are more clearly visible for the undamaged case of figure 4.38 a) than for the damaged case of figure 4.38 c). Corresponding indications show up in the frequency analyses of the Wigner-Ville distribution, figures 4.38 b) and 4.38 d), at 3 Hz. Peaks are visible in the band between the first sideband above and second sideband below the epicyclic meshing frequency, as well as on the gear pump mesh frequency of figure 4.38 b) and d).

Peaks are visible at f_a=7.6 Hz, the "planet to annular gear corresponding tooth mesh frequency", between the fourth and seventh sidebands above the epicyclic meshing frequency on the frequency analyses of figure 4.38 b) and d). As before this indicates a slight modulation of the gear mesh carrier signal at this frequency.

Wide-band transient events are more apparent on the pseudo Wigner-Ville distribution of figure 4.38 c) than on the spectrogram of figure 4.37 c). These spectral phenomena are possibly associated with damage to the epicyclic transmission. To determine whether these phenomena are associated with damage to the transmission, it needs to be confirmed that the spacing between the artefacts are multiples of the planet rotation period of 0.13 seconds. From the figure it does indeed seem that the spacing between the events is wholly divisible by 0.13. Planet rotation period here does not refer to the period associated with the absolute planet rotation frequency, but rather to the period with which a single tooth contacts the annulus. This frequency may be computed by equation 4.4, and the inverse taken to obtain the period. Using values as per table 4.5 this computes to approximately 0.13 seconds in both damaged and undamaged cases.

Adaptive filtering by the LMS based adaptive line enhancer has not enhanced the pseudo Wigner-Ville distributions displayed in figures 4.39 a) and b), when comparing to figures 4.38 a) and c). The structure associated with the hydraulic gear pump's first meshing harmonic at approximately 208 Hz that extended across the time record has largely been obliterated, without any perceivable gain around the epicyclic meshing frequencies of approximately 186 Hz. No enhancement is observed at any of the expected epicyclic meshing sidebands either. The energy criterion has also been affected detrimentally. It is pointed out however that this is due to the lack of convergence of the LMS algorithm, and is not an intrinsic effect resulting from the use of the LMS based adaptive line enhancer.

Figures 4.40 and 4.41 show the spectrograms and pseudo Wigner-Ville distributions for SQSD filtered signals. Comparing the SQSD filtered signal to the plain band-pass filtered signal leads to the conclusion that the SQSD based filtering process has made a small contribution to the clarity of the time-frequency distributions. It is to be noted that adaptive filtering is known to introduce noise into a signal, especially as the filter length increases

(Widrow & Stearns, 1985). Care has to be taken that cross terms resulting from noise introduced in such a manner does not influence the Wigner-Ville distribution detrimentally.

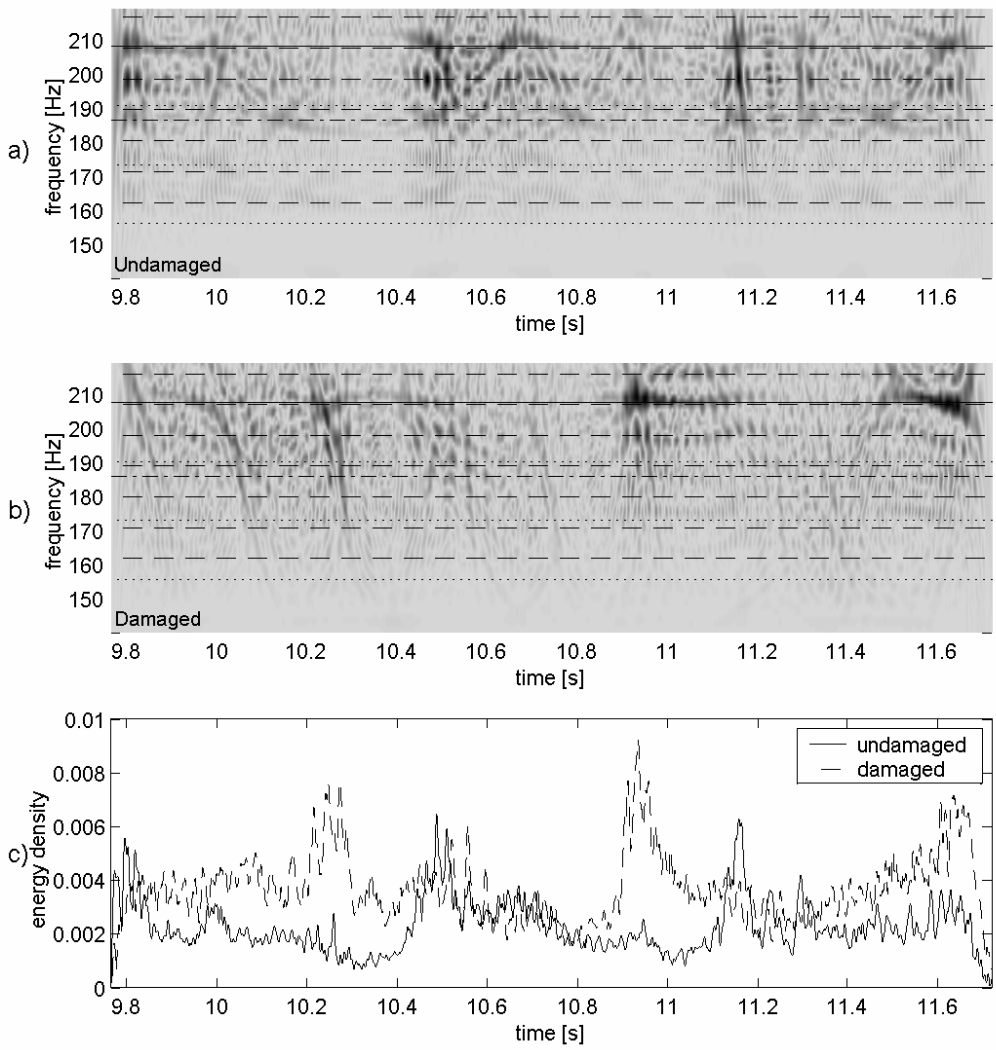

Figure 4.39: Pseudo Wigner-Ville Distributions, LMS Filtered Signals

Features of the spectrogram are slightly better defined with respect to time resolution. Frequency transients identified in figure 4.37 c) are also present in figure 4.40 c), and have slightly enhanced resolution in the latter case. Frequency resolution appears better in the case of the filtered data. This can be attributed to the effect of the adaptive filtering, as the same parameters were used to generate the figures. Irrespective of these improvements, the Wigner-Ville distribution still provides substantially better resolution on both the time and frequency axes. Figure 4.40 a) presents the SQSD filtered undamaged condition's spectrogram data, figure 4.40 c) the SQSD filtered damaged condition's data, and figure 4.40 e) the instantaneous energy densities computed from the spectrograms of the two damage scenarios. Figure 4.40 b) and d) represent frequency analyses performed along the time axis of the time-frequency distributions. As before activity at frequencies of 3

Hz and 6.7 Hz are evident, but with marginally improved resolution and clarity.

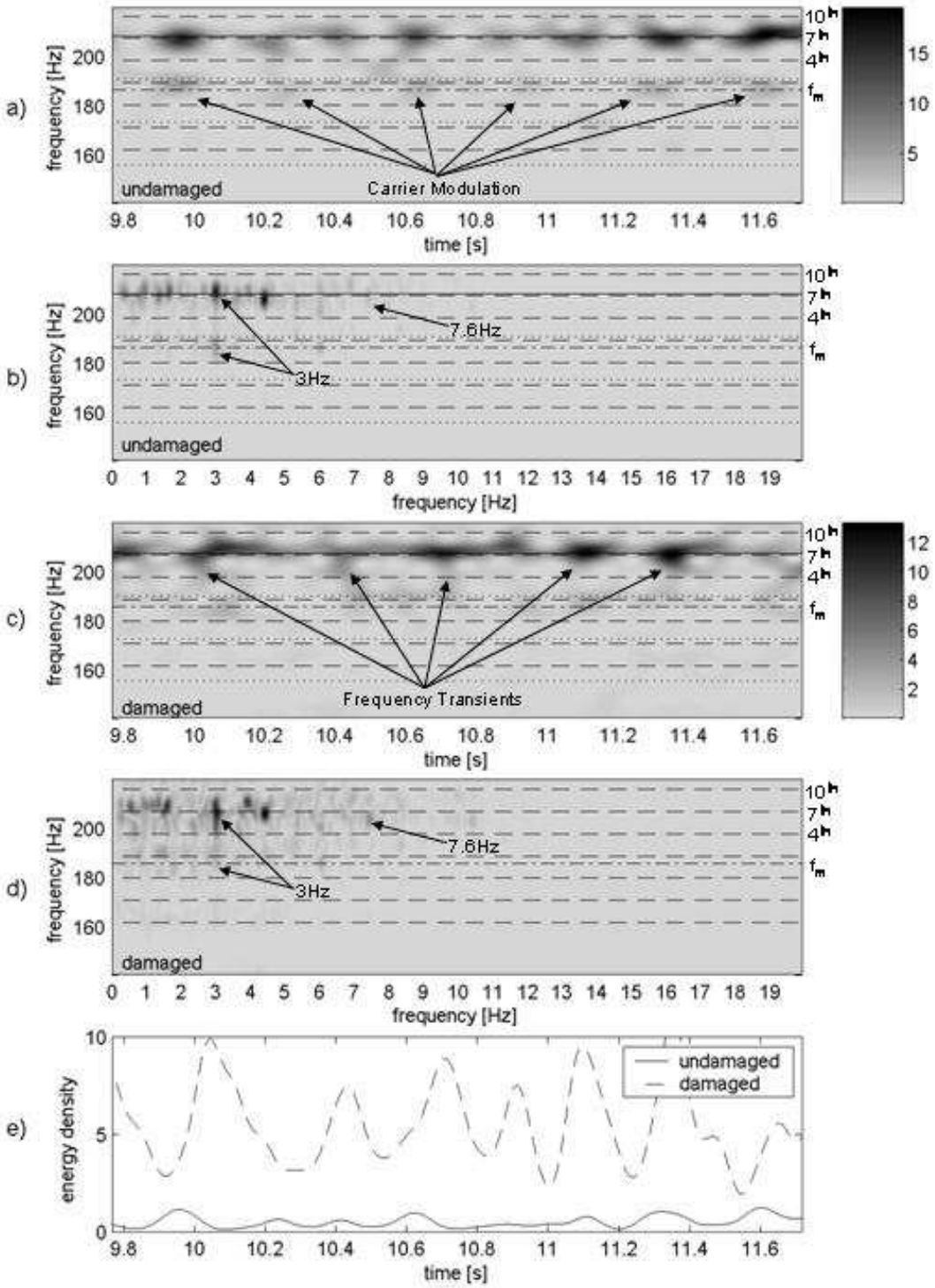

Figure 4.40: Spectrograms, SQSD Filtered Signals

Artefacts related to the structure of the events on the Wigner-Ville distribution of figure 4.41 do seem to have been enhanced, when comparing to figure 4.38. It is stressed that the change is by no means phenomenal. A

small improvement is nevertheless recognised. The most significant improvement is the enhancement of the vertical features, occurring across the frequency axis. These wide-band features may be indicative of damage to the epicyclic transmission.

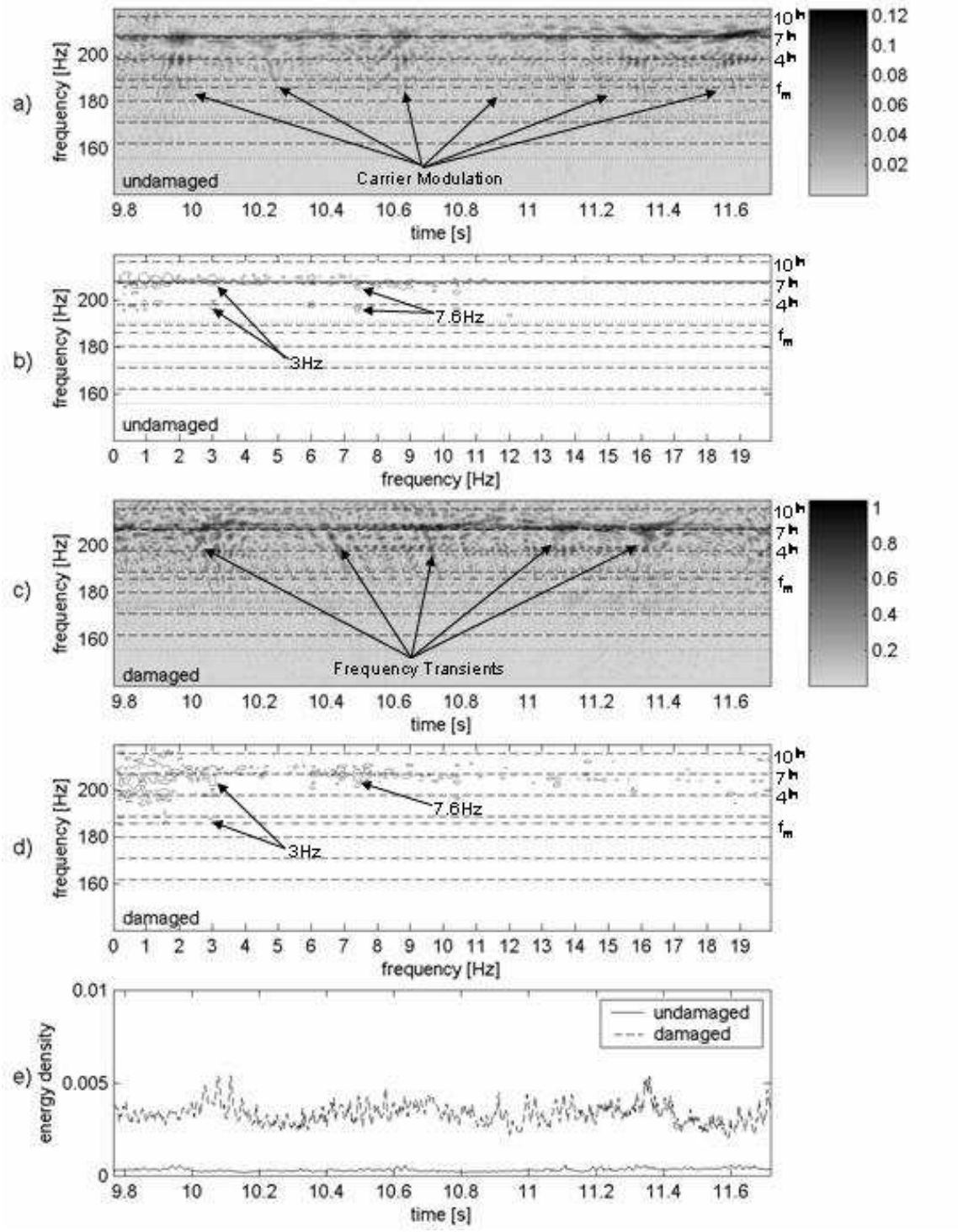

Figure 4.41: Pseudo Wigner-Ville Distributions, SQSD Filtered Signals

Transients associated with shock events are visible as vertical smudges on the time-frequency distribution of figure 4.41 c): the pseudo Wigner-Ville distributions computed over 2 seconds of the adaptively filtered signals. It is expected that these will increase only very slightly when compared to the undamaged case's data, due to the nature of the damage seeded on the gears: only a small amount of the flank was filed away from one of the teeth of one of the planetary gears, as shown in figure 4.28.

When comparing the damaged case of figure 4.41 c) to the undamaged case of figure 4.41 a), the frequency axis transients are indeed perceived to be slightly longer along the frequency axis. This indicates that more of the total signal energy is contained in these transient events: an observation further borne out by observing the level of the instantaneous energy densities also shown on the graphs. In the damaged cases the instantaneous energy density was consistently found to maintain a higher level than for the undamaged case, in spite of the similarity in load and speed conditions.

It should be noted that the transducers used to record the signals had to be moved between the experiments. System components had to be removed from the test bench in order to seed the damage to the gears, and were subsequently reinserted and realigned. Although reasonable precautions have been taken to ensure similar experimental conditions, strictly identical conditions are not practically achievable. These differences in the experimental setups will also contribute to the differences in the measured data. Especially the mounting of the transducers could have a marked effect on the signal levels, and hence the instantaneous energy density.

Adaptive filtering by the SQSD method has emphasized these transient phenomena on the pseudo Wigner-Ville distributions of figure 4.41. The underlying structure of the frequency content is more clearly observable on the graphs. The presence of cross-term interference is however also noted. As before, the frequency analyses of figure 4.41 b) and c) show activity at 3 Hz and 7.6 Hz, as expected.

Loutridis' (Article in Press) energy criterion also proves to be a useful aid in damage identification using time-domain data. Computing the instantaneous energy density from data filtered by adaptive methods provides for a spikier curve though. The enhancement of the time-frequency distribution itself has to be weighed against the deterioration in the cleanliness of the energy density.

From the cases presented in this current and the preceding section it is concluded that adaptive filtering may be used as an aid to damage identification from time-domain data for epicyclic gearboxes, especially when used in conjunction with time-frequency methods. Differences in the signals before and after adaptive filtering were more pronounced on the

time-frequency graphs than was the case for the PSDs. Although convergence is easier to attain with the newly proposed SQSD based adaptive line enhancer, the price to be paid is often a noisier weight vector solution. In the cases where convergence is hard to obtain by the LMS based filter, there is however a clear advantage in using the SQSD based filter.

5 Conclusion

Strictly time domain based diagnostic techniques operating on mechanical vibration signatures forms the central theme of this work. Filtering of the time domain data was performed using adaptive filtering methods. Damage identification was performed via signal analysis by time-frequency methods belonging to Cohen's general class.

Adaptive time domain filtering techniques for the removal of random noise from periodic or pseudo-periodic vibration signals were presented. The well known least mean squares algorithm was used in an adaptive line enhancer configuration in this context. A new unconditionally convergent adaptive filtering algorithm, based on the spherical quadratic steepest descent method was applied to the vibration signatures recorded from an epicyclic gearbox.

Damage identification was performed by examination of the vibration signatures using the spectrogram and pseudo Wigner-Ville distributions. Wide-band transient events were sought on the time-frequency distributions to identify the presence of damage. The instantaneous energy density as defined by Loutridis (Article in Press) was applied to the spectrogram and pseudo Wigner-Ville distributions.

5.1 Summary of Findings

5.1.1 Cantilever Beam Experiments

From the squared prediction errors it can be seen that the spherical quadratic steepest descent based filter and the least mean squares filter exhibit similar convergence behavior. Although the squared prediction error may indicate convergence, solution quality needs to be considered also.

Choosing an excessively small step size parameter will lead to excessively slow convergence, and a loss of tracking ability for non-stationary signals for both algorithms. Larger step size parameters may converge more quickly, but offers a poorer quality solution in terms of the severity of the random fluctuations of the weight vector about the optimal solution. It is noted that for the spherical quadratic steepest descent algorithm with constant step size parameter, the filtered signal tends to be slightly noisier than for the corresponding least mean square case. It was found, as expected, that the step size parameter has a pronounced effect on the convergence behavior, as well as the solution quality of the filtered signal. Squared prediction error may be used to good effect as an indicator of convergence for the algorithms presented. It is advisable however to also consider the solution in terms of the filtered signal and filter coefficients to ensure a satisfactory solution.

Exponential decrease of the step size offered the fast initial convergence of using a larger step size parameter, combined with the higher quality solution associated with smaller step size parameters. It was found during

experimentation with exponentially decreasing step size that a decrease in prediction error may be indicated as a result of forcing the exponential decay of the step size parameter, while the algorithm has not successfully converged to an acceptable stable solution. Care thus has to be exercised when applying a forcing function to the step size parameter.

5.1.2 *Conventional Helical Gearbox Experiments*

When applied to quadratic objective functions, the spherical quadratic steepest descent algorithm has demonstrated a distinct advantage of unconditional convergence over the conventional least mean squares algorithm. Instances where the least mean squares algorithm failed to converge, while the spherical quadratic steepest descent algorithm converged successfully have been demonstrated for both the conventional helical and the epicyclic gear vibration data. In addition the data filtered by the spherical quadratic steepest descent based filter provided signals with emphasized periodic content. Less experimentation was required with the spherical quadratic steepest descent algorithm to obtain a suitable step size parameter than with the least mean squares algorithm.

Both the least mean squares algorithm and the spherical quadratic steepest descent algorithm have been shown to have useful application to time domain gear vibration data. The time domain amplitude and phase modulated vibration signatures recorded from conventional gearboxes may be filtered successfully for random noise reduction using the algorithms. More experimentation may however be required to find suitable parameters for the least mean squares algorithm than for the spherical quadratic steepest descent algorithm.

A case where clear evidence of damage was absent from the time-frequency representation of a time domain vibration signature from a conventional helical gearbox has been demonstrated. On the spherical quadratic steepest descent based adaptively filtered signal's pseudo-Wigner-Ville distribution, the damage could clearly be identified from the wide-band transient events observed, spaced at multiples of the gear rotation period. Time-frequency methods and the associated instantaneous energy density (Loutridis, Article in Press) have been shown to provide a viable alternative damage identification methodology to conventional spectral analysis, using strictly time domain data.

Time-frequency methods, and in particular the pseudo Wigner-Ville distribution, combined with adaptive time domain filtering has been shown to aid in damage identification from strictly time domain data. The adaptive filtering has successfully enhanced the time domain signals such that damage features could be more easily identified on the time-frequency graphs produced by the pseudo Wigner-Ville distribution.

5.1.3 *Epicyclic Gearbox Experiments*

Traditional spectral analysis may not be suitable for epicyclic gearbox vibration diagnosis in general. Differences in traditional spectra may be too small to indicate appreciable damage to the transmission, as was the case in the epicyclic gearbox data presented.

Adaptive filtering by the least mean squares algorithm failed to converge to an acceptable solution with the time domain data presented here. In contrast, the spherical quadratic steepest descent adaptive filter converged and successfully emphasized transients on the pseudo Wigner-Ville distribution, enabling the clear identification of damage to the transmission. These transient events were less clear on the band-pass filtered only signal. Adaptive time domain filtering has thus been shown to be useful as an aid to damage identification from time domain vibration data for epicyclic gearboxes, especially when used in combination with sensitive time-frequency techniques. As for the conventional gear vibration case, the epicyclic case has demonstrated that adaptive time domain filtering can be used to enhance artefacts associated with damage to the transmission, visible on the time-frequency plane.

Spherical quadratic steepest descent based adaptive filtering has been shown to outperform the conventional least mean squares algorithm in the cases presented. Clearly the spherical quadratic steepest descent based filter has been demonstrated to deal satisfactorily with amplitude and phase modulated epicyclic gear vibration data, which includes modulation at the planet carrier rotation frequency.

Instantaneous energy density (Loutridis, Article in Press), computed from time-frequency representations has proven itself to be useful in epicyclic gearbox diagnostics from time-domain vibration data.

5.2 General Additional Conclusions

Antoni and Randall's (2001) method to determine number of filter coefficients has proved useful. In all experiments the method was used with success to determine the filter length for the least mean squares filter as well as the spherical quadratic steepest descent based filter.

It was found that the instantaneous energy density criterion in isolation presents some difficulty when used with the spherical quadratic steepest descent filtered data's pseudo Wigner-Ville distributions. The instantaneous energy density generally appears more active when computed from the Wigner-Ville distributions presented. Used in parallel with observations from the pseudo Wigner-Ville distributions, it is however a valuable aid to determining whether damage is in deed present. The instantaneous energy density was generally smoother when computed from spectrograms.

The spectrogram, although successfully used by other researchers, has a distinct disadvantage of poorer time- and frequency resolution. The Wigner-Ville distribution exhibited better resolution, and was found to paint a clearer picture of the underlying structure of the time-frequency representation. Wide-band transients were clearer on pseudo-Wigner-Ville distributions than on spectrograms.

In spite of unconditional convergence, discretion is still required when choosing parameters of the spherical quadratic steepest descent algorithm. The algorithm was found to be generally more stable than the least mean squares counterpart. In spite of this, care has to be taken to ensure that the algorithm converges to an acceptable solution. It was found that when the step size parameter was set too large, the filter weights would in some cases tend to unity and allow the signal to pass through the filter largely unaffected.

Although convergence was found to be easier to attain with the newly proposed spherical quadratic steepest descent based adaptive line enhancer, the price to be paid is often a noisier weight vector solution. In the cases where convergence is hard to obtain by the least mean squares based filter, there is however a clear advantage in using the spherical quadratic steepest descent based filter in spite of the possibility of a noisy weight vector solution.

5.3 Recommendations

Synchronous averaging is widely used by practitioners of gearbox vibration analysis. The technique performs well when used to reduce the random or asynchronous noise present in gear vibration signals. A disadvantage of the technique is that it requires data sampled in the angular domain, i.e. order tracked data. Order tracking removes the evidence of speed variation from time domain data.

Should the variation of shaft speed be important for some or other reason, synchronous averaging will be unattractive. The additional hardware required to perform the order tracking operation is another downside of the technique. In such cases, the analyst may be forced to make use of strictly time domain data.

It has been demonstrated here that incipient faults may be recognised from the time-frequency distributions computed from strictly time domain data. The adaptive filtering algorithms used have been shown to aid in this process. The preservation of shaft speed information may point to issues other than those associated with a damaged gearbox, such as misuse or inappropriate operation. Time domain data offers a maximised amount of possible information regarding the operation of a gearbox.

5.4 Future Work

Time-frequency methods applied to vibration data have been shown to be effective in the field of gearbox condition monitoring. Further work is required to make full use of the diagnostic information carried in time domain data and associated time-frequency techniques.

Adaptive filter techniques have also been shown to be of good use when applied to strictly time domain data. Periodically occurring damage signatures may be emphasised by judicious adaptive filtering. The newly presented spherical quadratic steepest descent based algorithm may yet prove to be of greater use in the field of vibration signature analysis. Further developmental work is hence required. Investigations into the convergence behaviour and the optimization of the algorithm's parameters are suggested.

As yet, no clear connection has been made between vibration signature analysis and residual life estimates. The penultimate goal of a condition monitoring technique is a prediction of the residual safe operating time of a machine. Residual life estimation based on current vibration signature analysis techniques needs to be addressed.

References

1) S.T. Alexander, 1986; Adaptive signal processing: theory and applications; Springer-Verlag
2) J. Antoni, F. Bonnardot, A. Raad, M. El Badaoui 2004; Mechanical Systems and Signal Processing 18, 1285 – 1314; Cyclostationary modeling of rotating machine signals.
3) J. Antoni and R.B. Randall 2001; Condition Monitoring and Diagnostic Engineering Management, 89 – 96; Optimization of SANC for separating gear and bearing signals.
4) J. Antoni and R.B. Randall 2004; Mechanical Systems and Signal Processing 18, 89 – 101; Unsupervised noise cancellation for vibration signals: part I – evaluation of adaptive algorithms.
5) J. Antoni and R.B. Randall 2004; Mechanical Systems and Signal Processing 18, 103 – 117; Unsupervised noise cancellation for vibration signals: part II – a novel frequency-domain algorithm.
6) N. Baydar, A. Ball, 2001; Mechanical Systems and Signal Processing 15, 1091 – 1107; A comparative study of acoustic and vibration signals in detection of gear failures using Wigner-Ville distributions.
7) F. Bonnardot, M. El Badaoui, R.B. Randall, J. Daniere, F. Guillet, in press; Mechanical Systems and Signal Processing; Use of the acceleration signal of a gearbox in order to perform angular resampling (with limited speed fluctuation).
8) K.M. Bossley, R.J. McKendrick, C.J. Harris, C. Mercer 1999; Mechanical Systems and Signal Processing 13, 627 – 641; Hybrid computed order tracking.
9) S. Braun 1975; Acoustica Vol. 32, 69 – 77; The extraction of periodic waveforms by time domain averaging.
10) S.G. Braun, B.B. Seth, 1979; Journal of Sound and Vibration 65, 37 – 50; On the extraction and filtering of signals acquired from rotating machines.
11) D. Brie, M. Tomczak, H. Oehlmann and A. Richard 1996; Mechanical Systems and Signal Processing 11, 149 – 167; Gear crack detection by adaptive amplitude and phase demodulation.
12) C. Capdessus, M. Sidahmed, J.L. Lacoume 2000; Mechanical Systems and Signal Processing 14, 371 – 385; Cyclostationary processes: Application in gear faults early diagnosis.
13) L. Cohen 1989; Proceedings of the IEEE, Vol. 77, No. 7; Time-Frequency Distributions – A Review.
14) L. Cohen 1994; Time-Frequency and Time-Scale Analysis, 1994, Proceedings of the IEEE-SP International Symposium, 182 – 185; The uncertainty principle in signal analysis.
15) L. Cohen, 1995; Time-Frequency Analysis; Prentice Hall
16) G. Dalpiaz, A. Rivola and R. Rubini 2000; Mechanical Systems and Signal Processing 14, 387 – 412; Effectiveness and sensitivity of vibration processing techniques for local fault detection in gears.

17) M.J. Dowling, 1993; IEEE, I-59 – I-62; Application of non-stationary analysis to machinery monitoring.
18) M. El Badaoui, F. Guillet, J. Daniere, 2004; Mechanical Systems and Signal Processing 18, 1031 – 1046; New applications of the real cepstrum to gear signals, including definition of a robust fault indicator.
19) S.J. Elliott 2001; Encyclopedia of Vibration, Vol. 1, 81 – 87; Adaptive Filters
20) D. Forrester, D. Blunt 2003; HUMS 2003 Conference, 510-1 – 510-7; Analysis of epicyclic gearbox vibration.
21) F.R. Fyfe and E.D.S. Munck 1997; Mechanical Systems and Signal Processing 11, 187 – 205; Analysis of computed order tracking.
22) H. Garudadri, M.P. Beddoes, A.-P. Benguerel and J.H.V. Gilbert, 1987; Proceedings of the IEEE ICASSP-87, 1521 – 1524; On computing the smoothed Wigner distribution.
23) S. Goldman, 1999; Vibration spectrum analysis: a practical approach; New York : Industrial Press
24) A. Grall, C. Bérenguer, L. Dieulle 2002; Reliability Engineering and System Safety 76, 167 – 180; A condition-based maintenance policy for stochastically deteriorating systems.
25) F. Gustafsson, 1996; IEEE Transactions on Signal Processing, Vol. 44, No. 4, 988 – 992; Determining the initial states in forward-backward filtering.
26) S.S. Haykin, 1986; Adaptive Filter Theory; Englewood Cliffs, N.J : Prentice Hall London : Prentice-Hall International
27) W. Hernández 2001; Sound and Actuators A 88, 198 – 208; Improving the response of an accelerometer by using optimal filtering.
28) W. Hernández 2003; Measurement 33, 229 – 240; Improving the response of a wheel speed sensor using an adaptive line enhancer.
29) E.C. Ifeachor and B.W. Jervis, 2002; Digital signal processing: a practical approach; Harlow, England ; New York : Prentice Hall
30) P. Jonsson, 2000; Journal of Operations Management 18, 701 – 718; Towards an holistic understanding of disruptions in Operations Management.
31) S.K. Lee and P.R. White 1998; Journal of Sound and Vibration 217, 485 – 505; The enhancement of impulsive noise and vibration signals for fault detection in rotating and reciprocating machinery.
32) S.J. Loutridis, Article in Press; Mechanical Systems and Signal Processing, 1 – 15; Instantaneous energy density as a feature for gear fault detection
33) S. L. Marple, Jr., Computing the discrete-time analytic signal via FFT, IEEE Transactions on Signal Processing, Vol. 47, No. 9, September 1999, pp.2600--2603.
34) P.D. McFadden and J.D. Smith 1985; Proceeding of the Institution of Mechanical Engineers Vol. 199, 65 – 70; An explanation for the asymmetry of the modulation sidebands about the tooth meshing frequency in epicyclic gear vibration.
35) P.D. McFadden and J.D. Smith 1985; Proc Instn Mech Engrs Vol 199, 287 – 292; A signal processing technique for detecting local defects in a gear from the signal average of the vibration.

36) P.D. McFadden 1986; Journal of Vibration, Acoustics, Stress and Reliability in Design Vol. 108, 165 – 170; Detecting fatigue cracks in gears by amplitude and phase demodulation of the meshing vibration.
37) P.D. McFadden 1987; Mechanical Systems and Signal Processing 1, 83 – 95; A revised model for the extraction of periodic waveforms by time domain averaging.
38) P.D. McFadden 1988; Mechanical Systems and Signal Processing 2, 403 – 409; Determining the location of a fatigue crack in a gear from the phase of the change in the meshing vibration.
39) P.D. McFadden 1991; Journal of Sound and Vibration 144, 163 – 172; A technique for calculating the time domain averages of the vibration of the individual planet gears and the sun gear in an epicyclic gearbox.
40) G. Meltzer and Y.Y. Ivanov 2002; Mechanical Systems and Signal Processing 17, 1033 – 1047; Fault detection in gear drives with non-stationary rotational speed – part I: The time-frequency approach.
41) G. Meltzer and Y.Y. Ivanov 2002; Mechanical Systems and Signal Processing 17, 273 – 283; Fault detection in gear drives with non-stationary rotational speed – part II: The time-quefrency approach.
42) M. Naeem, R. Singh and D. Probert 2001; Applied Energy 70, 103 – 133; Consequences of aero-engine deteriorations for military aircraft.
43) S.B. Narayanan, K.M.M. Prabhu, 1989; IEEE Electronics Letters, vol. 25, no. 5, 336 – 338; New method of computing Wigner-Ville distribution.
44) H.Oehlmann, D. Brie, M. Tomczak and A. Richard, 1997; Mechanical Systems and Signal Processing 11, 529 – 545; A method for analyzing gearbox faults using time-frequency representations.
45) A.V. Oppenheim, R.W. Schafer, 1989; Discrete-time signal processing; Englewood Cliffs, N.J : Prentice Hall London : Prentice-Hall International
46) R.B. Randall 1982; Journal of Mechanical Design Vol. 104, 259 – 267; A new method of modeling gear faults
47) R.B. Randall 2001; Condition Monitoring and Diagnostic Engineering Management, 1 – 11; Bearing diagnostics in helicopter gearboxes.
48) P.D. Samuel, D.J. Pines 2004; Journal of Sound and Vibration – Article in press; A review of vibration-based techniques for helicopter transmission diagnostics
49) J.D. Smith, 1983; Gears and their vibration; Marcel Dekker : The MacMillan Press Ltd.
50) J.A. Snyman, A.M. Hay, 2001; Computers and Mathematics with Applications 42, 169 – 178; The spherical quadratic steepest descent method for unconstrained minimization with no explicit line searches.
51) W.J. Staszewski, K. Worden, G.R. Tomlinson 1997; Mechanical Systems and Signal Processing 11, 673 – 692; Time–frequency analysis in gearbox fault detection using the Wigner-Ville distribution and pattern recognition.
52) H. Wang, 2002; European Journal of Operational Research 139, 469 – 489; A survey of maintenance policies of deteriorating systems.

53) W.J. Wang, P.D. McFadden 1993; Mechanical Systems and Signal Processing 7, 193 – 203; Early detection of gear failure by vibration analysis – I: Calculation of the time-frequency distribution.

54) W.J. Wang, P.D. McFadden 1993; Mechanical Systems and Signal Processing 7, 205 – 215; Early detection of gear failure by vibration analysis – II: Interpretation of the time-frequency distribution using image processing techniques.

55) W.Q. Wang, F. Ismail and M. F. Golnaraghi 2001; Mechanical Systems and Signal Processing 15, 905 - 922; Assessment of gear damage monitoring techniques using vibration measurements.

56) B. Widrow and M. Kamenetsky 2003; Neural Networks 16, 735 – 744; Statistical Efficiency of adaptive algorithms.

57) B. Widrow and S.D. Stearns, 1985; Adaptive Signal Processing; Englewood Cliffs, N.J : Prentice Hall New York

58) B. Widrow, E. Walach 1984; IEEE Transactions on Information Theory, vol. IT-30, no. 2, 211 – 221; On the Statistical Efficiency of the LMS Algorithm with Nonstationary Inputs

59) J.R. Zeidler, E.H. Satorius, D.M. Chabries, H.T. Wexler, 1978; IEEE transactions on acoustics, speech and signal processing, Vol. ASSP-26, No. 3, 240 – 254; Adaptive Enhancement of Multiple Sinusoids in Uncorrelated Noise.